Book of Abstracts

7^{th} International Conference on Inverse Problems, Control and Shape Optimization

PICOF 2014

May 7-9, 2014

Hammamet, Tunisia

Organizing committee

Skander Belhaj (ISAMM)
Nabil Gmati (ENIT)
Moncef Mahjoub (ENIT)
Ibrahim Trabelsi (ISAMM)

Scientific committee

Chair

Belhassen Dehman

International Program Committee

Grégoire Allaire (France)
Rajae Aboulaich (Morocco)
Amel Ben Abda (Tunisia)
Jacques Blum (France)
Houssem Haddar (France)
Mohamed Jaoua (France)
Enrique Zuazua (Spain)

Book of Abstracts of the 7^{th} International Conference on Inverse Problems, Control and Shape Optimization (PICOF 2014)

May 7-9, 2014, Hammamet, Tunisia

Conference homepage
http://www.lamsin.tn/picof14/

Slides at
http://www.lamsin.tn/picof14/

Online Book of Abstracts at
http://www.lamsin.tn/picof14/

Table of contents

Invited Talks

Control of partial differential equations and nonlinearities

Jean-Michel Coron*

Abstract: In this talk we survey some methods which can used in order to study control issues for physical systems modeled by means of nonlinear partial differential equations. A special emphasis is put on cases where the nonlinearities play a crucial role. These tools include Lie brackets, return method, scaling, quasistatic deformations, power series expansion, phantom tracking, Fredholm transformations. We present applications to various physical control systems (Euler and Navier-Stokes equations of incompressible fluids, shallow water equations, Korteweg-de Vries equations...) and open problems on the control of these control systems.

Keyworlds: Control, nonlinear partial differential equations, Fredholm transformations.

*Laboratoire Jacques-Louis Lions Université Pierre et Marie Curie, France, coron@ann.jussieu.fr,

Microscopic modeling of crowd motion

Aline Lefebvre-Lepot*

Abstract

We are interested in modeling crowd motion. Such models can be divided into two classes: the first one involves a macroscopic description of the crowd (which is represented by a local density) and the second one uses a microscopic description (each individual is represented). In this talk, we focus on microscopic modeling of crowds.

After a brief review of the existing microscopic models, we will focus on the model proposed by B. Maury and J. Venel (2007). In this model, each person is modeled by a disk and has a desired velocity (for example, the quickest path to leave a room). Since people can not overlap, the actual velocities has to take congestion into account. To do so, the authors propose to define the actual velocities as the projection of the desired ones onto the set of admissible velocities (that is, the velocities that preserve the non-overlapping constraint). To compute solutions to this model, the authors propose a numerical algorithm based on a projection step, initially described by B. Maury in order to simulate inelastic collisions in granular flows. Numerical simulations of crowd emergency exit using this model will be shown.

The previous model is based on a projection of the global vector of desired velocities $V = (V_1, \cdots, V_N)$ on the set of admissible velocities (N being the number of persons). As a consequence, in this model, the crowd can be seen as a unique entity which optimizes its satisfaction. This leads for example to pressure arches which blocks the exits. These situations are well known for granular materials and are realistic in case of emergency evacuation for crowd motion. We will discuss of different approach allowing to add "social" contributions to the behavior of people in order to simulate more general situations.

This work is a joint work with B. Maury, J. Venel, S. Faure and J-B. Lagaert.

*CNRS - CMAP/Ecole Polytechnique

On identification of fixed immersed obstacles in a Stokes fluid from boundary measurements

Laurent Bourgeois*

Abstract: In this talk we present an "exterior approach" in order to retrieve some fixed obstacles immersed in a Stokes fluid from boundary measurements. Such iterative approach is a combination of a quasi-reversibility method and of a level set method : the first one enables us to update the solution of the ill-posed Cauchy problem outside the obstacle obtained at previous iteration, while the second one enables us to update the obstacle with the help of the solution obtained at previous iteration. The main feature of our approach is that it does not rely on an optimization process. Concerning the quasi-reversibility method, which dates back to LattÃ¨s and Lions (67), we introduce two new mixed formulations which transform the classical fourth-order problem of quasi-reversibility into a system of two second-order problems. We compare these two mixed formulations and illustrate them numerically on a 2D data completion problem. Concerning the level set method, we introduce a new method based on a simple Poisson equation that is well adapted to Dirichlet obstacles. Our exterior approach is finally applied to some 2D numerical examples of inverse obstacle problems.

Keyworlds: Identification, immersed obstacles, Stokes fluid.

*UMA Equipe POEMS, France, laurent.bourgeois@ensta-paristech.fr,

Topological sensitivities for crack problems

Günther Leugering*

Abstract: Control of crack propagation by the way of optimal placement material inclusions in composite materials is a field of current interest. We show that the energy release in brittle materials admits a conical derivative with respect to to topological changes. The prove is based on a nonoverlapping domain decomposition technique using the Dirichlet-to-Neumann mapping.

Keyworlds:

*Friedrich-Alexander-Universität Erlangen-Nürnberg, leugering@math.fau.de,

Data assimilation for geophysical problems

Didier Auroux*

Abstract: We present a new data assimilation scheme, based on observers, and we compare it with variational and sequential methods, on a realistic ocean model.
Keywords: data assimilation, geophysics, optimal control, nudging, observers.

Data assimilation consists in estimating the state of a system by combining via numerical methods two different sources of information: models, and observations. Data assimilation makes it possible to answer a wide range of questions such as: the optimal identification of the initial state of a system, and then reliable numerical forecasts; the systematic identification of error sources in the models; the optimization of observation networks; the extrapolation, using a numerical model, of the values of non observed variables. Thus, data assimilation is increasingly used in the community of geophysical sciences, in relation with mathematicians. In external geophysics (meteorology, oceanography, ...), the model is chaotic and hence very dependent on the initial condition. The inverse problem consists then in identifying the initial condition for the data assimilation period. There are two main classes of data assimilation methods, the first based on estimation theory (sequential assimilation), and the other based on optimal control theory (variational assimilation).

The most sophisticated variational method, currently used in many centers of operational forecast (in oceanography and in meteorology), is the 4D-VAR (four-dimensional variational) algorithm [5]. It consists of assimilating all the available information (contained both in the model and the observations) during the work (or assimilation) period. The problem of identifying the state of a system at a given time can then be written as the minimization of a criterion measuring the difference between the forecasts of the model and the observations of the system in the given time window. In general, the initial state of the time interval is taken as the control variable for the minimization process. This provides an advantage to the 4D-VAR algorithm is that for each time step, the estimation of the state vector depends not only on the previous observations, but also on the future observations. Propagative phenomena, such as waves, are generally well represented by the 4D-VAR method. The disadvantages of the 4D-VAR algorithm are on one hand its quite difficult implementation, because it requires both the adjoint of the physical model and a powerful minimization algorithm, and on the other hand the lack of estimation of the errors in the assimilated state. Contrarily to the 4D-VAR, the sequential methods only require the physical model in the direct mode.

The spearhead of sequential methods, which are also operational (but more marginally than 4D-VAR), is the Kalman filter. The Kalman filter is designed to provide, for each time step, the optimal estimate (of variance of minimal error) of the system state, by using only the estimates of the state and the last observations. It alternates propagation steps (with the physical model) and correction steps (using the observations) of the state and of its error statistics. The main advantage of the Kalman filter is that it provides *in real time* an estimation of the statistics of errors of the state, in addition to the state itself, and thus it is able to provide a statistically optimal estimate of the state. Its weakness is its inability to take into account future observations like the 4D-VAR algorithm does. Extended forms of the Kalman filter are designed to integrate future observations then to smooth the model trajectory [4]; they are called the Kalman smoothers. 4D-VAR and Kalman filter or smoothers can be shown to be theoretically equivalent under certain hypotheses. However, the assumptions necessary to implement them are usually different and the equivalence is always lost in practice.

*University of Nice Sophia Antipolis, France, auroux@unice.fr

Nudging can be seen as a degenerate, oversimplified form of the Kalman filter. It consists in applying a Newtonian recall of the state value towards its direct observation. In spite of the differences, the term *nudging* is also sometimes used in the context of statistical interpolation. The standard nudging algorithm, which initially appeared in meteorology, is the first data assimilation method used in an operational way in oceanography. Some recent studies have shown that it is possible to determine in a systematic way the optimal weighting coefficients of the recall force to the observations, and then nudging is equivalent to the Kalman filter, or to 4D-VAR.

One of the main disadvantages of the sequential data assimilation methods is that they cannot, at a given time, take into account the future observations. They do not improve the estimation of the initial condition of the system. A simple idea, allowing at the same time the improvement of the estimation of the initial condition and the assimilation of future observations, consists of applying a second time the sequential method, but on the backward (in time) model, using the estimation of the final state (obtained by the forward assimilation) as a new initial guess. Thus, at the end of this process, one obtains a new estimation of the system state at the initial time (which makes it possible to use this estimation in a variational data assimilation method), and at each time of the backward assimilation, the corrections actually use the previous observations in the backward model, therefore future observations, to improve the estimated states. The backward problems are generally very ill posed (the heat equation is a very good example), and it is not a priori easy to apply a traditional data assimilation method to a backward model. However, if one uses a degraded version of the Kalman filter for complete observations of the system (in time and space), it is possible to stabilize backward integrations thanks to the assimilation corrective term.

A more recent approach of backward and forward nudging (or back and forth nudging, BFN) has been developed, consisting in initially solving the forward equations with a nudging term, and then, using the final state as an initial condition, in solving the same equations in a backward direction with a feedback term (with the opposite sign compared to the feedback term of forward nudging). This process is then repeated iteratively until convergence. The implementation of the BFN algorithm has been shown to be very easy, compared to other data assimilation methods [1].

However, several theoretical and numerical studies showed that it was difficult to deal with diffusion processes during backward integrations, leading to instabilities or explosion of the numerical solutions [2]. We present here an improved Back and Forth Nudging algorithm for diffusive equations in the context of meteorology and oceanography. In these applications, the theoretical equations are usually diffusive free (e.g. Euler's equation for meteorological processes). But then, in a numerical framework, a diffusive term is often added to the equations (or a diffusive scheme is used), in order to both stabilize the numerical integration of the equations, and take into consideration some subscale phenomena. In such situations, it is physically coherent to change the sign of the diffusion term in the backward integrations, in order to keep unchanged both roles of the diffusion term [3].

References

[1] D. Auroux and J. Blum, *A nudging-based data assimilation method for oceanographic problems: the Back and Forth Nudging (BFN) algorithm*, Nonlin. Proc. Geophys., 15:305-319, 2008.

[2] D. Auroux and M. Nodet, *The back and forth nudging algorithm for data assimilation problems: theoretical results on transport equations*, ESAIM Control Optim. Calc. Var., 18(2):318-342, 2012.

[3] D. Auroux, J. Blum, and M. Nodet, *Diffusive Back and Forth Nudging algorithm for data assimilation*, C. R. Acad. Sci. Paris, Ser. I, 349(15-16):849-854, 2011.

[4] G. Evensen and P.J. van Leeuwen, *An Ensemble Kalman Smoother for Nonlinear Dynamics*, Mon. Wea. Rev., 128:1852-1867, 1999.

[5] F.-X. Le Dimet and O. Talagrand, *Variational algorithms for analysis and assimilation of meteorological observations: theoretical aspects*, Tellus, 38A:97-110, 1986.

Regularization in Banach Spaces

Barbara Kaltenbacher*

Abstract: Making use of special features of certain Banach space norms such as the L^1 norm for promoting sparsity or the L^∞ norm for modelling uniform noise, enables an enhanced treatment of many practical inverse problems and has thus become quite popular recently. Motivated by this fact, much of the methodology and convergence theory for regularization has been generalized from the classical Hilbert space setting to Banach spaces in the last five to ten years. This talk is supposed to provide a short (probably incomplete) overview of the existing results and a report on recent joint work with Uno Hamarik, Bernd Hofmann, Urve Kangro, Christiane Poschl, Elena Resmerita, Otmar Scherzer, Frank Schopfer, Thomas Schuster, and Ivan Tomba.

Keyworlds: Banach spaces, Regularization, inverse problem.

*University of Graz, Institute for Mathematics and Scientific Computing, Austria, Barbara.Kaltenbacher@uni-klu.ac.at,

INVERSE PROBLEMS FOR A SPACE FRACTIONAL ADVECTION DISPERSION EQUATION

Taous-Meriem Laleg-Kirati

CEMSE, King Abdullah University of Science and Technology (KAUST), Thuwal, Kingdom of Saudi Arabia, taousmeriem.laleg@kaust.edu.sa

Abstract

Fractional advection dispersion equation is usually used to model solute transport in heterogeneous porous media. Identifying the source and the parameters for such an equation is important to understand how chemical or biological contaminates are transported throughout surface aquifer system. For instance, an estimate of the differentiation order in a ground water contaminant transport model can provide information about soil properties, such as the heterogeneous of the media.

We are interested in some inverse problems for a space fractional advection dispersion equation. We will discuss both the inverse source problem and the simultaneous estimation of the coefficients and the fractional differentiation order.

For the inverse source problem, we will derive the solution of the direct problem and study the well-posedness of the problem. We will then propose a numerical algorithm to compute the unknown source from final time solution.

In the second part, we will be interested in identifying the average velocity, the dispersion coefficient and the differentiation order for a space fractional advection dispersion equation using the measurements of the concentration and the flux at final time. Estimating the coefficients for fractional differential equations is not a trivial problem. Moreover, the problem becomes more challenging when it involves the identification of the differentiation order, where usually using standard optimization approaches fails. We propose a novel approach for more efficient and accurate results, where the so-called modulating functions method is combined with an optimization problem to estimate all three parameters simultaneously. The efficiency of the proposed method will be illustrated through some numerical examples.

Convexity constraints and Jordan - Kinderlehrer - Otto gradient flow

Édouard Oudet*

Abstract

We discuss new convergent schemes well suited for the numerical resolution of problems of calculus of variations under convexity constraints. We illustrate the versatility and the efficiency of our approach on three types of problems : 3D denoising, the principal agent problem, and optimization within the class of convex bodies. Then, we discuss recent progresses on the simulation of Jordan-Kinderlehrer-Otto flow to approximate elliptic, non necessary local, partial differential equations.

*LJK, Université Joseph Fourier Grenoble

Globules rouges et vésicules: modélisation et simulations

Olivier Pantz*

Abstract: Le modèle de Helfrich décrivant le comportement des vésicules (des membranes bilidiques) peut Ã[a]tre obtenu comme limite asymptotique d'un modèle tridimensionnel. On se propose d'utiliser cette approximation afin d'introduire de nouvelles méthodes numériques de type lignes de niveau pour minimiser l'énergie de Helfrich.

Keyworlds: Modèle de Helfrich, lignes de niveau, minimisation d'energie.

*CMAP, Ecole Polytechnique, France, olivier.pantz@polytechnique.org,

Characterization of interior eigenvalues from multi-frequency time-harmonic scattering data

Armin Lechleiter*

Abstract: It is well-known that the interior eigenvalues of the Laplacian in a bounded domain share connections to scattering problems posed in the exterior of this domain. For instance, certain boundary integral equations for exterior scattering problems fail at interior resonances.

Similar connections also exist for inverse scattering problems: For instance, if zero is an eigenvalue of the far field operator at a fixed wave number, then the squared wave number is an interior eigenvalue. Despite it is in general wrong that interior eigenvalues correspond to zero being an eigenvalue of the far field operator, one can prove a pretty direct characterization of interior eigenvalues via the behaviour of the phases of the eigenvalues of the far field operator for positive wave numbers.

In this talk, we present such analytic characterizations for impenetrable and penetrable scatterers in the context of the scalar Helmholtz equation. In the case of a penetrable scattering object, the interior eigenvalues are so-called interior transmission eigenvalues. These analytic results can be extended to more complex scattering problems (e.g., anisotropic scatterers or electromagnetic scattering), and they can further be exploited numerically.

Our motivation to study this so-called inside-outside duality is on the one hand due to the recent interest in interior transmission eigenvalues and on the other due to an older paper by Eckmann and Pillet (1995).

The results given in the talk are joint work with Andreas Kirsch (KIT, Karlsruhe, Germany) and Stefan Peters (University of Bremen, Germany).

Keyworlds: Interior eigenvalues, scattering data, boundary integral equations.

*ZeTeM, Zentrum fur Technomathematik, Universitat Bremen, Germany, lechleiter@math.uni-bremen.de,

Elastic energy, area and perimeter of plane domains

Antoine Henrot*

Abstract: In this talk, we will investigate the links between the elastic energy (in the sense of Euler), the area and the perimeter of a convex domain in the plane. The aim being to plot the *Blaschke-Santalò* diagram involving these three quantities.
Keyworlds: elastic energy, area, perimeter, Blaschke-Santalò diagram

1 Content of the talk

This is a joint work with Chiara Bianchini from Florence and Takéo Takahashi from Nancy.

For a regular planar convex compact set Ω (a planar convex body) let us introduce the three geometric quantities: its area $A(\Omega)$, its perimeter $P(\Omega)$ and its elastic energy $E(\Omega) = \frac{1}{2}\int_{\partial\Omega} k^2\, ds$ where k is the curvature (and s the arc length). The elastic energy of a curve seems to have been introduced by L. Euler who studied the *elasticae* which are the curves, satisfying some boundary conditions, critical points of the elastic energy. This question has been widely studied and has many applications in geometry, kinematics (the ball-plate problem), numerical analysis (non linear splines), computer vision (reconstruction of occluded edges)... For a good overview and historical presentation, we refer e.g. to [3].

The aim of this talk is to study the links between $E(\Omega)$, $A(\Omega)$ and $P(\Omega)$. It can be done in investigating the set of points in $\mathbb{R}^3$ corresponding to the triple $(A(\Omega), E(\Omega), P(\Omega))$ (or some a-dimensional version in the plane corresponding to $(A(\Omega)/P(\Omega)^2, E(\Omega)P(\Omega))$):

$$\mathcal{E} := \left\{ (x,y) \in \mathbb{R}^2, x = \frac{4\pi A(\Omega)}{P(\Omega)^2}, y = \frac{E(\Omega)P(\Omega)}{2\pi^2},\ \Omega \text{ convex} \right\}. \tag{1}$$

This kind of diagram is often called a *Blaschke-Santaló diagram* since W. Blaschke in [2] introduced this kind of diagram where the three quantities in consideration were the volume, the surface area and the integral of the mean curvature for a three-dimensional convex body. Later on, L. Santaló in [4] proposed a systematic study of this kind of sets for planar convex body and geometric quantities like the area, the perimeter, the diameter, the minimum width, the inradius and the circumradius.

For that purpose, we will consider the minimization problem

$$\min_{\Omega\in\mathcal{A}} E(\Omega) + \mu A(\Omega), \tag{2}$$

where $\mu \geq 0$ and where $\mathcal{A}$ is the class of regular planar convex bodies Ω such that

$$P(\Omega) = P_0. \tag{3}$$

*IECL - Universit'e de Lorraine, antoine.henrot@univ-lorraine.fr,

Obviously the disk would like to minimize the first term, due to Cauchy-Schwarz inequality while it would like to maximize the second one by the isoperimetric inequality. Thus we can expect that the penalization parameter μ plays an important role and that the solution is close to the disk when μ is small and far (actually close to the segment) when μ is large. By solving this minimization problem, our objective is to describe precisely the lower boundary of the set $\mathcal{E}$ defined in (1).

We prove

Theorem 1.1 *For all $\mu \geq 0$, there exists $\Omega^* \in \mathcal{A}$ which minimizes $J_\mu(\Omega) = E(\Omega) + \mu A(\Omega)$. The domain Ω^* is (at least) C^2. More precisely, it is C^∞ on the strictly convex parts and the curvature is continuous at junctions with flat parts of the boundary. Moreover, there exists one solution which is centrally symmetric.*

We also discuss when the disk is or is not the solution of that problem. More precisely:

- we prove that the disk is the solution when $\mu \leq 1$,
- we prove that the disk cannot be the solution for $\mu > 3$

Numerically, we observe that it is the solution when $\mu \leq 3$.
We also discuss the presence of segments on the boundary of the optimal domain. We are able to prove that such segments exist for μ large enough ($\mu \geq 9.22$.

Finally we give some properties of the set $\mathcal{E}$ defined in (1). In particular we prove that this set in convex in the horizontal and the vertical direction.

2 Bibliography

References

[1] C. BIANCHINI, A. HENROT, T. TAKAHASHI, Elastic energy of a convex body, submitted

[2] W. BLASCHKE, *Eine Frage über Konvexe Körper*, Jahresber. Deutsch. Math. Ver., **25** (1916), 121-125.

[3] YU. L. SACHKOV, Maxwell strata in the Euler elastic problem, *J. of Dynamical and Control Systems*, **vol. 14**, no 2 (2008), 169-234.

[4] L. SANTALÓ, *Sobre los sistemas completos de desigualdades entre tres elementos de una figura convexa plana*, Math. Notae, **17** (1961), 82-104.

Minisymposia

2.1 Inverse problems in cardiac electrophysiology (IPCE)

Minisymposium organized by Nejib Zemzemi

Inverse Problem in Electrocardiography via the Factorization Method of Boundary Value Problems

Julien Bouyssier, Nejib Zemzemi, Jacques Henry,

CARMEN team, Inria Bordeaux Sud-Ouest
200 avenue de la vieille tour, 33405 Talence Cedex

Electrocardiographic Imaging (ECGI) is a new imaging technique that noninvasively images cardiac electrical activity on the heart surface. In ECGI, a multi-electrode vest records body-surface potential maps (BSPMs); then, using geometrical information from CT-scans and a mathematical algorithm, electrical potentials, electrograms and isochrones are reconstructed on the heart surface. The reconstruction of cardiac activity from BSPMs is an ill-posed inverse problem. In this work, we present an approach based on an invariant embedding method: the factorization method of boundary values problems [1, 2]. The idea is to embed the initial problem into a family of similar problems on subdomains bounded by a moving boundary from the torso skin to the epicardium surface. For the direct problem this method provides

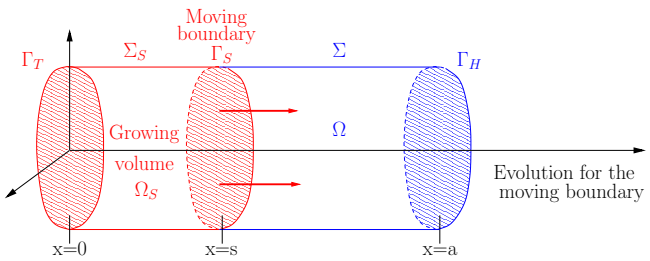

Figure 1: Illustration of the moving boundary. Γ_T the torso surface, Γ_H the heart surface, and Γ_S the moving surface.

an equivalent formulation with two Cauchy problems evolving on this moving boundary and which have to be solved successively in opposite directions. This method calculates Neumman-Dirichlet and Dirichlet-Neumann operators on the moving boundary using Riccati equations. Mathematical analysis allows to write an optimal estimation of the epicardial potential based on a quadratic criterion. The analysis of the inverse problem ill-posedness allows to compare different regularisation terms. For numerical simulations we first construct a synthetical data based on the ECG solver [3]. The electrical potential on the torso boundary is then extracted from the forward solution to be used as an input of the inverse problem. The method was first presented in [2] for a cylindrical domain. Here the numerical approximation of the method is thoroughly studied and the method is extended to 3D domains of arbitrary shapes. Numerical simulations in the case of spheres are presented.

References

[1] Jacques Henry and Angel Manuel Ramos , *La méthode de factorisation des problèmes aux limites*, book (in preparation), (2013)

[2] Fadhel Jday, *Complétion de données frontières : la méthode de plongement invariant*, PHD thesis, (2012)

[3] Nejib Zemzemi, *Étude théorique et numérique de l'activité électrique du coeur: Applications aux électrocardiogrammes*, PHD thesis, (2009)

A Nash-game approach to solve the Cauchy problem for elliptic equations

Moez Kallel* Abderrahmane Habbal†

Abstract: We consider the Cauchy problem for an elliptic operator, formulated as a Nash game. The over specified Cauchy data are split among two players : the first player solves the elliptic equation with the Dirichlet part of the Cauchy data prescribed over the accessible boundary, and a variable Neumann condition (which we call first player's strategy) prescribed over the inaccessible part of the boundary. The second player makes use correspondingly of the Neumann part of the Cauchy data, with a variable Dirichlet condition prescribed over the inaccessible part of the boundary. The first player then minimizes the gap related to the non used Neumann part of the Cauchy data, and so does the second player with a corresponding Dirichlet gap. The two costs are coupled through a difference term.
Keyworlds: elliptic Cauchy problem, data completion, Nash games

1 Introduction

We consider the following elliptic Cauchy problem :

$$\left\{\begin{array}{rcccc} \nabla.(k\nabla u) & = & 0 & \text{in} & \Omega \\ u & = & f & \text{on} & \Gamma_c \\ k\nabla u.\nu & = & \Phi & \text{on} & \Gamma_c \end{array}\right. \tag{1}$$

where Ω is a bounded open domain in $\mathbb{R}^d$ $(d = 2, 3)$ with a sufficiently smooth boundary $\partial\Omega$ composed of two connected disjoint components Γ_c and Γ_i. The parameters k, f and Φ are given functions, ν is the unit outward normal vector on the boundary. The Dirichlet data f and the Neumann data Φ are the so-called Cauchy data, which are known on the accessible part Γ_c of the boundary $\partial\Omega$ and the unknown field u is the Cauchy solution.

The solution of Cauchy problem does not always exist for any pair of data (f, Φ), and if such a solution exists, it does not always depend continuously on the data (Hadamard's ill-posedness, see [4]). The Cauchy data (f, Φ) are called compatible (or consistent) if the corresponding Cauchy problem (1) has a solution (it is then unique thanks to classical continuation arguments).

Our purpose is to introduce an original method to solve the Cauchy problem, based on a game theory approach.

2 A Nash game formulation of the Cauchy problem

We assume that the boundary $\partial\Omega$ and the data k, Φ and f are smooth enough. In this case, the Cauchy solution u, if it exists, belongs to the space $H^1(\Omega)$.

For given $\eta \in H^{-\frac{1}{2}}(\Gamma_i)$ and $\tau \in H^{\frac{1}{2}}(\Gamma_i)$, let us define $u_1(\eta)$ and $u_2(\tau)$ as the unique solutions in $H^1(\Omega)$ of the following elliptic boundary value problems :

$$(SP1)\left\{\begin{array}{rcccc} \nabla.(k\nabla u_1) & = & 0 & \text{in} & \Omega \\ u_1 & = & f & \text{on} & \Gamma_c \\ k\nabla u_1.\nu & = & \eta & \text{on} & \Gamma_i \end{array}\right. \qquad (SP2)\left\{\begin{array}{rcccc} \nabla.(k\nabla u_2) & = & 0 & \text{in} & \Omega \\ u_2 & = & \tau & \text{on} & \Gamma_i \\ k\nabla u_2.\nu & = & \Phi & \text{on} & \Gamma_c \end{array}\right. \tag{2}$$

*ENIT–LAMSIN, moez.kallel@ipeit.rnu.tn,
†J.A.Dieudonné, Université de Nice, habbal@polytech.unice.fr

The fields $u_1(\eta)$ and $u_2(\tau)$ are aiming at the fulfillment of a possibly antagonistic goals, namely minimizing the Neumann gap $\|k\nabla u_1.\nu - \Phi\|_{H^{-\frac{1}{2}}(\Gamma_c)}$ and the Dirichlet gap $\|u_2 - f\|_{H^{\frac{1}{2}}(\Gamma_c)}$. This antagonism is intimately related to Hadamard's ill-posedness character of the Cauchy problem, and rises as soon as one requires that u_1 and u_2 coincide, which is exactly what the coupling term $\|u_1 - u_2\|_{L^2(\Gamma_i)}$ is for. Thus, one may think of an iterative process which minimizes in a smart fashion the three terms, namely Neumann-Dirichlet-Coupling terms.

Let us define the following two costs : for any $\eta \in H^{-\frac{1}{2}}(\Gamma_i)$ and $\tau \in H^{\frac{1}{2}}(\Gamma_i)$,

$$J_1(\eta,\tau) = \frac{1}{2}\|k\nabla u_1.\nu - \Phi\|^2_{H^{-\frac{1}{2}}(\Gamma_c)} + \frac{\alpha}{2}\|k\nabla u_1.\nu - k\nabla u_2.\nu\|^2_{H^{-\frac{1}{2}}(\Gamma_i)}. \tag{3}$$

$$J_2(\eta,\tau) = \frac{1}{2}\|u_2 - f\|^2_{H^{\frac{1}{2}}(\Gamma_c)} + \frac{\alpha}{2}\|k\nabla u_1.\nu - k\nabla u_2.\nu\|^2_{H^{-\frac{1}{2}}(\Gamma_i)}. \tag{4}$$

where the fields $u_1(\eta)$ and $u_2(\tau)$ are the unique solutions to (SP1) and (SP2), respectively and α is a given positive parameter (e.g. $\alpha = 1$).

We shall say that there are two players, referred to as player 1 or Neumann-gap, and player 2 or Dirichlet-gap. Player 1 controls the strategy variable η, and player 2 controls the strategy variable τ. Each of the two players tries to minimize its own cost, namely J_1 for player 1, and J_2 for player 2. As classical, the fact that each player controls only his own strategy, while there is a strong dependance of each player's cost on the joint strategies (η,τ) justifies the use of the game theory framework (and terminology), a natural setting which may be used to formulate the negotiation between these two costs.

In order to be consistent with the initial formulation of the Cauchy problem, the relevant game theoretic framework to deal with is a static with complete information one. In this case, a commonly used solution concept (roughly speaking, in the game vocabulary, a rational and stable one) is the one of Nash Equilibria.

We prove that there always exists a unique Nash equilibrium, which turns out to be the reconstructed data when the Cauchy problem has a solution. We also prove that the completion Nash game has a stable solution with respect to noisy data. Some numerical 2D and 3D experiments are performed to illustrate the efficiency and stability of our algorithm. We made a comparison with the method introduced in [1].

References

[1] R. Aboulaïch, A. Ben Abda, M. Kallel (2008) Missing boundary data reconstruction via an approximate optimal control, *Inverse Problems and Imaging*, 2, pp. 411-426.

[2] A. Habbal, M. Kallel (2012) Data completion problems solved as Nash games, *J. Phys.: Conf. Ser.*, 386, 012004.

[3] A. Habbal, M. Kallel (2013) Neumann–Dirichlet Nash strategies for the solution of elliptic Cauchy problems, *SIAM J. Control Optim.*, 51, pp. 4066-4083.

[4] J. Hadamard (1953) *Lectures on Cauchy's Problem in Linear Partial Differential Equation*, Dover, New york USA

Parameter identification in the cardiac electro-mechanical problems

Cesare Corrado* J-F. Gerbeau† P. Moireau‡

In the recent years, data assimilation techniques have been proposed to estimate the state and the parameters of patient-specific mechanical models of the myocardium. In the present work, we consider a coupled electromechanical model in order to take advantage of different sources of clinical exams (typically MRI and ECG).

The mathematical structure of the electrocardiology equations (nonlinear reaction-diffusion problems) makes it difficult to extend the techniques used in mechanics, namely a nudging filter for the state and a Reduced Order Unscented Kalman filters (RO-UKF) for the parameters only. To address this challenging task, we propose to project the electrical state on a basis obtained by Proper Orthogonal Decomposition (POD) and to only filter the first components with the RO-UKF algorithm. This approach allows in particular to estimate parameters when error on state initial condition is considerable, as in the case of Fig. 1. This is the first contribution of this work.

The second contribution is to address the state-parameter estimation on a coupled system including the mechanics of the myocardium, the bidomain equations for the heart electrophysiology and an ECG simulator. Of particular interest is the information on electrophysiology provided by mechanical observations, that would not have been detectable by the ECG only. We show in particular that for some electrical parameters the mechanical response is longer in time than the electrical response observed on the ECG. Of particular interest is the case when uncertainty on parameters is considerable as in the case of Fig. 2. The proposed approach paves the way for the personalization of a complete electromechanical heart model.

Keyworlds: Electro-mechanics, electrocardiogram, MRI, RO-UKF, POD

References

[1] M. Boulakia, M.A. Fernández, J.-F. Gerbeau, N. Zemzemi *Mathematical modelling of electrocardiograms: a numerical study.* In: *Ann. Biomed. Eng*, 38(3):1071-1097, 2010.

[2] P. Moireau, D. Chapelle *Reduced-order Unscented Kalman Filtering with application to parameter identification in large-dimensional systems* SIAM *ESAIM: Control, Optimisation and Calculus of Variations*, 17:380-405, 2011.

[3] Chapelle, Fernández, Gerbeau, Moireau, Sainte-Marie Zemzemi *Numerical Simulation of the Electro-Mechanical Activity of the Heart*, volume 331 of *FIMH 2009*, LNCS 5528, pp. 357-365, 2009 Longman, 1995.

[4] P. Moireau, D. Chapelle, P. Le Tallec *Joint state and parameter estimation for distributed mechanical systems*, In: *Computer Methods in Applied Mechanics and Engineering*, 197:659-677, 2008

[5] S. Julier, J. Uhlmann, H.F. Durrant-Whyte *A new method for the nonlinear transformation of means and covariances in filters and estimators* IEEE *Transactions on Automatic Control*, 45(3):477–482, 2000.

*INRIA-Bordeaux Sud-Ouest, cesare.corrado@linria.fr,
†INRIA-Rocquencourt, jean-frederic.gerbeau@inria.fr
‡INRIA-Saclay, philippe.moireau@inria.fr

Mathematical Modelling of the electrical wave in the heart from ion-channels to the body surface: Direct and inverse problems

Nejib Zemzemi

CARMEN team, Inria Bordeaux Sud-Ouest
200 avenue de la vieille tour, 33405 Talence Cedex

We developed a 3D computational model of the electrical wave in the heart. This multi-scale mathematical model is heavy in terms of computational cost. Different numerical schemes are used in order to reduce the computational cost: We use domain decomposition methods combined with different time decoupling schemes [1]. We present a 3D anatomically based model of the whole human with a biophysically detailed representation of human membrane kinetics, realistic cardiac geometry, fibre orientation and heterogeneity in electrophysiological properties of cardiac ventricles. The 3D multi-scale model is used to simulate different heart conditions in order to test different method introduced to solve the inverse problem in electrocardiography.

The mostly used mathematical formulation of the inverse problem in electrocardiography is based on a least method using a transfer matrix that maps the electrical potential on the heart to the body surface potential (BSP). Lots of works have been concentrating on the regularization term without thinking of reformulating the problem itself. We propose in this study to solve the inverse problem based on two methods: The first is based on the classical Steklov-Poincaré approach [3, 2] for the Cauchy problem and the second is based on a domain decomposition technique on a fictive mirror-like boundary conditions. We conduct BSP simulations to produce synthetic data and use it to evaluate the accuracy of the inverse problem solution.

2.2 Shape and Topological Optimization (TO)

Minisymposium organized by Mohamed Masmoudi

Methods and Strategies for imposing a Maximum Feature Size in Shape and Topology Optimization

G. Michailidis[1*], G. Allaire[1], F. Jouve[3]

[1]Ecole Polytechnique, Centre de Mathématiques Appliquées (CMAP)
91128 Palaiseau, France
michailidis@cmap.polytechnique.fr, allaire@cmap.polytechnique.fr

[2]Laboratoire J.L. Lions (UMR 7598), University Paris Diderot, Paris,France
Bâtiment des Grands Moulins, 75205 PARIS CEDEX 13
jouve@math.jussieu.fr

ABSTRACT

Shape and topology optimization methods usually result in optimized structures that violate industrial fabrication constraints related to a notion of thickness. For example, in casting, too thick, thin, or closely spaced features should be avoided. Post-treating the optimized shape is usually a non-trivial task and can lead to a complete loss of its optimal characteristics. Therefore, it seems preferable to integrate thickness constraints in the optimization algorithm. Beyond finding a satisfying formulation of thickness constraints for continuous structures, efficient strategies for their handling need also to be applied. We discuss several such formulations and strategies for imposing a maximum feature size and show examples in 2d and 3d.

References

[1] G. Allaire, F. Jouve, and G. Michailidis. Thickness constraints in structural optimization via a level-set method. (In preparation.)

[2] S. Chen, M.Y. Wang, and A.Q. Liu. Shape feature control in structural topology optimization. Computer-Aided Design, 40(9):951-962, 2008.

[3] JK Guest, JH Prevost, and T. Belytschko. Achieving minimum length scale in topology optimization using nodal design variables and projection functions. International Journal for Numerical Methods in Engineering, 61(2):238-254, 2004.

[4] J.K. Guest. Imposing maximum length scale in topology optimization. Structural and Multidisciplinary Optimization, 37(5):463-473, 2009.

Geometric inverse problem for time-dependent PDE systems

Maatoug Hassine*

Abstract: In this talk, we consider a geometric inverse problem constrained by time-dependent partial differential equations. We propose an alternative approach based on the Kohn-Vogelius formulation and the topological gradient method. The Kohn-Vogelius formulation rephrase the geometrical inverse problem into a shape optimization one. The obtained shape optimization problem is treated using the topological gradient method.

In the first pat of the talk we derive a topological sensitivity analysis for the considered time-dependent partial differential equations. The obtained results are valid for large class of cost functions.

In the second part of the talk, we propose a one-shot reconstruction algorithm. The efficiency and accuracy of the proposed algorithm are illustrated by some numerical results.

Keyworlds: Inverse problem, topological gradient, topological sensitivity, reconstruction algorithm.

*FSM–Monastir University, maatoug.hassine@enit.rnu.tn,

Optimal design problems in a dynamical context: an overview

Arnaud Munch*

Abstract: We review here the problem which consists to minimize the norm of HUM controls for the wave and heat-like equations with respect to their support. The problem reduces to an optimal design problem for a dynamical equation defined on a bounded cylinder. As is well-known, this type of problem may have no solution in the class of characteristic functions. First, we show how, by the use of convex analysis, one may associate a well-posed reformulation in the class of density functions. Then, we present some numerical experiments that allow to separate qualitatively the heat situation from the wave one. We also discuss some recent contributions where the support evolves in time, the minimization over weighted Carleman type norms and the related stabilization issue.

Keyworlds: Hum control, optimal design problems, convex analysis.

*Université Blaise Pascal (Clermont Ferrand), France, arnaud.munch@math.univ-bpclermont.fr,

Nonstandard topological optimization methods

Mohamed Masmoudi*

Abstract: Mathematical analysis is a powerful tool to solve applied mathematics problems. Even topological optimization, which can be seen as a part of discrete mathematics, is using intensively variational methods.

In this presentation we will show two "analysis free" industrial topological optimization problem.

The goal of the first application is to find the optimal mask of a highly accurate resistor. This problem has been solved using number representation techniques.

The second application deals with optimal design of the feeding system (repartitor) of a spatial antenna. We used algebraic approaches to solve this problem.

In both cases, the classical topological optimization tools are likely to fail in solving these two real life problems.

Keyworlds: Topological optimization, variational methods, number representation techniques.

*Institut Mathématiques de Toulouse, France, masmoudi@math.univ-toulouse.fr,

2.3 Inverse problems and Carleman estimates (CE1)

Minisymposium organized by Mourad Bellassoued

lnverse spectral conductivity problem in a periodic waveguide

E. Soccorsi (Marseille)

Abstract

Given an unbounded cylindrical domain $\Omega = \omega \times \mathbb{R}$, where ω is a $\mathcal{C}^1$ connected bounded open subset of $\mathbb{R}^2$, we consider the operator $A = -\mathrm{div}(a\nabla\cdot)+V$, acting in $L^2(\Omega)$, with Dirichlet boundary conditions. Here $V \in L^\infty(\Omega)$ and $a \in W^{2,\infty}(\Omega) \cap \mathcal{C}^1(\overline{\Omega})$ are 2π-periodic functions with respect to the infinite variable of Ω. The operator A admits a fiber decomposition A_θ, $\theta \in [0, 2\pi)$, and its spectrum is absolutely continuous. We prove that a and V may be uniquely determined from the partial knowledge of the spectral data of any A_θ, for $[0, 2\pi)$.

This is joint work with O. Kavian (Versailles) and Y. Kian (Marseille).

STABILITY ESTIMATE IN DETERMINATION OF A COEFFICIENT IN TRANSMISSION WAVE EQUATION BY BOUNDARY OBSERVATION

BOCHRA RIAHI

ABSTRACT

We consider a transmission wave equation in two embedded domains in $\mathbb{R}^2$, we study the global stability in determination of a discontinuous coefficient which is variable on each subdomain and their traces are constant at the interface from data of the solution in a subboundary over a time interval.
Providing regular initial data, we prove an hölder stability estimate in the inverse problem with a single measurement. Moreover the exponent in the stability estimate depends on the regularity of initial data.
The key is the global Carleman estimate.

Inverse problems associated with linear and non-linear parabolic systems: two different approaches

M. Cristofol
(michel.cristofol@univ-amu.fr)

I2M, Ecole Centrale, Universite Aix-Marseille.

Abstract. In this talk I am interested to give an overview of recent results concerning the reconstruction of one or several coefficients associated to systems of linear and non linear parabolic equations.
The main goal is to obtain these results minimizing the observations. The first results (see [1], [2], [3] and [4]), involve Carleman inequalities and give a Lipschitz stability results but a measurement of the components of the system on all the domain is necessary. The last result (see [5]) avoids this constraint and concerns an uniqueness result for a strong non linear parabolic system (Lotka Volterra type).

References

[1] M Cristofol, P Gaitan, and H Ramoul. Inverse problems for a two by two reaction-diffusion system using a Carleman estimate with one observation. *Inverse Problems*, 22:1561–1573, 2006.

[2] M Cristofol, P Gaitan, H Ramoul, and M Yamamoto. Identification of two independant coefficients with one observation for a nonlinear parabolic system. *Applicable Analysis*, 91, Issue 11, 2073-2081, 2012

[3] M Cristofol, P Gaitan, K Niinimaki, and O Poisson. Inverse problem for a coupled parabolic system with discontinuous conductivities. *Inverse problem and imaging*, Volume 7, Issue 1, 159-182, 2013

[4] A Benabdallah, M Cristofol, L de Teresa and P Gaitan. Controllability to trajectories for some parabolic systems of three and two equations by one control force. *Mathematical control and related fields*, Volume 4 , Issue 1, 17-44, 2014

[5] M Cristofol and L Roques. The inverse problem of determining several coefficients in a nonlinear Lotka-Volterra system, *Inverse Problems*, 28 , 075007, 12 pp, 2012.

A data completion algorithm using boundary integral equations

Yosra Boukari[‡], Houssem Haddar[⋆]

[‡]CPT, University of Aix-Marseille.

[⋆]Defi, CMAP, Ecole Polytechnique.

Email: boukari@cmap.polytechnique.fr

Email: haddar@cmapx.polytechnique.fr

Abstract

The aim of the present work is to solve the Cauchy problem for the Helmholtz and the Laplace equations using a non-iterative method based on the surface representation of the solution. More specifically, we would like to determine the Cauchy data associated with a solution of the Helmholtz or the Laplace equation in a part of the boundary of a bounded domain from the knowledge of the Cauchy data on the complementary part. We consider the setting of a lipschitz domain that contains an inclusion, which means that the boundary of this domain can be split in two parts: an exterior boundary and an interior boundary that we denote by Γ_e and Γ_i respectively. Hence, the inverse problem under concern consists in reconstructing the interior Cauchy data on Γ_i by knowing the Cauchy data on the exterior boundary Γ_e. This problem has been shown to be an ill-posed problem since 1953.

We propose a new method to solve this inverse problem. Using the boundary integral equation representation along with the trace of the solution and its normal derivative on Γ_e and Γ_i, we derive a linear integral equation system that combines the known and unknown Cauchy data. The ill posedness of the problem shows up in the compactness of the component of the operator that has to be inverted. We prove the injectivity and the densness of the range of this operator in appropriate Sobolev spaces. Moreover, we show that our method naturally handles the case of noisy data. In fact, in our formulation the available Cauchy data are multiplied by an operator that has the same range as the operator to be inverted, which makes possible the use of classical regularization techniques for noisy data, such as the Thikonov regularization. Some numerical results are provided that show the efficiency of the method

for different shapes of the domain, different values of the wave number and also for noisy data. Note in addition that the implemented algorithm has the advantage to be fast as it does not rely on an iterative scheme.

Keys words: Inverse Problem, Helmholtz equation, Laplace equation, Data completion, Integral equations.

2.4 Inverse problems and Carleman estimates (CE2)

Minisymposium organized by Mourad Bellassoued

DETERMINATION OF A TIME-DEPENDENT COEFFICIENT IN A QUANTUM CYLINDRICAL WAVE GUIDE

Abstract. Let $\Omega = \omega \times \mathbb{R}$ be a cylindrical open subset of $\mathbb{R}^3$, with ω a bounded domain of $\mathbb{R}^2$. These domains are also called cylindrical wave guide. We study the inverse problem which consists in determining a scalar time-dependent potential $q(t, x)$, appearing in a boundary value problem associated to the Schrödinger equation $-i\partial_t u - \Delta u + qu = 0$ on $Q = (0, T) \times \Omega$, from boundary measurement on Q. The observation is given by an operator closed to the so called Dirichlet-Neumann map. We obtain uniqueness as well as stability for this inverse problem.

New Kind of Observations in an Inverse Parabolic Problem

Kaddouri Isma
University of Sciences and technology Houari Boumediene,
Algiers, Algerie and Aix-Marseille University
Marseille, France,
email: isma.kaddouri@gmail.com
Joint work with M. Cristofol, G. Nadin and L. Roques

Abstract

In this talk, I analyze the inverse problem of determining the reaction term $f(x,u)$ in reaction-diffusion equations of the form $\partial_t u - D\partial_{xx}u = f(x,u)$, where f is assumed to be periodic with respect to $x \in \mathbb{R}$. Starting from a family of exponentially decaying initial conditions $u_{0,\lambda}$, I will show that the solutions u_λ of this equation propagate with constant asymptotic spreading speeds w_λ. The main result shows that the linearization of f around the steady state 0, $\partial_u f(x,0)$, is uniquely determined (up to a symmetry) among a subset of piecewise linear functions, by the observation of the asymptotic spreading speeds w_λ.

Boundary Voltage Perturbations Resulting from the Presence of Thin Interfaces

Abdessatar Khelifi * Habib Zribi †

Abstract

In this talk, we derive high-order asymptotic formulae for two- or three-dimensional steady state voltage potentials associated with thin conductivity imperfections having no uniform thickness. These formulae recover highly conducting inclusions and those with interfacial resistance. Our calculations are rigorous and based on layer potential techniques.

Keywords: Small surface perturbations, full-asymptotic expansions, generalized polarization tensors, boundary integral method

1 Problem formulation

Consider a homogeneous conducting object occupying a bounded domain $\Omega \subset \mathbb{R}^d$ $(d = 2, 3)$, with a connected $\mathcal{C}^2$-surface $\partial\Omega$. We assume, for the sake of simplicity, that its conductivity is equal to 1. Let D be a bounded $\mathcal{C}^{2,\eta}$ domain in Ω for some $\eta > 0$, and of conductivity equal to some positive constant $k \neq 1$. We assume that $\text{dist}(D, \partial\Omega) \geq C > 0$. The voltage potential in the presence of the inclusion D is denoted by u. It is the solution to

$$\begin{cases} \nabla\cdot\Big(1 + (k-1)\chi_D\Big)\nabla u = 0 \quad \text{in } \Omega, \\ \dfrac{\partial u}{\partial \nu}\big|_{\partial\Omega} = g, \displaystyle\int_{\partial\Omega} u = 0, \end{cases} \tag{1}$$

where χ_D is the indicator function of D. Here ν denotes the unit outward normal to the domain Ω and g represents the applied boundary current; it belongs to the set $L^2_0(\partial\Omega) = \{f \in L^2(\partial\Omega), \int_{\partial\Omega} f = 0\}$.

Let D_ϵ be an ϵ-perturbation of D, *i.e.* ∂D_ϵ be given by

$$\partial D_\epsilon := \{\tilde{x} = x + \epsilon h(x)\nu(x) := \Psi_\epsilon(x),\ x \in \partial D\}, \tag{2}$$

where ν is the unit outword normal to the domain D and the function $h \in \mathcal{C}^2(\partial D)$. We assume that $h(x) \geq C > 0$ for all $x \in \partial D$.
Let u_ϵ be the solution to

$$\begin{cases} \nabla\cdot\Big(1 + (k-1)\chi_{D_\epsilon}\Big)\nabla u_\epsilon = 0 \quad \text{in } \Omega, \\ \dfrac{\partial u_\epsilon}{\partial \nu}\big|_{\partial\Omega} = g, \displaystyle\int_{\partial\Omega} u_\epsilon = 0. \end{cases} \tag{3}$$

The main achievement of this work is to adopt the FE method to derive formal high-order terms in the asymptotic expansion of $(u_\epsilon - u)|_{\partial\Omega}$ as $\epsilon \to 0$.

2 Formal derivations: field expansion (FE) method

In order to derive a formal asymptotic expansion for u_ϵ to order an integer N, we apply the FE method, see [5]. Firstly, we expand u_ϵ in powers of ϵ, *i.e.*

$$u_\epsilon(x) = u_0(x) + \epsilon u_1(x) + \epsilon^2 u_2(x) + \cdots, \quad x \in \Omega,$$

*Département de Mathématiques, Faculté des Sciences de Bizerte, Tunisia (abdessatar.khelifi@fsb.rnu.tn)

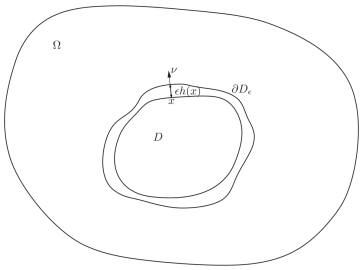

Figure 1: Main domain and thin inclusion

where u_n is well defined in $\Omega\backslash\partial D$ and satisfies

$$\Delta u_n = 0 \quad \text{in } \Omega\backslash\overline{D}, \quad \Delta u_n = 0 \quad \text{in } D, \quad \frac{\partial u_n}{\partial \nu} = g\delta_{0n} \quad \text{on } \partial\Omega, \tag{4}$$

for $n = 0, \cdots, N$. Here δ_{0n} is the Kronecker symbol. We formally obtain the following theorem.

Theorem 2.1 *The following asymptotic formula formally holds*

$$u_\epsilon(x) = u(x) + \sum_{n=1}^{N} \epsilon^n u_n(x) + O(\epsilon^{N+1}), \quad x \in \partial\Omega, \tag{5}$$

where the remainder $O(\alpha^{N+1})$ depends on N, Ω, the $\mathcal{C}^2$-norm of X, the $\mathcal{C}^1$-norm of ϱ, and $dist(D, \partial\Omega)$, u_1 is the unique solution os some PDE'equation.

2.1 Relationship between boundary measurements and h

For $f \in L^2_0(\partial\Omega)$, let v be the solution of

$$\begin{cases} \nabla\Big(\big(1 + (k-1)\chi(D)\big)\nabla v)\Big) = 0 & \text{in } \Omega, \\ \frac{\partial v}{\partial \nu}\Big|_{\partial\Omega} = f, \qquad \int_{\partial\Omega} v = 0. \end{cases}$$

It then follows from (5) that

$$\int_{\partial\Omega} f(u_\epsilon - u)d\sigma = \epsilon \int_{\partial\Omega} f u_1 d\sigma + O(\epsilon^2) = \epsilon \int_{\partial\Omega} (f u_1 - v\frac{\partial u_1}{\partial \nu})d\sigma + O(\epsilon^2).$$

Finally, we find the following relationship between boundary measurements and the shape deformation h:

$$\int_{\partial\Omega} f(u_\epsilon - u)d\sigma(x) = \epsilon(1-k)\int_{\partial D} h\ \Big[k\frac{\partial u}{\partial \nu}\Big|_- \frac{\partial v}{\partial \nu}\Big|_- + \frac{\partial u}{\partial T}\cdot\frac{\partial v}{\partial T}\Big]d\sigma(x) + O(\epsilon^2), \tag{6}$$

where $\dfrac{\partial}{\partial T} = \dfrac{\partial}{\partial T_\varphi}T_\varphi + \dfrac{\partial}{\partial T_\theta}T_\theta$.

The formula (6) can play a key role in developing effective algorithms to determine certain properties of the shape of an inhomogeneity from measurements on $\partial\Omega$.

3 Layer potential techniques method

Let B be a bounded Lipschitz domain in $\mathbb{R}^3$. Let $\Gamma(x)$ be the fundamental solution of the Laplacian Δ: $\Gamma(x) = -\frac{1}{4\pi|x|}$. The single and double layer potentials of the density function ϕ on ∂B are defined by

$$\mathcal{S}_B\phi(x) = \int_{\partial B} \Gamma(x-y)\phi(y)d\sigma(y), \quad x \in \mathbb{R}^3, \tag{7}$$

The following formulae give the jump relations obeyed by the double layer potential and by the normal derivative of the single layer potential on general Lipschitz domains:

$$\frac{\partial(\mathcal{S}_B\phi)}{\partial\nu}\big|_{\pm}(x) = \big(\pm\frac{1}{2}I + (\mathcal{K}_B)^*\big)\phi(x) \quad \text{a.e. } x \in \partial B, \tag{9}$$

$$(\mathcal{D}_B\phi)\big|_{\pm}(x) = \big(\mp\frac{1}{2}I + \mathcal{K}_B\big)\phi(x) \quad \text{a.e. } x \in \partial B, \tag{10}$$

for $\phi \in L^2(\partial B)$, where $\mathcal{K}_B$ is the operator defined by

$$\mathcal{K}_B\phi(x) = \text{p.v.}\frac{1}{4\pi}\int_{\partial B}\frac{< y-x, \nu(y) >}{|x-y|^3}\phi(y)d\sigma(y),$$

and $\mathcal{K}_B^*$ is the L^2-adjoint of $\mathcal{K}_B$, that is,

$$\mathcal{K}_B^*\phi(x) = \text{p.v.}\frac{1}{4\pi}\int_{\partial B}\frac{< x-y, \nu(x) >}{|x-y|^3}\phi(y)d\sigma(y). \tag{11}$$

The following lemma is of importance to us. For proof, see [6].

Lemma 3.1 *The operator $\lambda I - \mathcal{K}_B^*$ is invertible on $L_0^2(\partial B)$ if $|\lambda| \geq \frac{1}{2}$, and for $\lambda \in (-\infty, -\frac{1}{2}]\cup(\frac{1}{2}, +\infty)$, $\lambda I - \mathcal{K}_B^*$ is invertible on $L^2(\partial B)$.*

3.1 Asymptotic expansion of the layer potential $\mathcal{K}_{D_\epsilon}^*$

Let $\mathcal{K}_{D_\epsilon}^*$ be the integral operator defined for any density $\tilde{\psi} \in L^2(\partial D_\epsilon)$ by

$$\mathcal{K}_{D_\epsilon}^*\tilde{\psi}(\tilde{x}) = \frac{1}{4\pi}\int_{\partial D_\epsilon}\frac{< \tilde{x}-\tilde{y}, \tilde{\nu}(\tilde{x}) >}{|\tilde{x}-\tilde{y}|^3}\tilde{\psi}(\tilde{y})d\sigma_\epsilon(\tilde{y}). \tag{12}$$

For $(\varphi,\theta),(\alpha,\beta) \in \vartheta$. Set

$$x = X(\varphi,\theta), \qquad \tilde{x} = \tilde{X}(\varphi,\theta) = x + \epsilon\varrho(\varphi,\theta)\nu(x),$$

$$y = X(\alpha,\beta), \qquad \tilde{y} = \tilde{X}(\alpha,\beta) = y + \epsilon\varrho(\alpha,\beta)\nu(y).$$

Introduce a sequence of integral operators $(\mathcal{K}_D^{(n)})_{n\in\mathbb{N}}$, defined for any $\psi \in L^2(\partial D)$ by

$$\mathcal{K}_D^{(n)}\psi(x) := \frac{1}{4\pi}\int_{\partial D}\Bbbk_n(x,y)\psi(y)d\sigma(y), \quad \text{for } n \geq 0.$$

In particular $\mathcal{K}_D^{(0)} = \mathcal{K}_D^*$. Let Ψ_ϵ be the diffeomorphism from ∂D onto ∂D_ϵ given by $\Psi_\epsilon(x) = x + \epsilon h(\varphi,\theta)\nu(x)$, where $x = X(\varphi,\theta)$. The following theorem holds.

Theorem 3.1 *Let $N \in \mathbb{N}$. There exists C depending only on N, $\|X\|_{\mathcal{C}^2}$ and $\|h\|_{\mathcal{C}^1}$, such that for any $\tilde{\phi} \in L^2(\partial D_\epsilon)$,*

$$\Big\|\mathcal{K}_{D_\epsilon}[\tilde{\phi}]\circ\Psi_\epsilon - \mathcal{K}_D^*(\phi) - \sum_{n=1}^{N}\epsilon^n\mathcal{K}_D^{(n)}(\phi)\Big\|_{L^2(\partial D)} \leq C\epsilon^{N+1}\|\phi\|_{L^2(\partial D)},$$

where $\phi := \tilde{\phi}\circ\Psi_\epsilon$, $\mathcal{K}_D^*$ is defined in (11), and $\mathcal{K}_D^{(1)}$ is given by:

$$\begin{aligned}\mathcal{K}_D^{(1)}\phi(x) =& 2h(x)\hbar(x)\mathcal{K}_D^*\phi(x) - 2\mathcal{K}_D^*(h\hbar\phi)(x) + \frac{\partial(\mathcal{D}_D(h\phi))}{\partial\nu}(x)\\ &- \frac{1}{\sqrt{det(\mathcal{G})}}\Big(\nabla_{\varphi,\theta}\cdot\Big(h\sqrt{det(\mathcal{G})}\mathcal{G}^{-1}\nabla_{\varphi,\theta}\mathcal{S}_D\phi\Big)\Big)(x).\end{aligned} \tag{13}$$

Define

$$\phi^{(0)} = (\lambda I - \mathcal{K}_D^*)^{-1}G_0 = (\lambda I - \mathcal{K}_D^*)^{-1}\Big(\frac{\partial H_\epsilon}{\partial\nu}\big|_{\partial D}\Big), \tag{14}$$

and for $1 \leq n \leq N$,

$$\phi^{(n)} = (\lambda I - \mathcal{K}_D^*)^{-1}\Big(G_n + \sum_{0}^{n-1}\mathcal{K}_D^{(n-p)}\phi^{(p)}\Big). \tag{15}$$

Lemma 3.2 *Let $N \in \mathbb{N}$. There exists C depending only on N, the $\mathcal{C}^2$-norm of X, and the $\mathcal{C}^1$-norm of h such that*

$$||\phi_\epsilon - \sum_{n=0}^{N} \epsilon^n \phi^{(n)}||_{L^2(\partial D)} \leq C\epsilon^{N+1},$$

where $\phi^{(n)}$ are defined by the recursive relation (15).

If we define the operator $\mathcal{E}$ on $L_0^2(\partial\Omega)$ by

$$\mathcal{E}(v)(x) := \mathcal{N}_D(\lambda I - \mathcal{K}_D^*)^{-1}\Big(\frac{\partial}{\partial\nu}(\mathcal{D}_\Omega v)\big|_{\partial D}\Big)(x), \quad x \in \partial\Omega,$$

then it follows that

$$(I + \mathcal{E})(u_\epsilon - u)(x) = -\sum_{n=1}^{N} \epsilon^n v_n(x) + O(\epsilon^{N+1}), \quad x \in \partial\Omega, \tag{16}$$

where, for $n \in \mathbb{N}$ and for $x \in \partial\Omega$,

$$v_n(x) := \sum_{i+j+k=n} \int_{\partial D} \Big(\sum_{|\alpha|=i} \frac{1}{\alpha!}(h(y)\nu(y))^\alpha \partial_y^\alpha N(x,y)\Big)\sigma^{(j)}(y)\phi^{(k)}(y)d\sigma(y). \tag{17}$$

We need the following lemma, see [3] for a proof.

Lemma 3.3 *The operator $I + \mathcal{E}$ is invertible on $L_0^2(\partial\Omega)$.*

Observe that

$$(u_\epsilon - u)|_{\partial\Omega} = O(\epsilon),$$

and hence,

$$H_\epsilon(x) - H(x) = O(\epsilon).$$

Thus if we define G_n^1, $n \in \mathbb{N}$, for H_ϵ replaced with H, and define $\phi_1^{(n)}$ and v_n^1 by (14), (15), and (17), then $v_n - v_n^1 = O(\epsilon)$. Therefore we get

$$u_\epsilon(x) - u(x) = -\epsilon(I + \mathcal{E})^{-1}(v_1^1)(x) + O(\epsilon^2), \quad x \in \partial\Omega. \tag{18}$$

Repeat the same procedure with $H - \epsilon\mathcal{D}_\Omega(I + \mathcal{E})^{-1}(v_n^1)$ instead of H to get v_n^2. Then $v_n - v_n^2 = O(\epsilon^2)$ and hence

$$u_\epsilon(x) - u(x) = -\sum_{n=1}^{2} \epsilon^n (I + \mathcal{E})^{-1}(v_n^2)(x) + O(\epsilon^3), \quad x \in \partial\Omega.$$

Repeating the same procedure until we get v_n^N, and we obtain the following theorem.

Theorem 3.2 *Let v_n^N, $n = 1, \ldots, N$, be the functions obtained by the above procedure. Then the following formula holds uniformly for $x \in \partial\Omega$:*

$$u_\epsilon(x) - u(x) = -\sum_{n=1}^{N} \epsilon^n (I + \mathcal{E})^{-1}(v_n^N)(x) + O(\epsilon^{N+1}).$$

The remainder $O(\epsilon^{N+1})$ depends only on N, Ω, the $\mathcal{C}^2$-norm of X, the $\mathcal{C}^1$-norm of h, and dist$(D, \partial\Omega)$.

4 Generalized polarization tensors (GPTs)

Definition 4.1 *Let D a Lipschitz bounded domain in $\mathbb{R}^3$ and the conductivity of D be k, $0 < k \neq 1 < +\infty$. For two multi-index α and β, we define the generalized polarization tensor $M_{\alpha\beta}$ by*

$$M_{\alpha\beta}(k, D) := \int_{\partial D} y^\beta \phi_\alpha(y) d\sigma(y), \tag{19}$$

where ϕ_α is given by

$$\phi_\alpha(y) := (\lambda I - \mathcal{K}_D^*)^{-1}\Big(\nu_x \cdot \nabla x^\alpha\Big)(y), \quad y \in \partial D. \tag{20}$$

The following theorem concerning perturbations of the GPTs can be done in exactly the same manner as in two dimensions.

Theorem 4.1 *Suppose that a_α and b_β are constants such that $H = \sum_\alpha a_\alpha x^\alpha$ and $F = \sum_\beta a_\beta x^\beta$ are harmonic polynomials. Then*

$$\sum_{\alpha,\beta} a_\alpha b_\beta M_{\alpha\beta}(k, D_\epsilon) - \sum_{\alpha,\beta} a_\alpha b_\beta M_{\alpha\beta}(k, D) = \epsilon(k-1) \int_{\partial D} h(y) \left[\frac{\partial v}{\partial \nu}\Big|_- \frac{\partial w}{\partial \nu}\Big|_- + \frac{1}{k} \frac{\partial w}{\partial T}\Big|_- \cdot \frac{\partial v}{\partial T}\Big|_- \right] (y) d\sigma(y)$$

$$+ O(\epsilon^2),$$

where v and w satisfy suitable transmission problems.

According to [4] and [2], the PT associated with an unknown inclusion can be detected from boundary measurements. Following once again [4], given an arbitrary shape, one can find an equivalent ellipsoid with the same PT. Therefore, recovering more shape details than the equivalent ellipsoid using a finite number of GPTs is an ambitious question.

References

[1] H. Ammari and H. Kang, *High-order terms in the asymptotic expansions of the steady-state voltage potentials in the presence of conductivity inhomogeneities of small diameter,* SIAM J. Math. Anal., 34 (2003), 1152–1166.

[2] H. Ammari, H. Kang, E. Kim, and M. Lim, Reconstruction of closely spaced small inclusions, SIAM J. Numer. Anal., 42 (2005), 24082428.

[3] H. Ammari, H. Kang, M. Lim, and H. Zribi, *Conductivity interface problems. Part I: small perturbations of an interface,* Trans. Amer. Math. Soc., 362 (2010), 2435–2449.

[4] M. Brühl, M. Hanke, and M.S. Vogelius, A direct impedance tomography algorithm for locating small inhomogeneities, Numer. Math., 93 (2003), 635–654.

[5] R.R. Coifman, M. Goldberg, T. Hrycak, M. Israeli, and V. Rokhlin, An improved operator expantion algorithm for direct and inverse scattering computations, Waves Random Media 9 (1999), 441-457.

[6] G.B. Folland, *Introduction to partial differential equations*, Princeton University Press, Princeton, New Jersey, 1976.

[7] E. Beretta, E. Francini, and M.S. Vogelius, Asymptotic formulas for steady state voltage potentials in the presence of thin inhomogeneities. A rigorous error analysis, J. Math. Pures Appl., 82 (2003), 1277–1301.

[8] A. Khelifi, and H. Zribi, *Asymptotic Expansions for the Voltage Potentials with Twoand Three-Dimensional Thin Interfaces*. Math. Methods. Appl. Sci., 34 (2011), 2274–2290.

[9] C.F. Tolmasky and A. Wiegmann, Recovery of small perturbations of an interface for an elliptic inverse problem via linearization, Inverse Problems 15 (1999), 465–487.

Stability estimate for an inverse problem for the wave equation from boundary measurements

Abstract

In this work, we study the inverse problem of determining the electric potential q involved in the wave equation, in a bounded domain from boundary observations. where q is depending not only on the spatial variable but also on the time variable. We prove a log-type estimate which shows that q depends stably on the Dirichlet to Neumann-map, in a subset S of our domain, assuming that it is known outside this region.

2.5 Analysis of some inverse problems from physical applications (IPPA)

Minisymposium Juliette Leblond

Spectral properties of the Neumann Poincaré operator in composite media with close to touching inclusions

Eric Bonnetier*

Abstract

We study an integral formulation of a diffusion equation in a 2D composite medium, that contains smooth, close to touching inclusions, in view of characterizing the regularity properties of the gradient of the solution. Two parameters play an impor- tant role: the conductivity contrast and the inter-inclusion distance. We study the spectral properties of the corresponding integral operator, the Neumann-Poincaré operator, as these parameters degenerate. Joint work with F. Triki.

*Université Joseph Fourier Grenoble, Laboratoire Jean Kuntzmann

An ill-posed parabolic evolution system for dispersive deoxygenation-reaeration in waters.

Faker Ben Belgacem*

Abstract

We consider an inverse problem that arises in the management of water resources and pertains to the analysis of the surface waters pollution by organic matter. Most of physical models used by engineers derive from various additions and corrections to enhance the earlier deoxygenation-reaeration model proposed by Streeter and Phelps in 1925, the unknowns being the biochemical oxygen demand (BOD) and the dissolved oxygen (DO) concentrations. The one we deal with includes Taylor's dispersion to account for the heterogeneity of the contamination in all space directions. The system we obtain is then composed of two reaction-dispersion equations. The particularity is that both Neumann and Dirichlet boundary conditions are available on the DO tracer while the BOD density is free of any condition. In fact, for real-life concerns, measurements on the dissolved oxygen are easy to obtain and to save. In the contrary, collecting data on the biochemical oxygen demand is a sensitive task and turns out to be a long-time process. The global model pursues the reconstruction of the BOD density, and especially of its ux along the boundary. Not only this problem is plainly worth studying for its own interest but it can be also a mandatory step in other applications such as the identification of the pollution sources location. The non-standard boundary conditions generate two difficulties in mathematical and computational grounds. They set up a severe coupling between both equations and they are cause of ill-posedness for the data reconstruction problem. Existence and stability fail. Identifiability is therefore the only positive result one can seek after ; it is the central purpose of the paper. We end by some computational experiences to assess the capability of the mixed finite element capability in the missing data recovery (on the biochemical oxygen demand). Joint work with M. Azaez, F. Hecht, C. Le Bot (http://hal.archives-ouvertes.fr/hal00820289).

*UT Compiègne, Laboratoire de Math. App. de Compiègne, LMAC

An inverse problem of magnetization in geoscience

Sylvain Chevillard*

Abstract

When rocks are heated (typically when they are formed, or after subsequent alter- ation), they can become magnetized by the ambient magnetic

eld. This remanent magnetization is used to study important processes in Earth sciences, since it pro- vides records of past variations of the geodynamo. It has been used, e.g., to study motion of tectonic plates and geomagnetic reversals. SQUID microscopes are sen- sitive instruments, able to measure the magnetic

eld produced by the remanent magnetization of thin slabs of rocks. More precisely, it can measure the normal component of the magnetic

eld on a plane slightly above the sample, with a good spatial resolution. We will present on- going research on the inverse problem consist- ing in recovering the magnetization distribution of the sample, from the measures given by a SQUID microscope.

*INRIA Sophia Antipolis, Equipe Apics

Parameter estimation using macroscopic models of the diffusion MRI signal

Jing-Rebecca Li *

Abstract

The water proton magnetization in biological tissue due to diffusion-encoding magnetic field gradient pulses can be modeled by a microscopic-scale diffusive PDE posed in an image voxel. Two macroscopic models governing the time evolution of the magnetizations in different diffusion subdomains of the voxel have been for- mulated and take form of a system of coupled ODEs. We solve the least squares problem of fitting the signal predicted by the microscopic PDE model to the two macroscopic ODE models to obtain estimates of the model parameters, such as the cellular volume fraction and the total cellular surface to volume ratio. We discuss the different aspects of this parameter estimation problem in view of the potential application to experimentally acquired diffusion MRI data in biological tissue.

*INRIA Saclay et Ecole Polytechnique CMAP, Equipe Défi

2.6 Application of inverse methods in aerospace industry (AI)

Minisymposium organized by Bernard Troclet

Cavities identification problems with missing data

Amel Ben Abda * Emne Jaïem † Sinda Khalfallah ‡ Abdelmalek Zine §

Abstract: The main idea of this work is an analysis of geometric inverse problems related to the identification of cavities in a special case where the problem is compounded by missing data in two spatial dimensions. The overdetermined data is given by the displacement field and the shear stress whereas no information is given on the normal component of the normal stress. We introduce a Dirichlet-Neumann misfit function and we rephrase the inverse problem into a shape optimization one. The obtained optimization problem is solved by a steepest descent algorithm using the gradient information and the level set method.
Keyworlds: Cavities identification, missing data, shape derivative, level set method.

Résumé : Nous nous intéressons dans ce travail à l'analyse d'un problème inverse géométrique d'identification de cavités par des données "peu" surdéterminées sur le bord. La donnée surdéterminée pour la reconstruction de la frontière inconnue est la contrainte de cisaillement (en plus de champs de déplacement). En introduisant une approche Dirichlet-Neumann, nous transformons notre problème en un problème d'optimisation de forme. La combinaison de la notion de dérivée par rapport au domaine et de la méthode des ensembles de niveaux, a permis la mise en oeuvre d'un algorithme de descente de type gradient pour la résolution numérique du problème inverse en question.
Mots clés : Identification de cavités, données "peu" surdéterminées, dérivée par rapport au domaine, méthode des ensembles de niveaux.

1 Problem setting

Given a bounded domain $B \subset \mathbb{R}^2$, with boundary Γ_0, the problem consists in finding a bounded domain $\overline{A} \subset B$ with boundary Γ, a displacement u defined on $\Omega = B \setminus \overline{A}$ and the tensor

$$\sigma(u) = \frac{E}{1+\nu}\left[\varepsilon(u) + \frac{\nu}{1-2\nu}\mathrm{tr}(\varepsilon(u))\mathrm{Id}\right]$$

$$\text{such that } \begin{cases} -\operatorname{div}(\sigma(u)) = 0 & \text{in } \Omega, \\ \sigma(u)n = 0 & \text{on } \Gamma, \\ u = T & \text{on } \Gamma_0, \\ \sigma(u)n_0 \cdot \tau = g & \text{on } \Gamma_0. \end{cases} \tag{1}$$

Above, n respectively n_0 is the outer normal unit vector to the boundary Γ respectively Γ_0, τ is the tangent vector to the boundary Γ_0 and

$$\varepsilon(u) = \frac{1}{2}(\nabla u + \nabla u^T).$$

For a given Ω, let (σ_D, u_D) and (σ_N, u_N) be the solutions of the following Dirichlet, respectively Neumann problem

$$\begin{cases} -\operatorname{div}(\sigma(u_D)) = 0 & \text{in } \Omega, \\ \sigma(u_D)n = 0 & \text{on } \Gamma, \\ u_D = T & \text{on } \Gamma_0, \end{cases}$$

*ENIT–lamsin, amel.benabda@enit.rnu.tn,
†ENIT–lamsin, emna23jaiem@gmail.com,
‡ENIT–lamsin, sinda _khalfallah@yahoo.fr,
§Institut Camille Jordan, École Centrale de Lyon, abdel-malek.zine@ec-lyon.fr.

$$\text{and} \begin{cases} -\operatorname{div}(\sigma(u_N)) = 0 & \text{in } \Omega, \\ \sigma(u_N)n = 0 & \text{on } \Gamma, \\ u_N \cdot n_0 = T \cdot n_0 & \text{on } \Gamma_0, \\ \sigma(u)n_0 \cdot \tau = g & \text{on } \Gamma_0. \end{cases}$$

The problem (1) is formulated to a shape optimization one (see [1] and [2]).

$$\begin{cases} \text{Find } \Omega \text{ such that} \\ J(\Omega) = \min_{\tilde{\Omega}} J(\tilde{\Omega}), \end{cases}$$

using the error functional J

$$J(\Omega) := \frac{1}{2} \int_{\Omega} (\sigma(u_D) - \sigma(u_N)) : (\varepsilon(u_D) - \varepsilon(u_N)).$$

2 Shape derivative of the functional J

In order to implemente a numerical minimization algorithm using the gradient method, we use the notion of shape derivative. In fact, there exists a function G defined on Γ such that

$$J'(\Omega, h) = \int_{\Gamma} G(h \cdot n) \quad \text{where}$$

$$G = \frac{1}{2} \left[(\sigma_D : \epsilon(u_D)) - (\sigma_N : \epsilon(u_N)) \right] + \left[(n^T \sigma_N) \,.\, (\nabla u_N \, n) \right] - \left[(n^T \sigma_D) \,.\, (\nabla u_D \, n) \right].$$

This result opens the road to choose like a descent direction of the functional J

$$h \in Q \quad \text{such that} \quad h_{|\Gamma} = -G\, n \qquad \text{where}$$

$$Q = \{ h \in \mathcal{C}^{1,1}(\overline{\Omega})^2;\ h = 0 \text{ on } \Gamma_0 \}.$$

To obtain numerical solutions for our shape optimization problem, we use the level set method combined with the shape derivative. In fact, we parameterize the boundary of Ω by means of a level set function Ψ (see [3] and [4]) which evolution is governed by the following Hamilton-Jacobi transport equation

$$\frac{\partial \Psi}{\partial t} + V \, |\nabla \Psi| = 0 \quad \text{in } \Omega,$$

where we choose the normal velocity V equal G.

References

[1] A. Ben Abda, F. Bouchon, G. H. Peichl, M. Sayeh, R. Touzani. *A Dirichlet-Neumann cost functional approach for the Bernoulli problem.* Journal of Engineering Mathematics 81(1), 157–176, 2013.

[2] H. Ben Ameur, M. Burger and B. Hackl. *Level set methods for geometric inverse problems in linear elasticity.* Inverse Problems 12, 673–696, 2004.

[3] S. Osher and R. Fedkiw *Level Set Methods and Dynamic Implicit Surfaces.* Springer-Verlag, New York, 2003.

[4] K. Ito, K. Kunisch and Z. Li. *Level-set function approach to an inverse interface problem.* Inverse Problems 17, 1225–1242, 2001.

Hybrid Inverse Boundary Element Method for the determination of the optimal spectral characteristics of a complex radiating noise source.

Mohamed Ali Hamdi[1] and Slaheddine Frikha[2]

1. Laboratory Roberval UMR 7337 UTC-CNRS, CS 60319. 60203 Compiègne Cedex. FRANCE
2. ESI France, Parc SILIC, 99 rue des Solets, BP 80112, 94513 Rungis Cedex, France

ABSTRACT

A robust inverse method based on the combination of near field acoustic measurements with a novel Hybrid Inverse Boundary Element Method (HIBEM) is presented. Its combines Acoustic Reciprocity Principle (ARP) and Least Mean Square (LMS) or Single Value Decomposition (SVD) to optimally determine the generalized spectral characteristics of very complex noise sources, typically encountered in transportation industry (engine, tire, exhaust,..). The first and second sections of the paper briefly describes the theoretical background and the numerical procedures used to determine the optimal spectral characteristics of the radiating source. The third section of the paper gives results obtained with the developed software tool to characterize a car engine.

1. Integral representation of the radiated acoustic pressure

The acoustic pressure radiated by a complex acoustic source placed as shown in figure 1, inside a closed fictive surface *S* admits [1] the following integral representation in the acoustic domain Ω_a occupying the exterior of the surface *S*,

$$p(x) = -\int_S \mu(y) \frac{\partial G(x,y)}{\partial n(y)} dS(y) \qquad (1)$$

where, μ represents the density of a double layer potential distributed on the fictive surface *S*. $G(x,y) = -exp\,(ikR(x,y))\,/(4\pi R(x,y))$ is the free space Green's function corresponding to the elementary solution of acoustic wave equation written in an infinite three dimensional space with harmonic time dependence $(exp(-i\omega t))$; $k=\omega/c$ is the acoustic wave number, ω is the circular frequency and c is the speed of sound. $R(x,y)$ is the distance separating two points *x* et *y* located in the external acoustic domain Ω_a.

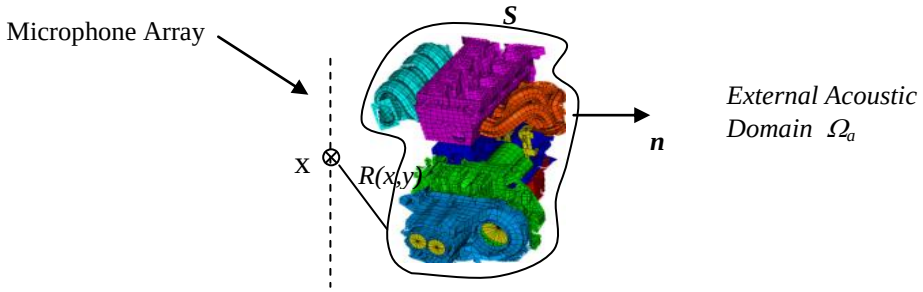

Figure 1 : Noise Source placed inside a fictive surface S

The density μ is related to the normal component γ of the acoustic acceleration of the acoustic media at the surface S by the following Fredholm integral equation of first kind,

$$\gamma(x) = \int_S \mu(y) \frac{1}{\rho} \frac{\partial^2 G(x,y)}{\partial n(x) \partial n(y)} dS(y) \qquad (2)$$

where ρ is the mass density of the acoustic media.

As shown in reference [4], the components of the density vector μ (defined at the nodes of the surface S) are related to the acceleration normal components of the vector γ (defined at the center of gravity of the boundary elements) by the following algebraic system of linear equations:

$$D\mu = C^t\gamma \tag{3}$$

where, *D* is the surface acoustic admittance square (N x N) complex matrix resulting from the BEM discrete form of the surface admittance operator,

$$D(\mu',\mu) = \int_{SxS} \mu'(x)\mu(y)\frac{1}{\rho}\frac{\partial^2 G(x,y)}{\partial n(x)\partial n(y)}dS(y)dS(x) \tag{4}$$

and, *C* is the surface coupling rectangular (E x N) real matrix resulting from the BEM discrete form of the coupling operator,

$$C(\mu',\gamma) = \int_S \mu'(x)\,\gamma(x) \tag{5}$$

Where N is the number of Nodes and E is the number of Elements of the BEM model of the fictive discrete surface S enveloping the real source.

Again as shown in reference [4], the acoustic pressure vector *P* measured by a microphone array (of dimension M) is given by,

$$P = B^t q \tag{6}$$

where B is the rectangular (N x M) Reciprocal Transfer Matrix(RTM), each column k of B corresponds to the "blocked" pressure vector induced on the surface S (considered as rigid) by an unitary point source placed at the microphone location x_k *. The vector,*

$$q = -C^t\gamma \tag{7}$$

corresponds to the acceleration flux vector of dimension N, the components of q are defined at the nodes of the fictive surface S. From equation (6) one can easily remarks that the so-called Acoustic Transfer Vectors (ATV) simply correspond to the rows of the reciprocal transfer matrix B (or to the columns of B transpose).These vectors are obtained by exploiting the Acoustic Reciprocity Principle(ARP) which is must faster than doing the direct transfer between field microphones and vibrating elements or nodes.

The inverse ill posed problem consists of determining the N components of the optimal flux vector q by minimizing the generalized Tikhonov functional,

$$J_\lambda(q) = \left\|B^t q - P_{meas}\right\|^2 + \lambda\left\|Lq\right\|^2 \tag{8}$$

where the first term corresponds to the "error"in the sense of the L2 norm $\|.\|$ ***between the vector*** P_{meas} ***measured by the antenna of M microphones (M<<N) and the predicted vector P resulting from the matrix equation (6); and the second term represents a penalty term involving the discrete L2 norm of q in order to prevent that the reconstructed acceleration flux grows without bound during the minimization procedure.***

The novel approach consist of representing the acceleration flux vector *q* on an ad hoc basis Φ,

$$q = \Phi\,\alpha \tag{9}$$

by choosing the Wave-Envelope Vectors (WEV) satisfying the following linear eigen-value problem:

$$K_S\Phi = M_S\Phi\Lambda \tag{10}$$

where K_s is a real symmetric semi-definite positive matrix resulting from the FEM discrete form of the surface bilinear operator given by,

$$K_S(\phi,\phi') = \int_S (grad_S\phi,\, grad_S\phi')dS \tag{11}$$

Where $grad_s$ is the surface Laplace operator; and where the matrix M_s is a real symmetric definite positive matrix resulting from the FEM discrete form of the surface bilinear operator defined by,

$$M_S(\phi,\phi') = \int_S \phi\phi' \, dS \tag{12}$$

Λ is a diagonal matrix composed by the eigen-values of the surface Laplace operator.
The matrix operator L appearing in the second term of the Thikonov functional (8) is chosen as the Cholesky decomposition of the symmetric matrix M_s such that,

$$L^t L = M_S \tag{13}$$

The Wave Envelope Vectors are normalized such that the matrices M_s and K_s satisfy respectively,

$$\Phi^t M_s \Phi = I \quad \text{and} \quad \Phi^t K_s \Phi = \Lambda \tag{14-1; 14-2}$$

The Thikonov functional could be now written in term of the components of the generalized vector α,

$$J_\lambda(\alpha) = \alpha^h (H^h H) + \lambda I)\alpha - 2\Re e(\alpha^h H^h P_{meas}) + P_{meas}^h P_{meas} \tag{15}$$

where,

$$H = B^t \Phi \tag{16}$$

corresponds to the Generalized Reciprocal Transfer Matrix (GRTM). The columns of the GRT Matrix corresponds to the so-called Modal Acoustic Transfer Vectors (MATV). Again these vectors are generated taking advantage of the Acoustic Reciprocity Principle (ARP).

2. Inverse technique for the reconstruction of the acceleration flux vector *q*

The minimum α_λ of the Thikonov functional is obviously given by,

$$\alpha_\lambda = R \,.\, P_{meas} \tag{17}$$

where,

$$R = \left(H^h H + \lambda I\right)^{-1} H^h \tag{18}$$

is the regularized pseudo-inverse of the Generalized Reciprocal Transfer Matrix H. The standard Least Mean Square (LMS) approach or Single Value Decomposition (SVD) of the GRT Matrix H could be used to compute the optimal vector α_λ. As discussed in references [2,5] *the optimal choice of the positive parameter λ could be done using ad hoc filtering techniques combined with the Morozov Discrepancy Principle (MDP) such that the reconstructed acceleration flux q_{rec}^λ solution of the functional (8), must satisfies the discrepancy equation:*

$$\left\| B^t q_{rec}^\lambda - P_{meas}^\sigma \right\|^2 = M\sigma^2 \tag{19}$$

where σ^2 is the variance of the noise in data and M is the number of microphones.

3. Results

The proposed Inverse Boundary Element Method (IBEM) has been applied to characterize a car engine in the low frequency band f < 1000Hz. Figure 1-b shows the experimental set up where a microphone array (60 microphones) is placed on the top of a running car engine at 3000 rpm. The microphone array has been placed on right, left, top and front sides of the engine. Figure 2-a shows the IBEM model corresponding to the fictive surface enveloping the car engine which is nearly a closed box meshed with approximately 250 quadrangular boundary elements. Figure 2-b shows the comparison between measured and predicted averaged sound pressure levels (240 microphones), where 20 eigen-functions (wave-envelopes) have been used to represent the acceleration flux through the enveloping surface S. Figure 2-c shows the comparison between measured and predicted sound pressure levels at the position of a microphone not included in the global cost function. The error between measured and predicted results remains less than 2 dB. This confirms the robustness of the proposed inverse method to predict and extrapolate the acoustic pressure radiated by the engine. Finally Figure 2-d shows the measured and the predicted acoustic pressures radiated by the engine at 600 Hz.

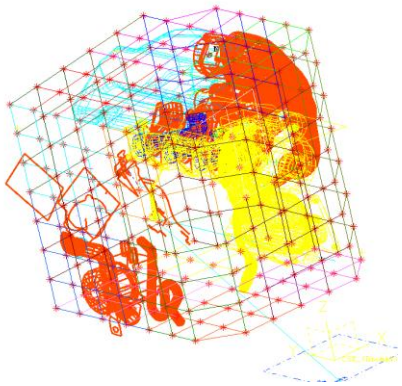

Figure 2-a. Engine IBEM Model

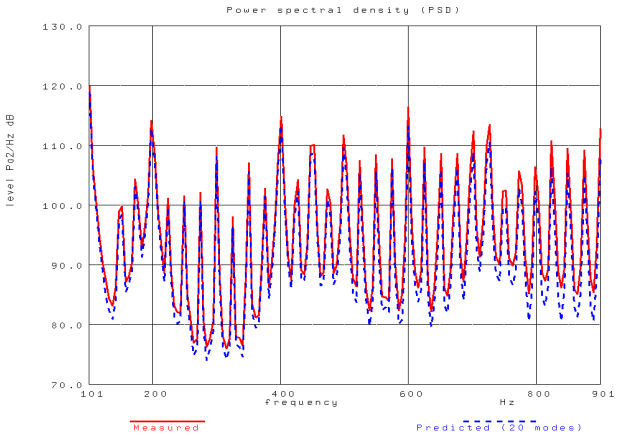

Figure 2-b. Averaged Sound Pressure Level

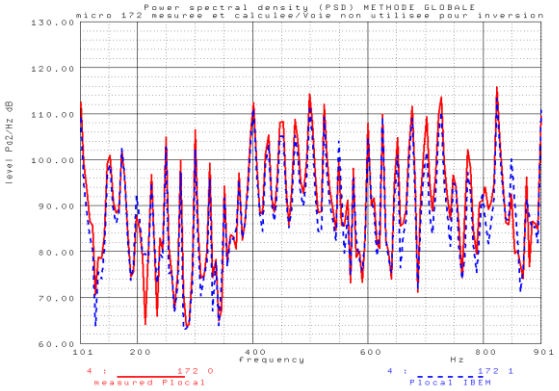

Figure 2-c. Local Sound Pressure Level

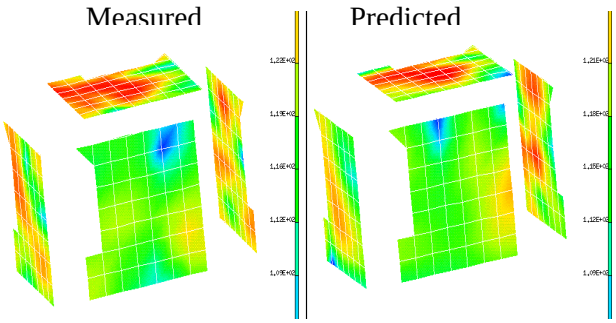

Figure 2-d. Radiated Acoustic Pressure at 600Hz

CONCLUSION

A hybrid inverse boundary element method based on the exploitation of the reciprocity principle in acoustics combined with a wave envelope technique has been developed and implemented in RAYON^{R}-IBEM solver. This method has been successfully applied to characterize a real car engine as a distributed noise source which could be used to excite the car body and predict either interior and exterior noise (pass by noise). This method which has a big potential of applications, could be advantageously used to characterize and identify noise sources in transportation industries [3].

REFERENCES

[1] M.A Hamdi and J.M. Ville, “Sound Radiation from Ducts/ Theory and Experiments”, Journal of Sound and Vibration, 107(2), 231-242, 1986.

[2] P.C. Hanson, “Rank-Deficient and Discrete ill-Posed Problems, Numerical Aspects of Linear Inversion”, SIAM, 1998.

[3] J.M. Auger, M.A. Hamdi, G. Amadasi, E. Girimondi, “Pass By Noise Modelling with Boundary Elements”,SAE Noise &Vibration Conf., Traverse City, May 20-22, 1997

[5] E.G. Williams, " Regularization Methods for Nearfield Acoustical Holography", JASA-Preprint, July, 2001

IDENTIFICATION OF OVERPRESSURE SOURCES AT LAUNCHER VEHICLE LIFT-OFF USING AN INVERSE METHOD IN THE TIME DOMAIN

B. Troclet[1], I. Terrasse[2], S.Alestra[2]

[1] Airbus Defence & Space, 78133 Les Mureaux, France

1 ENS Cachan, 94230 CACHAN, France

Bernard.troclet@astrium.eads.net

[2] Innovation Works, 92150 Suresnes, France

Keywords: Inverse Source Method, Acoustics, Overpressure, BEM, Time Domain, Launch Vehicle Lift-Off.

Abstract.

At lift-off, launch vehicles are subject to a very severe overpressure, which can induce loads acting on payloads in the low frequency domain. The overpressure starts at ignition of solid rocket motors. For a numerical prediction of the overpressure environment, AIRBUS Group Defence & Space has developed an inverse method via a Time Domain Boundary Integral Equations approach using an optimal control method, with direct and adjoint equations and Quasi Newton optimizer. The corresponding discrete schemes are highly accurate and unconditionally stable. As an industrial application, the identification of overpressure sources is shown, on the lift-off acoustic environment of ARIANE V.

Introduction

During the lift-off phase, the launch vehicles, such as the ARIANE 5 launcher, are subject to severe loads: the overpressure loads, which appear at ignition of solid rocket motors. The overpressure loads are among the most severe loads that a launcher can encounter during flight. The initial cause of the overpressure is the rocket-exhausts and their interactions with the launch pad. The overpressure is composed of the Ignition OverPressure (IOP), which originates from the launch table, and the Duct OverPressure (DOP), which originates from the launch ducts. Figure 1 illustrates this point with a picture of ARIANE 5 launch pad with the ducts. The overpressure is a deterministic load having discrete spikes at certain particular frequencies, with significant levels for frequencies lower than 40 Hz [1], [2].This low frequency excitation excites the launch vehicle and induces Quasi Static Loads (QSL) at the payload/launcher interface, which the payload has to endure. Consequently, it is important to predict these loads before launches.

To achieve this goal, an inverse method using an optimal control method (direct and adjoint equations), with a Time Domain Boundary Integral Equations approach, has been progressing for several years at Innovation Works, in collaboration with Airbus Defence & Space [3]. The corresponding discrete schemes are high accurate quality and unconditionally stable.

Having localized the overpressure sources from ARIANE 5 in-flight measurements, it will be easy to rebuild the unsteady pressure field and to estimate the pressure levels at any point of the vehicle for other flights. By integrating the unsteady pressures over all surfaces of the launchers, the loads created by the overpressure can be estimated. Consequently, the response of the launcher to this load case during the lift-off phase can be analyzed in the temporal domain by using any FEM software.

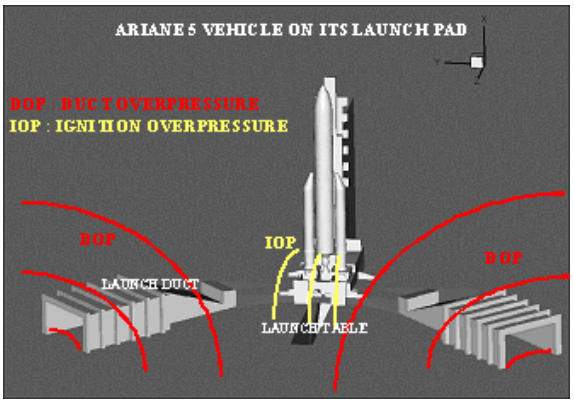

Fig 1 : Ignition and Duct OverPressure definition

Inverse Source Problem with BEM (Boundary Element Method) in Time domain

We wish to identify time domain acoustic source, emitted at point source x_0 parameterized by a real function *p* for each sampling time, which will be the control parameter variable used for the optimal control inverse method.
($p = \left(p_1; \cdots, p_p, \cdots, p_N \right)$ stands for parameter, N is the number of Time sampling for solving direct problem).
We associate the discrete emission function and the corresponding incident field $O_{inc}(p)$ to this parameter.

$$f_p(t) = \begin{pmatrix} p_1 = f(\Delta t) \\ \vdots \\ p_N = f(N\Delta t) \end{pmatrix} \qquad O_{inc}(p)(x,t) = \frac{f_p(t - |x - x_0|/c)}{4\pi |x - x_0|}$$

We consider the scattering problem of transient acoustic waves in a fluid medium by a submerged rigid object.
Let Ω^i be a three-dimensional object with a regular (without tip) bounded surface $\Gamma = \partial\Omega^i$.
Let $\Omega^e = R^3 \backslash \Omega^i$ denote the exterior domain occupied by the fluid medium.. We denote by O^e_{diff} the scattered acoustic pressure created in the fluid medium by an incident field $O_{inc}(p)$ (the wave propagating without the obstacle), which is the contribution of a time domain point source.
Therefore, we have the following initial boundary value problem:

$$\begin{cases} \dfrac{1}{c^2} \dfrac{\partial O^e_{diff}(x,t)}{\partial t^2} - \Delta O^e_{diff}(x,t) = 0 & \text{in } \Omega^e \times R^+, \\ O^e_{diff}(x,0) = \dfrac{\partial O^e_{diff}}{\partial t}(x,0) = 0 & \text{in } \Omega^e, \\ \dfrac{\partial O^e_{diff}}{\partial n} = -\dfrac{\partial O_{inc}}{\partial n}(p)(x,t) & \text{on } \Gamma \times \mathrm{R}^+. \end{cases}$$

where *n* denotes the unit normal vector to Γ, oriented from domain Ω^I to Ω^e. c is the speed of sound in the medium. We associate to the *exterior* problem an appropriate *interior* problem with O^i_{diff} in Ω^I . It is well-known that the scattered field O^e_{diff} has the following representation formula, using the Near Field Scattered operator Q :

$$O^e_{diff}(x,t) = QU = -\frac{1}{4\pi} \int_\Gamma n_y . \nabla_x \frac{U(y, t - |x-y|/c)}{|x-y|} dy \qquad \forall x \in \Omega^i \cup \Omega^e$$

where: $U = O^{i}_{diff} - O^{e}_{diff}$ is the jump O^{e}_{diff} crossing Γ, and τ = t-|x-y| is the *retarded time*. Using formula to compute the traces of O^{e}_{diff} ΓxR^{+}, as a function of *U*, and introducing the boundary conditions, one obtains the *Boundary Integral Equation* for the unknown function *U* :

$$RU(x,t)) = S(p)(x,t) \quad \forall (x,\, t) \in \Gamma$$

with the surface operator *R*, a Double layer Integral Operator coming from the variationnal formulation with function *U* in $H^2(R+, H^{1/2}(\Gamma))$, such that, for all Ψ in the same space:

$$RU(x,t) = \int_{\Re}\int_{\Gamma\times\Gamma} \frac{\vec{n}(x)\vec{n}(y)}{4\pi|x-y|}\frac{\partial^2 U}{\partial t^2}\left(y, t-\frac{|x-y|}{c}\right)\frac{\partial \Psi}{\partial t}(x,t)dxdydt$$
$$+c^2\int_{\Re}\int_{\Gamma\times\Gamma} \frac{curl_{\Gamma}U}{4\pi|x-y|}\left(y, t-\frac{|x-y|}{c}\right)curl_{\Gamma}\frac{\partial \Psi}{\partial t}(x,t)dxdydt$$

$$S(p)(x,t) = \int_{\Re}\int_{\Gamma}\left(\frac{\partial O_{inc}}{\partial n}(p)(x,t)\right)\frac{\partial \Psi}{\partial t}(x,t)dxdt$$

The equation is solved in space by a P1 surface finite element method. The boundary Γ of the object is meshed with triangular elements.

Finally, the direct problem consists in two main steps:
1) Computation of the pressure jump U by the Integral Equation operator R, and the excitation S
2) The radiating post-treatment equation to compute the acoustic pressure O by the scattered operator Q added with the Oinc incident field contribution :

$$1) \quad RU = S(p)$$
$$2) \quad O = QU + O_{inc}(p)$$

The quadratic error or cost function j(p), depending on the source parameters p, is defined by

$$J(O(p)) = j(p) = \min_{q\in X} j(q) = \frac{1}{2}\left\|O(q) - O_{mes}\right\|^2$$

Then after some derivations, we obtain

- The Adjoint Equations

$$\begin{cases} O^* = -\dfrac{dJ(O)}{dO} = -\left(O(p) - O_{mes}\right) \\ RU^* = Q^T O^* \end{cases}$$

- The Gradients Formula for multiparameter p

$$\frac{\nabla j}{\nabla p} = -<U^*, \frac{\partial S(p)}{\partial p}> - <O^*, \frac{\partial O_{inc}(p)}{\partial p}>$$

The expression of the gradients is now completely established. Starting with an initial guess for the estimated parameter p_0, a Quasi-Newton optimizer is used to update the parameter value *p* and to find the optimal p_{opt} which causes the gradients to vanish.

Some recent progresses :

- We can reduce the computation times by decomposing the sources parameters vector into a base of unitary sources (multilinear process): the time computation is then reduced by a factor 10.
- We have completed the identification of sources by optimizing on p and Δp (differences of pressures between opposite points; (The launcher is excited by the differences of pressures in the low frequency domain),
- We have introduced physical sources constraints in the optimization process

Numerical Results

For identifying the overpressure sources, the flight of concern is the 511 ARIANE 5 flight. Indeed, pressure measurements have been mounted on the lower (9 available measurements) and on the upper part of the launcher (4 available measurements).
The locations of sources are defined a priori from previous experience. 10 sources have been identified:

- one per EAP solid rocket booster and its image with regards to the mast, which was not modelled,
- one per solid rocket booster at launch duct exit and its image with regards to the mast,
- one source for the Vulcain engine.

After identification of the overpressure source locations, a direct problem is solved to compute simulated pressure levels and compare them with the real measured values on the same sensors. The comparisons were made on the pressures and the differences of pressure measured at diametrically opposite points. Indeed, this quantity is the adequate parameter for the calculations of low frequency dynamic response of the launch vehicle.

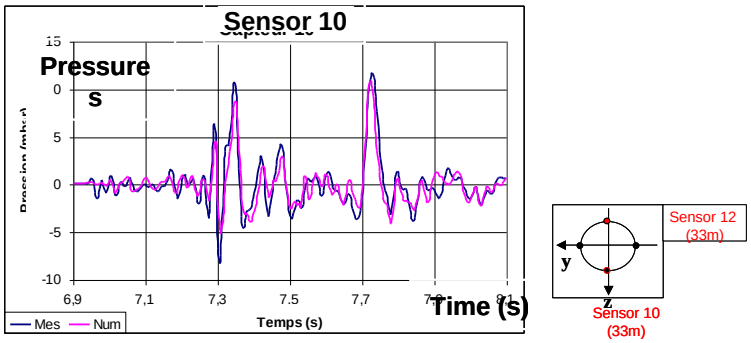

Fig 2 : Comparison of the measured and computed data (Sensor 10, Fairing)

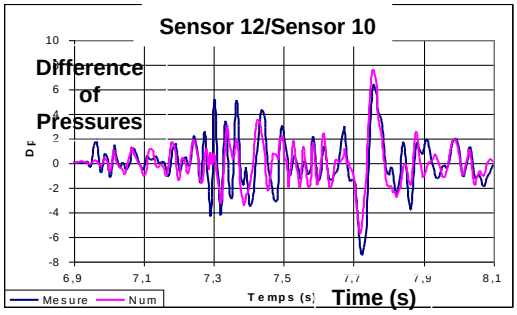

Fig 3 : Comparison of the measured and computed differences of pressure data (Sensor 10, 12 Fairing)

Good correlations are observed between the measured and calculated pressures. Also, the comparisons on the rebuilt and measured diametrically opposite pressures are good.
A deep robustness analysis of the method has then been performed, as follows,

- A calculation of the field of pressures on a number of necessary points was achieved, in order to check the physical character of the calculated pressures,

- The study of the robustness of the method with regards to the number of measurements,
- The comparison between the measured propulsion parameters and the evolution of the identified sources versus time, to check the physical meaning of the identified sources.

Summar,

A robust and accurate time domain integral equation for wave propagation was developed. The time marching scheme for the direct acoustic source problem is unconditionally stable (no CFL conditions). This allows a classical optimization approach for the inverse problem.

Direct and adjoint codes have exactly the same properties. Prior knowledge of the localization of sources and power parallel computers allow the industrial application of such an inverse problem.

We demonstrate the interest of the method on some examples of source reconstructions in low frequency acoustics for the ARIANE 5 overpressure source identification on the data from 511 ARIANE 5 flight: initial results are very promising and show a good identification of the multiparameter sources in the 0- 40 Hz frequency domain

For future launches from the same launch pad, that the one used for the identification, and having the same characteristics in terms of propulsion, the complete pressure field in the time domain can be estimated.

The dynamic response of the launcher will be investigated. This approach is now used in industrial activities.

References

[1] Troclet B, Chemoul.B, P. Roux, D. Gely and G. Elias.

"*Synthesis of Vibroacoustic Studies performed during ARIANE 5 Program", In Launch Vehicle Vibrations, Toulouse*, pages 201, 210, 1999

[2] H.Ikawa F.Laspesa

Ignition/Duct Overpressue Induced by Space Shuttle Solid Rocket Motor Ignition», Journal of Spacecraft, pages 4841- 488, Vol 22, n°4, July- August 1985

[3] S.Alestra, I.Terrasse, B.Troclet,

Inverse Method for Identification of Acoustic Sources at Launch Vehicle Lift-off", AIAA JOURNAL, Vol 41, Number 10, Octobre 2003

2.7 Inverse problems: Identification and stability (IS)

Minisymposium organized by Slim Chaabane

Pointwise inequalities of Logarithmic type in Hardy-Hölder spaces

Slim Chaabane* Imed Feki†

Abstract: We prove some optimal logarithmic estimates in the Hardy space $H^\infty(G)$ with Hölder regularity, where G is the open unit disk or an annular domain of $\mathbb{C}$. These estimates extend the results of [1, 3] established in the case of the Hardy-Sobolev space $H^{k,\infty}$. The proofs are based on a variant of Hardy-Landau-Littlewood inequality for Hölder functions. We apply those results to establish stability properties for inverse problem of identifying Robin's coefficients in corrosion detection by electrostatic boundary measurements.

Keyworlds: Hardy-Hölder space; Hardy-Landau-Little-wood inequality; Inverse problem

1 Optimal logarithmic estimates in Hardy-Hölder spaces

Let $\mathbb{D}$ be the open unit disk of $\mathbb{C}$ with boundary $\mathbb{T}$ and let $H^\infty(\mathbb{D})$ the space of bounded analytic functions on $\mathbb{D}$. For $s \in]0,1[$, we denote by $G_s = \mathbb{D}\backslash s\overline{\mathbb{D}}$ the annulus of inner boundary $s\mathbb{T}$ and outer boundary $\mathbb{T}$ and by $H^\infty(G_s)$ the Hardy space of bounded analytic functions on G_s.

In the sequel, we denote by G the open unit disk $\mathbb{D}$ or the annulus $G_s; s \in]0,1[$.
For $k \in \mathbb{N}$ and $\alpha \in]0,1[$, we designate by $H^{k,\infty}(G)$ the Hardy-Sobolev space of G:

$$H^{k,\infty}(G) = \{f \in H^\infty(G),\ f^{(j)} \in H^\infty(G), j = 0, ..., k\},$$

where $f^{(j)}$ denote the j^{th} complex derivative of f,
and by $\mathcal{H}^{k,\alpha}(G)$ the Hölder-Hardy space:

$$\mathcal{H}^{k,\alpha}(G) = \left\{ g \in H^{k,\infty}(G);\ \sup_{z_1 \neq z_2 \in G} \frac{|g^{(k)}(z_1) - g^{(k)}(z_2)|}{|z_1 - z_2|^\alpha} < \infty \right\},$$

We endow $H^{k,\infty}(G)$ with the usual norm:

$$||f||_{H^{k,\infty}} = \max_{0 \leq j \leq k} \left(||f^{(j)}||_{L^\infty(\partial G)} \right).$$

Let $\mathcal{B}^{k,\alpha}(G)$ denotes the unit ball of $\mathcal{H}^{k,\alpha}(G)$:

$$\mathcal{B}^{k,\alpha}(G) = \left\{ g \in \mathcal{H}^{k,\alpha}(G),\ \text{such that } [g]_{k,\alpha} \leq 1 \right\},$$

where $[g]_{k,\alpha}$ is the k^{th} Hölder quotient defined by

$$[g]_{k,\alpha} = \sup_{z_1 \neq z_2 \in G} \frac{|g^{(k)}(z_1) - g^{(k)}(z_2)|}{|z_1 - z_2|^\alpha}.$$

For any connected subset I of ∂G with length $2\pi\lambda; \lambda \in]0,1[$, the L^1 norm of f on I is given by:

$$||f||_{L^1(I)} = \frac{1}{2\pi\lambda} \int_I |f(re^{i\theta})| d\theta, \quad \text{where } r = s \text{ if } I \subset s\mathbb{T} \text{ and } r = 1 \text{ if } I \subset \mathbb{T}.$$

We present in this work the following main result:

*Faculty of Sciences of Sfax- LAMHA Laboratory. slim.chaabane@fsm.rnu.tn,
†Faculty of Sciences of Sfax- LAMHA Laboratory. imed.feki@fss.rnu.tn

Theorem 1.1. *Let $k \in \mathbb{N}$ and I a subarc of ∂G of length $2\pi\lambda; \lambda \in]0,1[$. There exists two non negative constants C and γ, depending only on k, α, s and λ, such that for every $f \in \mathcal{B}^{k,\alpha}(G)$ satisfying $||f||_{L^1(I)} < \gamma$, we have*

$$\|f\|_{L^\infty(\partial G)} \leq \frac{C}{|\log \|f\|_{L^1(I)}|^{\alpha+k}}. \tag{1}$$

Furthermore, for $I = \{e^{i\theta}, -\frac{\pi}{2} \leq \theta \leq \frac{\pi}{2}\}$, there exists a sequence $g_n \in \mathcal{B}^{k,\alpha}(G)$ such that:

$$\lim_{n\to+\infty} \|g_n\|_{L^\infty(\partial G)} \left|\log \|g_n\|_{L^1(I)}\right|^{\alpha+k} \geq \frac{(\log 2)^{\alpha+k}}{2^{1-\alpha}}. \tag{2}$$

2 Application

As application, we apply our results to obtain logarithmic stability estimates for an inverse problem of identifying Robin's coefficients by boundary measurements. Let consider a prescribed flux ϕ together with measurement f on a subarc I of the unit circle $\mathbb{T}$, the inverse problem considered is to recover a function q on $J = \mathbb{T} \setminus I$ such that the solution u of

$$(RP) \begin{cases} -\Delta u = 0 & \text{in} \quad \mathbb{D}, \\ \partial_n u = \phi & \text{on} \quad I, \\ \partial_n u + qu = 0 & \text{on} \quad \mathbb{T} \setminus I, \end{cases}$$

also satisfies $u_{|I} = f$.
Let $c,\ c' > 0$ and K be a non-empty connected subset of J, for which the boundary does not intersect that of I. We suppose that q belongs to the class of admissible Robin coefficients:

$$Q_{ad} = \{q \in \mathcal{C}_0^1(\overline{J}), \quad |q^{(k)}| \leq c', \quad 0 \leq k \leq 2, \text{ and } \ q \geq c\chi_K\},$$

where $\mathcal{C}_0^1$ is the set of differentiable functions, that vanish on the boundary as well as their first derivatives. Let $W_0^{1,2}(I)$ denote the closure of $\mathcal{C}_0^1(I)$ in $W^{1,2}(I)$.

As an application of Theorem 1.1, we establish the following stability result:

Theorem 2.1. *Let $\phi \in W_0^{1,2}(I)$ be a positive function which is not identically trivial. There exists then, a non negative constant C such that for any $q_1, q_2 \in Q_{ad}$, we have:*

$$\|q_1 - q_2\|_{L^\infty(J)} \leq \frac{C}{\left|log\left(\|u_1 - u_2\|_{L^1(I)}\right)\right|^{1/2}},$$

provided that $\|u_1 - u_2\|_{L^1(I)} < 1$, where u_i denotes the solution of (RP) with $q = q_i;\ i = 1, 2$.

Note that this result improves upon [2, Corollary 1] where the authors supposed that $\phi \in W_0^{2,2}(I)$. We note also that an $1/\log$-type estimate has been proved in [4, Theorem 4.3].

References

[1] Chaabane S and Feki I *Optimal logarithmic stability estimates in Hardy-Sobolev spaces $H^{k,\infty}$.* C.R. Acad. Sci. Paris, Ser. I **347**, 1001-1006, 2009.

[2] Chaabane S, Fellah I, Jaoua M and Leblond J *Logarthmic stability estimates for a Robin coefficient in two-dimensional Laplace inverse problems.* Inverse problem **20**, 47-59, 2004.

[3] Feki I *Estimates in Hardy-Sobolev spaces on annular domains: Stability results.* Czecholovak Mathematical Journal, **63-2**, 481-495, 2013.

[4] Feki I, Nfata H and Wielonsky F *Optimal logarithmic estimates in the Hardy-Sobolev space of the disk and stability results.* J. Math. Anal. Appl., **395**, 366–375, 2012.

Quelques estimations logarithmiques optimales dans les espaces de Hardy-Sobolev

Imed Feki * Houda Nfata † Franck Wielonsky ‡

Résumé : On démontre dans ce travail des estimations optimales de type $1/\log^k$ dans les espaces de Hardy-Sobolev $H^{k,2}; k \in \mathbb{N}^*$, du disque unité $\mathbb{D}$ améliorant ainsi les résultats établis par L. Baratchart et M. Zerner [2] et généralisant les travaux effectués dans le cas uniforme par S. Chaabane et I. Feki [3]. On généralise ensuite ces estimations au cas des espaces de Hardy-Sobolev $H^{1,p}$, $p \in [1, \infty]$. Un contre-exemple est aussi élaboré pour montrer que ces dernières estimations sont optimales.
Mots clés : Espace de Hardy-Sobolev, inégalité de Hardy-Landau-Littlewood, estimation logarithmique, stabilité, problème inverse.

1 Introduction

On établit dans ce travail des estimations logarithmiques dans les espaces de Hardy-Sobolev du disque unité $\mathbb{D}$ améliorant ainsi les résultats de [2] et généralisant les travaux de [3].
Pour tout $p \in [1, +\infty], r \in]0, 1[$ et f une fonction analytique dans $\mathbb{D}$, on note par :

$$M_p(f, r) = \left(\frac{1}{2\pi} \int_0^{2\pi} |f(re^{i\theta})|^p d\theta \right)^{\frac{1}{p}} \quad \text{si} \quad p < +\infty \quad \text{et} \quad M_\infty(f, r) = \max_{|z|=1} |f(z)|$$

On désigne par H^p l'espace de Hardy des fonctions f analytiques dans $\mathbb{D}$ ayant une moyenne $M_p(f, r)$ bornée sur les cercles de rayons $r \in]0, 1[$ que l'on munit de la norme suivante :

$$||f||_p = \lim_{r \to 1^-} M_p(f, r).$$

Pour $k \in \mathbb{N}^*$, on désigne par $H^{k,p}$ l'espace de Hardy-Sobolev du disque unité $\mathbb{D}$:

$$H^{k,p} = \{f \in H^p;\ f^{(j)} \in H^p,\ 1 \leq j \leq k\}$$

que l'on munit de la norme :

$$\|f\|^p_{H^{k,p}} = \sum_{j=0}^{k} \|f^{(j)}\|^p_p \quad \text{si} \quad 1 \leq p < \infty \ \ et \ \ \|f\|_\infty = \max_{0 \leq j \leq k} (\|f^{(j)}\|_{L^\infty(\mathbb{T})}).$$

Pour $1 \leq p < \infty$ et I un sous arc de $\mathbb{T}$ de longueur $2\pi\lambda$, $\lambda \in]0, 1[$, on désigne par

$$\|f\|_{p,I} = \left(\frac{1}{2\pi\lambda} \int_I |f(e^{i\theta})|^p \ d\theta \right)^{\frac{1}{p}},$$

la norme L^p de la fonction f sur I.
On note par $\mathcal{B}_{k,p}$ la boule unité de l'espace de Hardy-Sobolev $H^{k,p}$:

$$\mathcal{B}_{k,p} = \{f \in H^{k,p}\ ;\ \ \|f\|_{H^{k,p}} \leq 1\}.$$

Ce travail comporte deux parties.

*FSS–LAMHA, Imed.Feki@fss.rnu.tn,
†FSS–LAMHA, nfata.houda@yahoo.fr,
‡CMI–LATP, wielonsk@cmi.univ-mrs.fr

- On établit dans la première partie des estimations optimales de type logarithmique dans les espaces de Hardy-Sobolev $H^{k,2}$ permettant de contrôler en norme L^2 le comportement d'une fonction f dans la boue unité $\mathcal{B}_{k,2}$ à partir de son comportement en norme L^2 sur un sous-arc I de $\mathbb{T}$.
- Dans la deuxième partie, on généralise ces estimations de type logarithmique dans les espaces de Hardy-Sobolev $H^{1,p}$, $1 \leq p \leq \infty$.

2 Estimations dans les espaces de Hardy-Sobolev $H^{k,2}$

On démontre dans le théorème suivant une estimation logarithmique optimale dans les espaces de Hardy-Sobolev $H^{k,2}$ du disque, $k \in \mathbb{N}^*$.

Théorème 2.1. *Soit $k \geq 1$. Alors, il existe deux constantes positives α_k et γ_k, dépendant uniquement de k, tels que pour tout $f \in \mathcal{B}_{k,2}$ vérifiant $\|f\|_{2,I} \leq e^{-\gamma_k/\lambda}$, I étant un sous arc de $\mathbb{T}$ de longeur $2\pi\lambda$, on a :*

$$\|f\|_2 \leq \frac{\alpha_k}{|\lambda \log \|f\|_{2,I}|^k}. \tag{1}$$

De plus, pour $I = \{e^{i\theta}, -\pi/2 \leq \theta \leq \pi/2\}$ il existe une suite de polynômes

$$f_n = u_n/\|u_n\|_{H^{k,2}}, \qquad u_n(z) = (z-a)^n, \qquad n > 0, \qquad a > 1.$$

telle que la norme $\|f_n\|_{2,I}$ tend vers 0 lorsque n tend vers l'infini avec

$$0 < \beta_{k,a} := \lim_{n\to\infty} \|f_n\|_2 |\log \|f_n\|_{2,I}|^k, \qquad \lim_{a\to+\infty} \beta_{k,a} = 1. \tag{2}$$

Remarque Il résulte de (2) que l'estimation (1) du Théorème 2.1 est optimale : Il est impossible de remplacer la constante α_k par une fonction de la norme $\|f\|_{2,I}$ qui tend vers 0 en 0 telle que pour tout $f \in \mathcal{B}_{k,2}$, on a :

$$\|f\|_2 |\log(\|f\|_{2,I})|^k \leq \varepsilon(\|f\|_{2,I}).$$

3 Estimations dans les espaces de Hardy-Sobolev $H^{1,p}$

On démontre dans le théorème suivant une estimation logarithmique optimale dans les espaces de Hardy-Sobolev $H^{1,p}$ du disque, $1 \leq p \leq \infty$.

Théorème 3.1. *Il existe deux constantes positives α et Γ, dépendant uniquement de $1 \leq p \leq \infty$, tels que pour tout $f \in \mathcal{B}_{1,p}$ vérifiant $\|f\|_{1,I} \leq e^{-\Gamma}$, I est un sous arc de $\mathbb{T}$ de longueur $2\pi\lambda$, on a :*

$$\|f\|_p \leq \frac{\alpha}{|\lambda \log(\|f\|_{1,I})|}. \tag{3}$$

De plus, pour $I = \{e^{i\theta}, \ \frac{\pi}{2} \leq \theta \leq \frac{3\pi}{2}\}$ il existe une suite de fonctions $f_n \in \mathcal{B}_{1,p}$ telle que la norme $\|f_n\|_{1,I}$ tend vers 0 lorsque n tend vers l'infini avec

$$\lim_{n\to+\infty} \|f_n\|_p \, |\log \|f_n\|_{1,I}| \geq \frac{\log 5}{2}. \tag{4}$$

Références

[1] I. Feki, H. Nfata, F. Wielonsky, *Optimal logarithmic estimates in the Hardy-Sobolev space of the disk and stability results*, Journal of Mathematical Analysis and Applications 395 (2012), 366-375.

[2] L. Baratchart and M. Zerner. *On the recovery of functions from pointwise boundary values in a Hardy-Sobolev class of the disk*, Journal of computational and Applied Mathematics 46 (1993), 255-269.

[3] S. Chaabane, I.Feki, *Optimal logarithmic estimates in Hardy-Sobolev spaces $H^{k,\infty}$*, C. R. Acad. Sci. Paris, Ser. I 347 (2009), 1001-1006.

Plasma equilibrium reconstruction in a Tokamak using topological gradient method

Maatoug Hassine* Mohamed Jaoua† Souhila Sabit‡

Abstract: The Tokamak is an experimental machine which aims to confine the plasma in a magnetic field to control the nuclear fusion of atoms of mass law. The real-time reconstruction of the plasma magnetic equilibrium in a Tokamak is a key point to access high performance regimes.

In an axisymmetric configuration, the plasma equilibrium is described by the equation (see [2])

$$L\psi = 0 \text{ in } \Omega_v$$

where $\Omega_v = \Omega \backslash \overline{\Omega_p}$ is the vacuum region surrounding the plasma domain Ω_p, Ω is the vacuum vessel, and $\mathcal{L}$ is the Grad-Shafranov operator

$$\mathcal{L} = -\frac{\partial}{\partial r}(\frac{1}{r}\frac{\partial}{\partial r}) - \frac{\partial}{\partial z}(\frac{1}{r}\frac{\partial}{\partial z})$$

Due to its economic importance, the plasma control problem has long been receiving considerable attention by engineers and mathematicians[2,3]. Therefore, the most developed methods deal with control theory or parametric optimization.

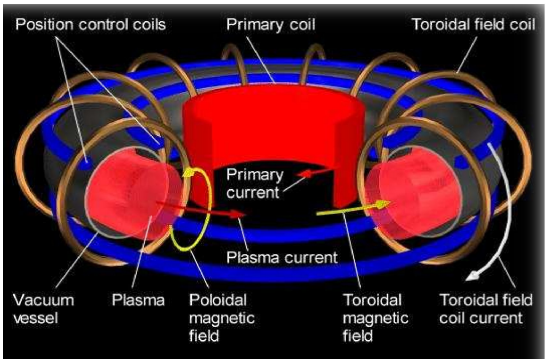

Figure 1: Tokamak

In this work, we propose a new method. Our approach is based on the topological sensitivity analysis[1,4]. The plasma domain defined by a level curve of a scalar function, called the topological gradient. The topological gradient is calculated from a topological asymptotic expansion for the Grad-Shafranov operator. The proposed approach leads to a fast and accurate numerical algorithm. The efficiency of the proposed method is illustrated by some numerical examples.

Keyworlds: Inverse problem, topological gradient, topological sensitivity, plasma reconstruction.

*FSM–lamsin, maatoug.hassine@enit.rnu.tn,
†Université Francaise d'Egypte, mb.jaoua@gmail.com
‡INRIA Rennes, France, souhila.sabit@inria.fr

1 The inverse problem

We consider here the inverse problem of determining plasma boundary Γ_p location from over-specified boundary data on $\Gamma = \partial\Omega_v$. Knowing a complete set of Cauchy data, the poloidal flux ψ satisfies the system

$$\left\{\begin{array}{lcll} L\psi & = & 0 & \text{in} \quad \Omega_v, \\ \dfrac{1}{r}\dfrac{\partial\psi}{\partial n} & = & \varphi^N & \text{on} \quad \Gamma, \\ \psi & = & \varphi^D & \text{on} \quad \Gamma, \\ \psi & = & 0 & \text{on} \quad \Gamma_p. \end{array}\right. \tag{1}$$

In this formulation the domain Ω_v is unknown since the free plasma boundary Γ_P is unknown. This problem is ill posed in the sense of Hadamard.

The considered inverse problem can be formulated as follows: given boundary data φ^N and φ^D, find the optimal location of the plasma boundary Γ_P minimizing the cost function

$$J(\psi^N, \psi^D) := \int_{\Omega_v} |\psi^N - \psi^D|^2 \tag{2}$$

where ψ^N and ψ^D are the solutions to the following systems

$$\left\{\begin{array}{lll} L\psi^N & = 0 & \text{in } \Omega_v, \\ \dfrac{1}{r}\dfrac{\partial\psi^N}{\partial n} & = \varphi^N & \text{on } \Gamma, \\ \psi^N & = 0 & \text{on } \Gamma_p, \end{array}\right. \quad \left\{\begin{array}{lll} L\psi^D & = 0 & \text{in } \Omega_v, \\ \psi^D & = \varphi^D & \text{on } \Gamma, \\ \psi^D & = 0 & \text{on } \Gamma_p. \end{array}\right. \tag{3}$$

2 Topological sensitivity analysis

The topological sensitivity analysis method consists in studying the variation of a cost function $j(\Omega)$ with respect to the insertion of small hole $\omega_\rho = X_0 + \rho\omega$ in the domain Ω, where $X_0 = (x_0, y_0) \in \Omega$, $\rho > 0$ and $\omega \subset I\!R^2$ is a fixed bounded domain containing the origin, whose boundary is connected and piecewise of class $\mathcal{C}^1$.

The topological gradient method leads to an asymptotic expansion of the form

$$j(\Omega\backslash\overline{\omega_\rho}) = j(\Omega) + f(\rho)\, g(X_0) + o(f(\rho)),$$

where f is a scalar positive function going to zero with ρ. The function g is called the topological gradient.

In order to minimise j, the best location to insert a small hole ω_ρ in the domain Ω is where g is negative. In fact if $g(X_0) < 0$, we have $j(\Omega\backslash\overline{\omega_\rho}) < j(\Omega)$.

In this section we give a topological asymptotic expansion for the Grad-Shafranov operator. The following Theorem describes the variation of the function j when creating a small hole ω_ρ inside the domain Ω with a Dirichlet boundary condition on $\partial\omega_\rho$.

For all $\rho \geq 0$, $j(\Omega\backslash\overline{\omega_\rho}) = \displaystyle\int_{\Omega\backslash\overline{\omega_\rho}} |\psi_\rho^N - \psi_\rho^D|^2$,

where ψ_ρ^N and ψ_ρ^D are the solutions to the systems

$$\left\{\begin{array}{lll} L\psi_\rho^N & = 0 & \text{in } \Omega\backslash\overline{\omega_\rho}, \\ \dfrac{1}{r}\dfrac{\partial\psi_\rho^N}{\partial n} & = \varphi^N & \text{on } \Gamma, \\ \psi_\rho^N & = 0 & \text{on } \partial\omega_\rho, \end{array}\right. \quad \left\{\begin{array}{lll} L\psi_\rho^D & = 0 & \text{in } \Omega\backslash\overline{\omega_\rho}, \\ \psi_\rho^D & = \varphi^D & \text{on } \Gamma, \\ \psi_\rho^D & = 0 & \text{on } \partial\omega_\rho. \end{array}\right.$$

Theorem: The function j admits the following asymptotic expansion

$$j(\Omega\backslash\overline{\omega_\rho}) = j(\Omega) - \frac{1}{\log(\rho)} g(X_0) + o(-\frac{1}{\log(\rho)})$$

where $g(X) = \dfrac{2\pi}{x}(\psi_0^N(X)\phi_0^N(X) + \psi_0^D(X)\phi_0^D(X))$, $X \in \Omega$. Here ϕ_0^N and ϕ_0^D are the solutions to the associated adjoint problems.

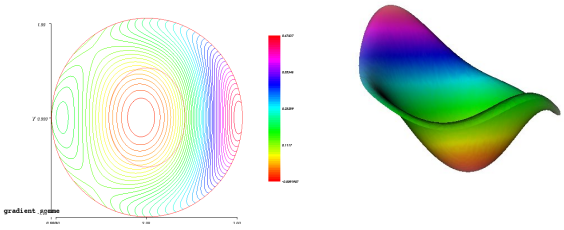

Figure 2: Isovalues(left) and 3D view (right) of the topological gradient g.

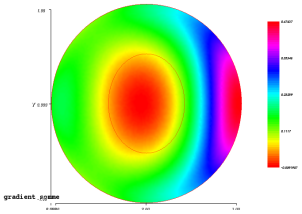

Figure 3: The exact (ellipse $\Omega_p^{ex} = B(Z_0, r_1, r_2)$) and the obtained (red zone) plasma domain.

3 Numerical experiments

We propose a fast and efficient identification procedure. Our numerical algorithm is based on the asymptotic expansion established in the previous Theorem. The unknown plasma boundary is defined by level set curve of the topological gradient $g(X)$ defined for all $X = (x, y) \in \Omega$. Our identification procedure is a one-shot algorithm based on the following steps:

– solve the direct and adjoint problems,

– compute the topological gradient g,

– determine the plasma domain $\Omega_p = \{X \in \Omega;\ g(X) \leq c < 0\}$, where c is chosen in such a way that the function j decreases as much as possible.

We present here the numerical results for one example using the following data:

– the vacuum vessel region is defined by the disc $\Omega = B(Z_0, 1)$, with $Z_0 = (2, 0)$.

– the exact plasma domain is defined by the ellipse $\Omega_p^{ex} = B(Z_0, r_1, r_2)$, with $r_1 = 0.4$ and $r_2 = 0.5$.

The obtained numerical results are described in Figures 2 and 3. One can note that the zone where the topological gradient g is negative (the red region) nearly coincides with the exact plasma domain Ω_p^{ex} (see Fig.3).

The numerical procedure is very fast, accurate and can be extended to real practical situations implying real measerements.

References

[1] Ben Abda A., Hassine M., Jaoua M., Masmoudi M. *Topological sensitivity analysis for the location of small cavities in Stokes flow*, SIAM J. Contr. Optim. **48** (2009), 2871-2900.

[2] Blum J. *Numerical simulation and optimal control in plasma physics with applications to the tokamaks*, Wiley/ Gauthier-Villars Series in Modern Applied Mathematics (1989).

[3] Blum J., Boulbe C., Faugeras B. *Real-time plasma equilibrium reconstruction in a Tokamak*, Proceedings of ICIPE 2008 Conference, Dourdan , France, June 2008.

[4] Masmoudi M. *The topological asymptotics*, Computational Methods for Control Applications, Ed. H. Kawarada and J.Periaux, International Series GAKUTO, 2002.

Reconstruction of multiple cracks using a self regularizing approach

S. Chaabane* M. Jaoua† A. Jaour

Abstract: We present in this paper a self regularizing approach to determine an unknown crack (s) in a bi-dimensional domain Ω using boundary measurements. We develop an identification algorithm based on the Kozlov method and we present some numerical results obtained by using this algorithm.

Keyworlds: Identification, cracks, Kozlov algorithm

1 The Kozlov algorithm with primitive data

We develop in this paper a new approach based on the Kozlov algorithm to determine an unknown linear crack (s) in a domain Ω of $\mathbb{R}^2$ with a smooth boundary Γ. If σ is a linear crack (s) of Ω, we denote by u_σ the solution of the following direct problem:

$$(\mathcal{P}) \begin{cases} -\Delta u_\sigma = 0 & \text{in} \quad \Omega \setminus \sigma, \\ \partial_n u_\sigma = \phi & \text{sur} \quad \Gamma, \\ \partial_n u_\sigma = 0 & \text{sur} \quad \sigma, \\ \int_\Gamma u_\sigma = 0. \end{cases}$$

where $\phi \in L^2(\mathbb{T})$ denotes the current flux such that: $\phi \not\equiv 0$ and $\int_{\mathbb{T}} \phi = 0$.

1.1 Identification of linear crack (s) using the Kozlov algorithm

In this part, we describe the method presented by Azaeiz et al [2] to solve the inverse problem of determining an unknown linear crack (s) σ_u in Ω by using the Kozlov algorithm. Let l be the support line of σ_u which divides Ω into two sub-domains Ω_1 and Ω_2, and let us denote by $\Gamma_i = \Gamma \cap \partial\Omega_i$, $i = 1, 2$. The method consists to solve on each sub-domain Ω_i the Cauchy problem :

$$(\mathcal{C}_i) \begin{cases} -\Delta u_i = 0 & \text{in} \quad \Omega_i, \\ \partial_n u_i = \phi & \text{on} \quad \Gamma_i, \\ u_i = f & \text{on} \quad \Gamma_i, \end{cases}$$

and to compute the jump $[u] = u_1 - u_2$ on the line l. Referring to Andrieux and Ben Abda [1], the crack (s) σ_u describe in the case of identifying flux ϕ the subset of l where the jump not vanish:

$$\sigma_u = \overline{\{x \in l \text{ such that } | \, [u(x)] \, | > 0\}}.$$

To solve the Cauchy problems $(\mathcal{C}_i)$; $i = 1, 2$, the authors apply the Kozlov algorithm.

*FSS–lamha, Sfax, Tunisia slim.chaabane@fsm.rnu.tn,
†Université Française d'Egypte, PO Box 21, Shorouq City, Cairo, Egypt, mb.jaoua@gmail.com

1.2 The Kozlov algorithm with primitive data

By introducing a conformal mapping Ψ transforming the domaine Ω into the unit disk $\mathbb{D}$ of $\mathbb{R}^2$, all the results obtained in this section are also valid in the case of $C^{1,\alpha}$ domain Ω of $\mathbb{R}^2; \alpha \in]0,1[$. So, with no loss of generality, we can assume in the sequel that the domain Ω is the unit disk $\mathbb{D}$ of $\mathbb{R}^2$ and we denote by $\mathbb{D}_1$ and $\mathbb{D}_2$, the upper and lower half disk of $\mathbb{R}^2$:

$$\mathbb{D}_1 = \{z \in \mathbb{D} \text{ such that } Im(z) > 0\} \quad ; \quad \mathbb{D}_2 = \{z \in \mathbb{D} \text{ such that } Im(z) < 0\}$$

Let u solve the problem $(\mathcal{P})$ with $\sigma = \sigma_u$. For $j = 1,\ 2$, we denote by $u_j = u_{|\mathbb{D}_j}$ and by $g_j = u_j + iv_j$, where v_j is the harmonic conjugate function associated to u_j such that $v_j(1) = 0$. We denote by G_j the primitive complex of g_j in the sub-domaine $\mathbb{D}_j$ such that $G_j(1) = 0$.

Given an identifying flux ϕ, there exists two unique functions g and G analytic on $\mathbb{D} \setminus \sigma_u$ and presenting the same discontinuity domain σ_u such that $g_{|\mathbb{D}_j} = g_j$ and $G_{|\mathbb{D}_j} = G_j$ for $j \in \{1,2\}$. In the sequel, we denote by U the real part of G, $F = U_{|\mathbb{T}}$ and $\Phi = \partial_n(U)$ over $\mathbb{T}$. From the Cauchy Riemann equations, we have:

$$F(e^{i\theta}) = -sin(\theta)\int_0^\theta \phi(s)ds + \int_0^\theta sin(s)\,[\phi(s) - f(s)]\,ds \ ; \ \Phi(\theta) = f(\theta)cos(\theta) - sin(\theta)\int_0^\theta \phi(s)ds.$$

The idea, consists then to applay the method presented in the previous section to the primitive data (F, Φ). In that case, the two following advantages show up:

- From the classical theory of regularity in PDE and the Privalov theorem, the function $g_j \in \mathcal{C}^{0,\beta}(\mathbb{D}_j)$; $\beta < 1/2$ and its primitive G_j belong to the Hardy-Holder space $\mathcal{C}^{1,\beta}(\mathbb{D}_j)$. This gain of regularity stabilizes the problem of data completion in each sub-domain $\mathbb{D}_j$; $j = 1, 2$.
- Let $(\varepsilon_n)_{n\in\mathbb{N}}$ be a sequence of $L^p(\mathbb{T})$; $p \in [1, +\infty[$ such that $\lim\limits_{n\to\infty} \|\varepsilon_n\|_{L^p(\mathbb{T})} = 0$ and $f_n = f + \varepsilon_n$ a sequence of noisy data. In the new approach, the function $\pi_n = \int \varepsilon_n$ represents the perturbation term of F and satisfies: $\lim\limits_{n\to\infty} \|\pi_n\|_{W^{1,p}(\mathbb{T})} = 0$. Then, the move from L^p convergence to $W^{1,p}$ convergence smoothes the data and erases the oscillations resulting from the noise, which constitutes what has been called a self regularization. The following numerical tests clearly confirm those observations:

1.3 Numerical results

To illustrate numerically this method, we consider first the case of $\Omega = \mathbb{D}$ and $u = Im(\sqrt{z-a}\,)$ as a solution of the problem $(\mathcal{P})$ with an unknown crack $\sigma_u = [-1, a] \times \{0\}$; $a \in]-1, 1[$. Using the Kozlov algorithm and the new approach, we obtain the following numerical results:

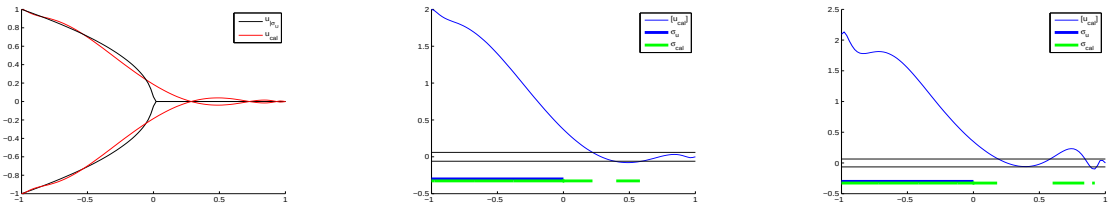

Figure 1: The graph of u in the left, the graph of [u] and reconstruction of σ_u in the middle, reconstruction of σ_u with 5% of noise in the right (Kozlov algorithm).

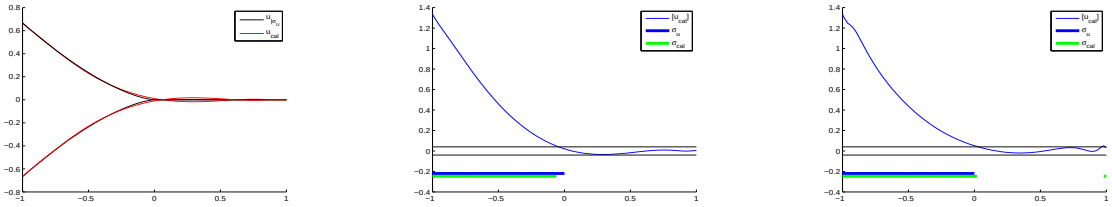

Figure 2: The graph of U in the left, the graph of [U] and reconstruction of σ_u in the middle, reconstruction of σ_u with 5% in the right (The new approach).

For the reconstruction of 2D multiple linear cracks, we obtain by using the Kozlov algorithm and the new approach the following numerical results.

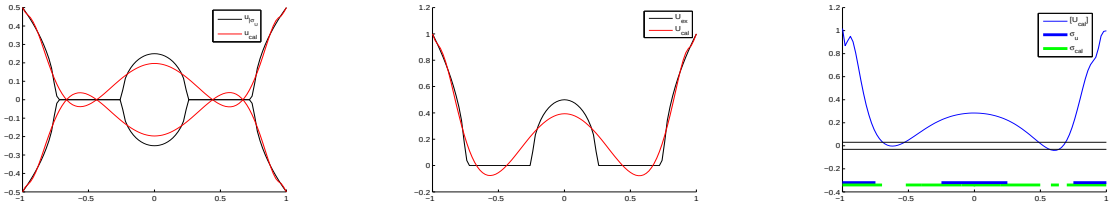

Figure 3: The graph of u in the left, the graph of [u] and reconstruction of σ_u in the middle, reconstruction of σ_u with 5% in the right (Kozlov algorithm).

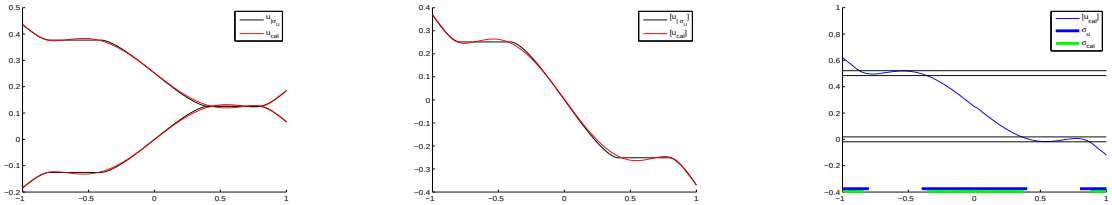

Figure 4: The graph of U in the left, the graph of [U] and reconstruction of σ_u in the middle, reconstruction of σ_u with 5% of noise in the right (The new approach).

References

[1] S. Andrieux and A. Ben Abda. *Identification of planar cracks by complete over determining data: inversion formula*. Inverse Problems **12**, 553-563, 1996.

[2] M. Azaiez, A. Ben Abda and J. Ben Abdallah. *Revesting the Dirichlet to Neumann solver for data complation and application to some inverse problems*. Int. J. of Appl. Math. and Mech.,**1**, 106-121, 2005.

2.8 Control and Stabilization Problems (CSP)

Minisymposium organized by Moez Khenissi

Energie limite et décroissance de l'Energie dans réseau dégénéré

Mohamed Jellouli*

Résumé : Nous présentons dans cet exposé quelques résultats concernant la décroissance de l'énergie (ou de l'énergie locale selon la situation) d'un système formé de cordes vibrantes à faible amplitudes. Ce système est décrit par des d'équations d'ondes définies sur un réseau contenant N branches ($N \geq 3$). Plus précisément, nous nous intéressons à deux cas de figures celui d'un arbre borné et celui d'un arbre contenant une tige de longueur infinie (nous parlerons ici d'énergie locale).
La stabilisation (même forte) d'un réseau demande une condition nécessaire (et parfois suffisante) sur la non rationalité des rapports des longueurs de ses cordes (voir par exemple ([1]) et on distinguera les deux cas : non dégénéré et dégénéré. nous savons que si l'arbre est non dégénéré et sous la présence d'un *feedback* linéaire, l'énergie totale décroît vers zéro mais non exponentiellement (voir les cas [1] et [2]). Notre travail consiste à étudier le comportement de l'énergie $E(t)$ d'un réseau dégénéré, et pour cet effet nous introduisons des opérateurs (voir [3]) qui permettent de calculer l'énergie emmagasinée E_∞ et de déterminer d'une façon optimale la décroissance de $E(t)$ vers E_∞.
Ces travaux sont en collaboration avec M. Mehrenberger (avec une étude numérique en parallèle) dans le cas borné et avec R. Assel et M. Khenissi dans le cas contenant une tige de longueur infinie (en étudiant aussi le problème spectral associé)
Mots clés : Réseau de cordes, décroissance de l'énergie, formule de D'Alembert, opérateur de type τ

1 Formulation Matématique

Les systèmes d'équations des ondes à faibles amplitudes s'écrivent (en se limitant à un arbre générique) :
Cas borné

$$(S_1):\begin{cases}\partial_t^2 u_j(t,x)-\partial_x^2 u_j(t,x)=0, & t>0,\ x\in(0,\ell_j) \text{ et } 1\leq j\leq N\\ u_j(t,\ell_j)=0, & t\geq 0 \text{ et } 2\leq j\leq N \text{ (Dirichlet aux extrémités)}\\ \partial_x u_1(t,0)=\alpha\partial_t u_1(t,0), & t\geq 0\ (\alpha>0 \text{ dissipation à l'origine})\\ u_1(t,\ell_1)=u_j(t,0), & t\geq 0 \text{ et } 2\leq j\leq N \text{ (continuité au nœud)}\\ \partial_x u_1(t,\ell_1)=\sum_{j=2}^N \partial_x u_j(t,0), & t\geq 0 \text{ (Kirchhoff au nœud)}\\ u_j(0,x)=a_j(x) \text{ et } \partial_t u_j(0,x)=b_j(x), & 2\leq j\leq N \text{ et } x\in[0,\ell_j] \text{ (condition de Cauchy)}\end{cases}$$

où $((a_j)_{1\leq j\leq N},(b_j)_{1\leq j\leq N})\in\mathcal{H}:=\prod_{j=1}^N H^2(0,\ell_j)\times\prod_{j=1}^N H^1(0,\ell_j)$, vérifiant les conditions de compatibilités

$$\begin{cases} a_1'(0)=\alpha b_1(0)\\ a_1'(\ell_1)=\sum_{j=2}^N a_j'(0)\end{cases} \quad \text{et } \forall 2\leq j\leq N, \begin{cases} a_j(\ell_j)=0,\\ a_1(\ell_1)=a_j(0).\end{cases} \tag{1}$$

On définie l'énergie totale $E(t)$ du système (S_1) par,

$$E(t)=\frac{1}{2}\sum_{j=1}^N \|\partial_t u_j(t)\|^2_{L^2(0,\ell_j)}+\frac{1}{2}\sum_{j=1}^N \|\partial_x u_j(t)\|^2_{L^2(0,\ell_j)}\,. \tag{2}$$

*Faculté des sciences de Monastir, mohamed.jellouli@fsm.rnu.tn,

Cas non borné Dans le cas où l'arbre contient une branche de longueur infinie, nous étudions le système dissipatif suivant

$$(S_2):\begin{cases}\partial_t^2 u_j(t,x)-\partial_x^2 u_j(t,x)=0, & t>0,\ x\in(0,\ell_j) \text{ et } 1\le j\le N\\ \partial_t^2 u_\infty(t,x)-\partial_x^2 u_\infty(t,x)=0, & t>0,\ x\in(0,\ell_\infty),\ \ell_\infty=+\infty\\ u_j(t,\ell_j)=0, & t\ge 0 \text{ et } j\in\{1,\cdots,N\}\\ u_j(t,0)=u_\infty(t,0), & t\ge 0 \text{ et } 1\le j\le N\\ \partial_x u_\infty(t,0)+\sum_{j=1}^N \partial_x u_j(t,0), & t\ge 0\\ u_j(0,x)=a_j(x) \text{ et } \partial_t u_j(0,x)=b_j(x), & j\in\{1,\cdots,N,\infty\} \text{ et } x\in[0,\ell_j]\end{cases}$$

où

$$((a_j)_{1\le j\le N},a_\infty,(b_j)_{1\le j\le N},b_\infty)\in\widetilde{\mathcal{H}}:=\prod_{j=1}^N H^2(0,\ell_j)\times\dot{H}^1\cap H^2(0,+\infty)\times\prod_{j=1}^N H^1(0,\ell_j)\times\dot{H}^1 \quad (3)$$

vérifiant les conditions de compatibilités

$$\sum_{j=2}^N a_j'(0)+a_\infty'(0)=0 \ \text{ et } \forall 1\le j\le N,\begin{cases} a_j(\ell_j)=0,\\ a_j(0)=a_\infty(0).\end{cases} \quad (4)$$

L'énergie locale est définit pour un $R>0$ par :

$$\begin{aligned}E_R(t)=\tfrac{1}{2}\Big(\|\partial_t u_\infty(t)\|^2_{L^2(0,R)}+\textstyle\sum_{j=1}^N\|\partial_t u_j(t)\|^2_{L^2(0,\ell_j)}\Big)+\\ \tfrac{1}{2}\Big(\|\partial_x u_\infty(t)\|^2_{L^2(0,R)}+\textstyle\sum_{j=1}^N\|\partial_x u_j(t)\|^2_{L^2(0,\ell_j)}\Big).\end{aligned} \quad (5)$$

Les énergies (2) et (5) vérifient les conditions de dissipations respectives:

$$E(t)=E(0)-\alpha\int_0^t|\partial_t u_1(s,0)|^2\ ds \quad (6)$$

et

$$E_R(t)=E_R(0)-\int_0^t|\partial_t u_\infty(s,R)|^2\ ds. \quad (7)$$

2 Résultats

Dans toute la suite, on supposera que toutes les longueurs finies sont égales : $\ell_j=\ell$.

Théorème 1 *Si $((a_j)_{1\le j\le N},(b_j)_{1\le j\le N})\in\mathcal{H}$ vérifiant (1), alors l'énergie limite de la solution du système (S_1) est donnée par*

$$E_\infty=\frac{1}{2(N-1)}\sum_{j=2}^N\sum_{k=j+1}^N\Big(\|(a_k'-a_j')\|^2_{L^2(0,\ell)}+\|(b_k-b_j)\|^2_{L^2(0,\ell)}\Big). \quad (8)$$

Le théorème suivant exprime la nature de la décroissance de $E(t)$ vers E_∞.
On note $\alpha_0=\frac{2\sqrt{N-1}}{N}$, $\Delta=\frac{4(\alpha^2N^2-4N+4)}{(\alpha+1)^2}$ et $\lambda=-\frac{\frac{2(N-2)}{\alpha+1}+\sqrt{\Delta}}{2N}$. [1] [2]

Théorème 2 *Il existe une constante $C=C_N(\alpha)>0$ telle que pour toute donnée $((a_j)_{1\le j\le N},(b_j)_{1\le j\le N})\in\mathcal{H}$ vérifiant (1),*

$$E(t)-E_\infty\le C\Big(\|a_1\|_1^2+\|b_1\|^2+\Big\|\sum_{j=2}^N a_j\Big\|_1^2+\Big\|\sum_{j=2}^N b_j\Big\|^2\Big)\frac{e^{-\gamma t}}{|\Delta|},\ \textit{if } \alpha\neq\alpha_0 \quad (9)$$

[1] $\sqrt{\Delta}=i\sqrt{-\Delta}$ si $\Delta<0$
[2] Notons que $\Delta<0$ (resp. $\Delta=0$) si et seulement si $\alpha\in]0,\alpha_0[$ (resp. $\alpha=\alpha_0$)

et

$$E(t)-E_\infty \le C\left(\|a_1\|_1^2+\|b_1\|^2+\left\|\sum_{j=2}^N a_j\right\|_1^2+\left\|\sum_{j=2}^N b_j\right\|^2\right)t^2e^{-\gamma_0 t},\ \text{if } \alpha=\alpha_0 \tag{10}$$

où $\gamma=\frac{1}{\ell}\log\frac{1}{|\lambda|}>0$ *et* $\gamma_0=\frac{1}{\ell}\log\frac{N+2\sqrt{N-1}}{N-2}$.

Consernant le système (S_2), on considère des données initiales dans $\widetilde{\mathcal{H}}$ vérifiant les conditions (4). On note

$$h=\sum_{j=1}^N\left(\mathcal{L}^+a_j'+\mathcal{L}^-b_j\right)\quad\text{et}\quad h_\infty=a_\infty'+b_\infty.$$

Théorème 3 *Soient* $R=2l$ *et* u *la solution de* (S_2) *alors*

$$\lim_{t\to+\infty}E_R(t)=E_R(\infty)=\frac{1}{2N}\sum_{1\le i<j\le N}\left(\left\|a_i'-a_j'\right\|_{L^2(0,l)}^2+\|b_i-b_j\|_{L^2(0,l)}^2\right),$$

et pour tout $t\ge 2R$, *on a*

$$C_1\left\|\frac{N-1}{2N}h+h_\infty\right\|_{L^2(0,2l)}^2e^{-\gamma t}\le E_R(t)-E_R(\infty)\le C_2\left\|\frac{N-1}{2N}h+h_\infty\right\|_{L^2(0,2l)}^2e^{-\gamma t}$$

où $C_1=\frac{N}{(N-1)^2}$, $C_2=\frac{N(N+1)^4}{(N-1)^6}$ *et* $\gamma=\dfrac{1}{l}\ln\left(\dfrac{N+1}{N-1}\right)$.

La preuve de ces théorèmes utilisent les opérateurs de type $\mathcal{T}$ dont le définition est (voir [2] et [3])

Définition 1 *Soient* $m=(m(j))_{j\ge1}$ *une suite réelle strictement croissante tendant vers* $+\infty$ *avec* $m(1)=0$ *et* $\gamma=(\gamma(j))_{j\ge1}$ *une suite complexe, on appelle opérateur de type* $\mathcal{T}$ *associé à ces deux suites, l'opérateur qui à une fonction causale* f *associe la fonction*

$$\mathcal{P}f(t)=\sum_{j=1}^q\gamma(j)f(t-m(j))\ ,\quad q\ge1\ \text{et}\ t\in]m(q),m(q+1)[.$$

L'intérêt principal de ces opérateurs, c'est qu'ils permettent d'exprimer suite à des opérations algébriques, les traces $\partial_t u_1(t,0)$ et $\partial_t u_\infty(t,R)$ (qui appraissent dans (6) et (7)) à l'aide des données initiales du problème correspondant.

References

[1] K. Ammari, M. Jellouli and M. Khenissi, *Stabilization of Generic Tree of String.* Journal of Dynamical and control System, Vol. 11, No. 2, April 2005, 177-193.

[2] K. Ammari and M. Jellouli, *Remark on Stabilization of Tree-Shaped Networks of Strings.* Application of Mathematics, Vol. 52, No. 4, 2007, 327-343.

[3] K. Ammari and M. Jellouli, *Méthode numérique pour la décroissance de l'énergie d'un réseau de cordes.* Bulletin of the Belgian Mathematical Socity-Simon Stevin, 4 (2010), 717-735.

[4] R. Dáger and E. Zuazua, *Controllability of tree-shaped networks of vibrating strings.* C. R. Acad. Sci Paris. Sér. I Math., 332 (2001), 1087-1092.

[5] R. Dáger and E. Zuazua, *Obsevation and control of vibration in tree-shaped networks of strings.* SIAM J. Control, 43 (2004), 590-623.

[6] G. Leugering and E. Zuazua, *Exact controllability of generic trees.* ESAIM Proc. 8 (2000), 95-105.

[7] J. Lagnese, G. Leugering and E.J.P.G. Schmidt, *Modeling, Analysis of Dynamic Elastic Multi-link Structures.* Birkh. . . auser

Stability estimates for the Calderón problem with partial data

Dos Santos Ferreira *

Abstract

This work is a follow up of a previous one where we proved local stability estimates for a potential in a Schrödinger equation on an open bounded set in dimension $n = 3$ from the Dirichlet-to-Neumann map with partial data. The region under control was the penumbra delimited by a source of light outside of the convex hull of the open set. These local estimates provided stability of log-log type corresponding to the uniqueness results in Calderón's inverse problem with partial data proved by Kenig, Sjöstrand and Uhlmann and relied on a quantitative version of the micro local version of Helgason's support theorem based on Kashiwara's Watermelon theorem. In this work, we prove the corresponding global estimates in all dimensions higher than three. The estimates are based on the construction of solutions of the Schrödinger equation by complex geometrical optics developed in the anisotropic setting by Dos Santos Ferreira, Kenig, Salo and Uhlmann to solve the Calderón problem in certain admissible geometries and relies on known stability estimates of the geodesic ray transform on caps of the hypersphere. This is a joint work with Pedro Caro and Alberto Ruiz.

*Institut Élie Cartan, Université de Lorraine France

WELL-POSEDNESS AND ASYMPTOTIC STABILITY FOR THE LAMÉ SYSTEM WITH INFINITE MEMORIES IN BOUNDED DOMAIN

AHMED BCHATNIA* AND AISSA GUESMIA**

Abstract. In this work, we consider the Lamé system in 3-dimension bounded domain with infinite memories. We prove, under some appropriate assumptions, that this system is well posed and still stable, and we get a general and precise estimate on the convergence of solutions to zero at infinity in term of the growth of the infinite memories.

Let Ω be a bounded domain in $\mathbb{R}^3$ with smooth boundary $\partial\Omega$. Let us consider the following Lamé system with infinite memories:

$$\begin{cases} u'' - \Delta_e u + \displaystyle\int_0^{+\infty} g(s)\Delta u(t-s)ds = 0, & \text{in } \Omega \times \mathbb{R}_+, \\ u = 0, & \text{on } \partial\Omega \times \mathbb{R}_+ \end{cases} \tag{0.1}$$

with initial conditions

$$\begin{cases} u(x,-t) = u_0(x,t), & \text{in } \Omega \times \mathbb{R}_+, \\ u'(x,0) = u_1(x), & \text{in } \Omega, \end{cases} \tag{0.2}$$

where $' = \frac{\partial}{\partial t}$, u_0 and u_1 are given history and initial data. Here Δ_e denotes the elasticity operator defined by

$$\Delta_e u = \mu\Delta u + (\lambda+\mu)\nabla \div u, \quad u = (u_1, u_2, u_3)^T$$

and λ and μ are the Lamé constants which satisfy the conditions

$$\mu > 0, \quad \lambda + \mu \geq 0. \tag{0.3}$$

Moreover,

$$g(s) = \begin{pmatrix} g_1(s) & 0 & 0 \\ 0 & g_2(s) & 0 \\ 0 & 0 & g_3(s) \end{pmatrix},$$

where $g_i : \mathbb{R}_+ \to \mathbb{R}_+$ are given functions, which represent the terms of dissipation.

Our aim in this work is to prove that the stability and/or bounded of our system holds with infinite memories and getting a general decay connection (exponential or polynomial or others) between the decay rates of the solutions and the growth of the memory functions. Now, we give our main stability results.

Theorem 1. *Assume that (0.3) and (H1)-(H3) are satisfied such that (??) holds or there exists a positive constant m_i satisfying*

$$\int_\Omega \left|\nabla \eta_0^i\right|^2 dx \leq m_i, \ \forall s \in \mathbb{R}_+. \tag{0.4}$$

Date: December 1, 2013.

1991 *Mathematics Subject Classification.* 35B37, 35B40, 35L55.

Key words and phrases. Well-posedness; General decay; Asymptotic behavior; Infinite memory; Lamé system; Semigroup theory; Energy method.

Then there exist positive constants c', c'' and ϵ_0 for which E satisfies

$$E(t) \leq c'' e^{-c't}, \quad \forall t \in \mathbb{R}_+ \tag{0.5}$$

if (??) is satisfied, for any $i = 1, 2, 3$, and

$$E(t) \leq c'' G_1^{-1}(c't), \quad \forall t \in \mathbb{R}_+ \tag{0.6}$$

otherwise, where

$$G_1(s) = \int_s^1 \frac{1}{\tau G'(\epsilon_0 \tau)} d\tau \ (s \in]0, 1]). \tag{0.7}$$

REFERENCES

[1] F. ALABAU-BOUSSOUIRA AND V. KOMORNIK, Boundary observability, controllability and stabilization of linear elastodynamic systems, SIAM J. Control and Optim., 37 (1999), 521-542.

[2] F. ALABAU-BOUSSOUIRA, P. CANNARASA AND V. KOMORNIK, Indirect internal stabilization of weakly coupled evolution equations, J. Evol. Equa., 2 (2002), 127-150.

[3] A. BCHATNIA AND M. DAOULATLI, Behavior of the energy for Lame systems in bounded domains with nonlinear damping and external force, Electron. J. Diff. Equa., 2013 (2013), 1-17.

[4] C. M. DAFERMOS, Asymptotic stability in viscoelasticity, Arch. Ration. Mech. Anal., 37 (1970), 297–308.

[5] C. GIORGI, J. E. MUOZ RIVERA AND V. PATA, Global attractors for a semilinear hyperbolic equation in viscoelasticity, J. Math. Anal. Appl., 260 (2001), 83–99.

[6] A. GUESMIA, Asymptotic stability of abstract dissipative systems with infinite memory, J. Math. Anal. Appl., 382 (2011), 748-760.

[7] A. GUESMIA AND S. MESSAOUDI, A general decay result for a viscoelastic equation in the presence of past and infinite history memories. Nonlinear Analysis, 13 (2012), 476-485.

[8] M. A. HORN, Implications of sharp trace regularity results on boundary Stabilization of the system of linear elasticity, J. Math. Anal. Appl., 223 (1998), 126-150.

[9] M. A. HORN, Stabilization of the dynamic system of elasticity by nonlinear boundary feedback, Internal Ser. Numer. Math., 133 (1999), 201-210.

[10] B. V. KAPITONOV, Uniform stabilization and exact controllability for a class of coupled hyperbolic systems, Comp. Appl. Math., 15 (1996), 199-212.

[11] V. KOMORNIK, Exact Controllability and Stabilization. The Multiplier Method, Masson-John Wiley, Paris, 1994.

[12] V. KOMORNIK, Boundary stabilization of linear elasticity systems, Lecture Notes in Pure and Appl. Math., 174 (1995), 135-146.

[13] J. E. LAGNESE, Boundary stabilization of linear elastodynamic systems, SIAM J. Control and Optim., 21 (1983), 968-984.

[14] J. E. LAGNESE, Uniform asymptotic energy estimates for solution of the equation of dynamic plane elasticity with nonlinear dissipation at the boundary, Nonlinear Anal. T. M. A., 16 (1991), 35-54.

[15] P. MARTINEZ, Stabilisation de systèmes distribués semi linéaires : domaines presques étoilés et inégalités intégrales généralisées, Ph. D. Thesis, Louis Pasteur university, France, 1998.

[16] A. PAZY, Semigroups of linear operators and applications to partial differential equations, Springer-Verlaag, New York, 1983.

[17] L. TEBOU, Energy decay estimates for some weakly coupled Euler-Bernoulli and wave equations with indirect damping mechanisms, MCRF, 2 (2012), 45-60.

*DEPARTMENT OF MATHEMATICS, FACULTY OF SCIENCES OF TUNIS, UNIVERSITY OF TUNIS EL MANAR, CAMPUS UNIVERSITAIRE 2092 - EL MANAR 2, TUNIS, TUNISIA.

E-mail address: ahmed.bchatnia@fst.rnu.tn

** LABORATORY OF MATHEMATICS AND APPLICATIONS OF METZ, BAT. A, LORRAINE - METZ UNIVERSITY, ILE DE SAULCY, 57045 METZ CEDEX 01, FRANCE.

E-mail address: guesmia@univ-metz.fr

NONLINEAR CONTROL FOR THE RADIATIVE-CONDUCTIVE HEAT TRANSFERT SYSTEMS

Mohamed Ghattassi* Mohamed Boutayeb† Jean Rodolphe Roche‡

Abstract: This contribution concerns the problem of finite dimensional control for a class of systems described by nonlinear hyperbolic-parabolic coupled partial differential equations (PDE's). Initially, Galerkin's method is applied to the PDE system to derive a nonlinear ordinary differential equation (ODE) system that accurately describes the dynamics of the dominant (slow) modes of the PDE system. After, we introduce a useful nonlinear controller to assure stabilization under convex sufficient conditions.

Keywords: Nonlinear control, Radiative transfer equation, Nonlinear heat equation, Galerkin method, Linear Matrix Inequalities (LMIs).

1 Introduction

A large number of industrially important transport-reaction processes are inherently nonlinear and are characterized by significant spatial variations because of the underlying diffusion and convection phenomena. Representative examples include rapid thermal processing, plasma reactors, and crystal growth processes, to name a few. The mathematical models which describe the spatiotemporal behavior of these processes are typically obtained from the dynamic conservation equations and consist of systems of parabolic and hyperbolic partial differential equations (PDEs). The main feature of parabolic PDE systems is that the eigenspectrum of the spatial differential operator can be partitioned into a finite-dimensional slow one and an infinite-dimensional stable fast complement [1]. Motivated by this fact, a typical approach to the control design of linear or semilinear parabolic PDE systems is to obtain an approximate ordinary differential equation (ODE) representation of the original PDE system by utilizing the spatial discretization techniques, which is then used for controller design purposes by applying different existing ODE-based linear or nonlinear control techniques. The standard Galerkin method was used to derive a finite-dimensional ODE model.

In this note, we construct a boundary controller to establish the stability of the coupled radiative-conductive heat transfer systems in the finite dimensional. Through Lyapunov analysis we established sufficient conditions for stability by the feasibility of the finite-dimensional Linear Matrix Inequalities(LMI)[4, 3].

2 The feedback control problem

Let $\mathcal{D} = \left\{\beta \in \mathbf{R}^2 : |\beta| \leqslant 1\right\}$ the unit disk, Ω a bounded domain in $\mathbf{R}^2$ and $t \in [0, \tau]$, for $\tau > 0$. Let $\mathbf{n}$ be the outward unit normal to the boundary $\partial\Omega$. We denote

$$\partial\Omega_- = \{(s, \beta) \in \partial\Omega \times \mathcal{D} \text{ such that } \beta.\mathbf{n} < 0\} \tag{1}$$

*UL–IECL, mohamed.ghattassi@univ-lorraine.fr,
†UL–CRAN, mohamed.boutayeb@univ-lorraine.fr,
‡UL–IECL, jean-rodolphe.roche@univ-lorraine.fr

The unknown of the RTE is the radiation intensity denoted $I(t, s, \beta)$ given at time t, position s and in the direction β. The unknown of the nonlinear heat equation is the temperature $T(t, s)$ at time t and position s. The RTE is given by (see,[2])

$$\beta.\nabla_s I(t, s, \beta) + \kappa I(t, s, \beta) = \kappa I_b(T(t, s)) \qquad \text{for } (t, s, \beta) \in [0, \tau] \times \Omega \times \mathcal{D} \tag{2a}$$

$$I(t, s, \beta) = I_b(T(t, s)) \qquad \text{for } (t, s, \beta) \in [0, \tau] \times \partial\Omega_- \tag{2b}$$

where κ is the absorption coefficient of the medium and $I_b(T)$ is the radiation intensity of the blackbody with, T, the temperature of the medium:

$$I_b(T) = \frac{\sigma_B}{\pi} T^4 \tag{3}$$

where $\sigma_B = 5.6698 \times 10^{-8}\ Wm^{-2}K^{-4}$ is the Stefan-Boltzmann constant.

Emission and absorption of radiation by the medium lead to a radiative source term in the energy equation function of $I_b(T)$ and the incident radiation intensity G defined by:

$$G(t, s) = \int_{\mathcal{D}} I(t, s, \beta)\ d\beta \qquad \text{for } (t, s) \in [0, \tau] \times \Omega. \tag{4}$$

The radiative transfer equation is strongly coupled by the incident radiation intensity G and the temperature T with the following nonlinear heat equation:

$$\rho c_p \frac{\partial T}{\partial t}(t, s) - k_c \triangle T(t, s) = \Psi(T(t, s)) \quad (t, s) \in [0, \tau] \times \Omega \tag{5}$$

where Ψ is a nonlinear function defined by $\Psi = 4\kappa G - 4\kappa\sigma_B T^4$. The equation (5) is associated with Dirichlet boundary conditions and the initial condition $T(0, s) = T_0(s)\ s \in \Omega$. The data ρ, c_p, and k_c are the density, the specific heat capacity, and the thermal conductivity of the medium, respectively.

In this work, we explore the Discontinuous and Continuous Galerkin method's to approximate the radiative transfer equation and the nonlinear heat equation, respectively. The Galerkin approximation for the nonlinear heat equation (5) has the following form

$$\mathbb{M}_h \dot{T}_h = \mathbb{A}_h T_h + \mathbb{B}_h U_h + \Psi_h(T_h), \tag{6}$$

where $\mathbb{M}_h, \mathbb{A}_h \in \mathcal{M}_N(\mathbf{R})$ and $\mathbb{B}_h \in \mathcal{M}_{N,n}(\mathbf{R})$ are the matrices of the Galerkin approximation method. $\mathbb{M}_h$ is a symmetric positive definite matrix and $\mathbb{A}_h$ is a negative definite matrix. $\Psi_h(T_h) \in \mathbf{R}^N$ is approximation of the nonlinear function $\Psi(T)$. $U_h \in \mathbf{R}^n$ is the input vector of boundary control.

We consider the following nonlinear control:

$$U_h = -\mathbb{K}_1 T_h - \mathbb{K}_2 \Psi_h(T_h), \tag{7}$$

where $\mathbb{K}_1$ and $\mathbb{K}_2$ are the control gain matrices. Using the Linear Matrix Inequality (LMI), we establish a convex sufficient conditions, such that a nonlinear control (7) guarantee the stabilization of the nonlinear systems.

References

[1] H. O. Fattorini. *Boundary Control Systems.* SIAM Journal on Control: Vol. 6, No. 3 :349-385, 1968.

[2] Asllanaj, F. and Jeandel, G. and Roche, J. R. *Numerical solution of radiative transfer equation coupled with nonlinear heat conduction equation.* International Journal of Numerical Methods for Heat & Fluid Flow: Vol. 11(5-6):449-472, 2001.

[3] Grandvallet, B. and Zemouche, A. and Souley-Ali, H. and Boutayeb, M. *New LMI Condition for Observer-Based $\mathcal{H}_\infty$ Stabilization of a Class of Nonlinear Discrete-Time Systems.* SIAM Journal on Control and Optimization: Vol. 51, No. 1 :784-800, 2013.

[4] Boyd, Stephen and Ghaoul, Laurent El and Feron, Eric and Balakrishnan, Venkataramanan. *Linear Matrix Inequalities in System and Control Theory.* SIAM, 1994.

2.9 Control of diffusion equations: Numerical methods (NM)

Minisymposium organized by Sidi Mahmoud Kaber and Faker Ben Belgacem

Variational formulations for the numerical resolution of control and inverse problems for the heat equation

Arnaud Munch *

Abstract

We address in this talk the numerical resolution of controllability problems as well as inverse problems for the heat equation posed in bounded domain. Due to the intrinsic strong regularization property of the heat operator, such kind of problems are generally ill-posed numerically. We present space-time variational formulations which allow to solve directly the optimality conditions related to some quadratic functionals usually introduced in control or inverse problem theory (for instance, least-squares type functional). In particular, such direct approach avoid in particular the use of iterative minimization process which may fail to converge numerically. The well-posedeness of such formulation as well as the numerical approximations are discussed.

*Université Blaise Pascal (Clermont-Ferrand, France)

Optimal observation of parabolic equations

Yannick Privat*

Abstract

In this talk, we consider parabolic equations on a bounded open connected subset of $\mathbb{R}^n$. We model and investigate the problem of optimal shape and location of the observation domain having a prescribed measure. We show that it is relevant to consider a spectral optimal design problem corresponding to an average of the classical observability inequality over random initial data. We prove that, under appropriate sufficient spectral assumptions, this optimal design problem has a unique solution, depending only on a finite number of modes, and that the optimal domain is semi-analytic and thus has a finite number of connected components. Our results cover the case of the Stokes equations.

*CNRS (Paris, France)

Parareal in time intermediate targets methods for optimal control problem

Mohamed Kamel Riahi*

Abstract

We present a time parallel method to solve the Euler-Lagrange system associated with the optimal control of a parabolic equation. Our approach, which gives rise to independent sub-problems, is based on both the definition and the iterative update of a sequences of intermediate targets and initial conditions. In order to accelerate the timeresolution, this method is coupled with the parareal in time algorithm. Numerical experiments show the efficiency of the methods.

*INRIA-Saclay, France

Ill-Conditioning versus Ill-Posedness for the boundary Controllability of the Heat Equation

Sidi-Mahmoud Kaber*

Abstract

Ill-posedness and/or Ill-conditioning are features users have to deal with appropriately in the controllability of diffusion problems for secure and reliable outputs. We investigate those issues in the case of a boundary Dirichlet control, in an attempt to underline the origin of the troubles arising in the numerical computations and to shed some light on the dificulties to obtain good quality simulations. The exact controllability is severely ill-posed while, in spite of its well-posedness, the null-controllability turns out to be very badly ill-conditioned. Theoretical and numerical results are stated on the heat equation in one dimension to illustrate the speci

c instabilities of each problem. The main tools used here are first a characterization of the subspace where the HUM control lies and the study of the spectrum of some structured matrices, of Pick and Lowner type, obtained from the Fourier calculations on the state and adjoint equations.

*Université Pierre et Marie Curie, (Paris, France)

Contributed talk abstracts

3.1 Boundary and cracks recovery (BCR)

Identification of fractures in porous medium

F. Cheikh* H. Ben Ameur† G. Chavent‡ V. Martin§ J.E. Roberts¶

Abstract: We consider the problem of identifying fractures as the least squares minimization of a function evaluating the misfit between a measured pressure and that calculated using a particular reduced discrete model for flow in porous media with fractures. Inspired by the idea of refinement indicators [2], we use fracture indicators to find the fractures as well as their hydraulic properties through an iterative process.
Keyworlds: inverse problems, flow in porous media, fracture indicators, parameter estimation.

The object of this communication is to present a method for identifying fractures in a porous medium as well as their hydraulic conductivity by means of fracture indicators. The idea of the method is to assume that the fractures lie on the edges of the mesh, and thus to avoid remeshing during the process.

1 The discrete fracture model

The forward model that we use is a reduced discrete fracture model for flow in a fractured porous medium, [1]. In this model the fractures are considered to be interfaces of co-dimension 1. Flow in the n-dimensional porous medium as well as that in the $(n-1)$-dimensional fracture, itself also a porous medium, is governed by Darcy's law together with the equation for mass conservation. Flow in the two media is coupled: the discontinuity of the flux across the fracture serves as a source/sink term for flow in the fracture, whereas the pressure in the fracture is used to give a Robin boundary condition on the fracture for the flow problem in the domain minus the fracture. We discretize this model with a mixed finite element or a finite volume method. The unknown values for the model are a value for the pressure at the center of each element of the discretization grid. We suppose that a fracture coincides with a "connected" subcollection of the interior edges of the grid, *i.e.* a subcollection the union of whose elements is a connected set. We also suppose that this subcollection consists of more than one edge.

2 The inverse problem

The above model depends on a parameter representing the effective permeability in the fractures. The problem of the identification of the fractures can be seen as a parameter estimation problem in which the parameter to be estimated is the effective permeability in the fractures. The least squares objective function for the estimation of these parameters is

$$J(\kappa) = \sum_{T \in \mathcal{T}_h} \left| P_T - \overline{P}_T \right|^2,$$

where $\mathcal{T}_h$ is the grid and $\forall T \in \mathcal{T}_h$, P_T is the pressure at the center of T given by the model with parameter κ and $\overline{P}_T$ is the corresponding measured pressure. To minimize J we calculate its gradient using the adjoint method. The parameter $\kappa \geq 0$ is assumed to have one constant value for each interior edge of $\forall T \in \mathcal{T}_h$. Since the location of the fracture is not known, the parameter κ contains *a priori* a value for each grid edge. However the fracture indicators reduce the size of the space where the parameters are looked for and hopefully help locating the fractures.

*ENIT–Lamsin, Tunis, Tunisia /INRIA Paris-Rocquencourt, France, cheikhfatmaenit@yahoo.fr,
†ENIT–Lamsin,Tunis, Tunisia, hbenameur@yahoo.ca,
‡INRIA Paris-Rocquencourt, France, guy.chavent@inria.fr,
§UTC, Compiègne, France, vincent.martin@utc.fr,
¶INRIA Paris-Rocquencourt, France, jean.roberts@inria.fr.

3 Fracture indicators

The strategy for localizing the fractures is based on the use of fracture indicators. We first define a set $\mathcal{S}$ of potential fractures, *i.e.* a set of acceptable (connected and containing more than one element) subcollections of the set of all interior edges. Then we define a fracture indicator function $\mathcal{I}$ that to each potential fracture $F \in \mathcal{S}$ associates a value dependent on the gradient of J as follows: for $F \in \mathcal{S}$ and $\epsilon > 0$, we define a parameter $\kappa(F, \epsilon)$ which has value ϵ on each edge belonging to F and value ϵ^2 on each other interior edge. Then the indicator has the value

$$\mathcal{I}(F) = \lim_{\epsilon \to 0^+} \frac{d}{d\epsilon} J(\kappa(F, \epsilon)).$$

The actual calculation of these indicators is quite simple. Two pressure values are obtained for each interior edge of the grid, one from the solution of the direct problem with no fractures and the other from the solution of the corresponding adjoint problem. (This calculation is completely independent of the set $\mathcal{S}$ of potential fractures and is only performed once.) From these values, a direct calculation gives for each pair (E, N), where E is an interior edge and N is a vertex of E, a flux along E in the direction of N. We obtain both state fluxes $V_{E,N}$ and adjoint fluxes $\nu_{E,N}$. We then put

$$\mathcal{I}(F) = \sum_{E \in F} \sum_{N \subset E} V_{E,N} \nu_{E,N}.$$

For the potential fractures F giving the largest (or close to the largest) value of the indicator, we now minimize the cost function J associated with the model in which F is considered to be a fracture, and we select the potential fracture F for which the minimized cost function is least. The minimization yields the value for the effective hydraulic conductivity κ. For the moment we consider only constant parameters. Several iteration strategies are considered.

4 Numerical result

We show a preliminary numerical result in which the domain, the square $(0, 3) \times (0, 3)$, contains one vertical fracture centrally located and of length 1.5 (depicted in blue in the Figure). The fracture connects two rectangles of size 1.5 by 1 in the lower left and the upper right corners in which the hydraulic conductivity is 10 times greater than that in the rest of the domain, except the fracture where the effective conductivity is 20 times greater. The domain is impermeable on top and bottom and has a pressure drop from left to right.

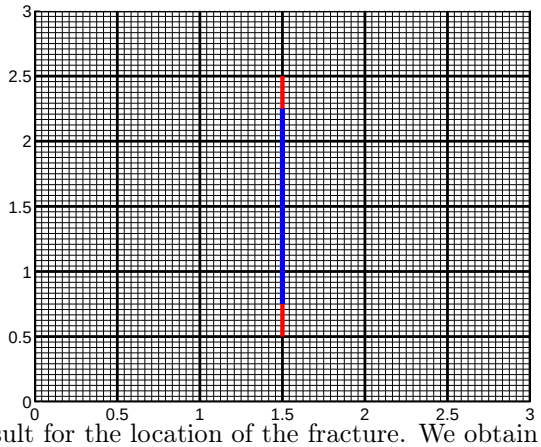

Using our method, we obtain a very reasonable result for the location of the fracture. We obtain the actual fracture but with its length extended by .25 on top and on bottom (by the portion in red in the Figure). However the permeability that we obtain is quite off the mark (8.51 instead of 20) as the cost function is very flat making it very difficult to obtain a correct minimum.

References

[1] V.Martin, J.Jaffré, J.E. Roberts. Modeling fractures and barriers as interfaces for flow in porous media. *SIAM J.Sci.Comput.*. 26,(5),1667-1691, 2005.

[2] H. Ben Ameur and G. Chavent and J. Jaffré. Refinement and coarsening indicators for adaptive parameterization application to the estimation of hydraulic transmissivities. *Inverse Problems* 775-794; 2002.

Submarine Groundwater Discharge as an inverse problem

Nejla Tlatli Hariga * Thouraya Nouri Baranger† Rachida Bouhlila‡

Abstract: The considered inverse problem concerns the interface land-sea identification and submarine groundwater exchange estimation from the known of over-specified boundary conditions on a part of the domain boundary. The approach consists on solving iteratively a data completion problem on a fictitious domain, which can be rather larger or smaller than the real one, and identifying the land-sea interface at the null hydraulic head isovalue then the water fluxes on this boundary represent the exchanged flow between the sea and the aquifer.
Keyworlds: Submarine Groundwater, Inverse Problem, Data Completion, Interface Identification, Energy Functional.

Résume : Nous présentons içi un problème inverse d'identification de l'interface entre un aquifére côtier et la mer, et par suite de la quantité d'eau échangée, à partir de la connaissance de données surabondantes sur une partie de la frontière du domaine. La démarche adoptée est itérative et consiste à résoudre un problème de Cauchy sur un domaine fictif, qui peut être plus grand ou plus petit que le domaine réel, ensuite l'interface est localisée comme étant l'isovaleur à charge hydraulique nulle et le flux d'eau à travers cette frontière représente le débit échangé entre la nappe et l'océan.
Mots clés : Eaux soutérraines soumarines, Problème Inverse, Complétion de données, Identification d'interface, Fonctionnelle energétique.

1 Introduction

Exchange of water between the sea and coastal aquifers is now recognized as being an important parameter for near shore marine water and groundwater systems. The oceanographic community divides this exchange into a submarine groundwater discharge (SGD), the flux of fresh water from the continent to the ocean, and a submarine groundwater recharge (SGR), the flux of seawater from the ocean to the aquifer. The net flux is therefore the difference between these parameters, known as submarine groundwater exchange (SGE) [5].
The numerical models and software used in SGE simulations vary in complexity, but all of them have in common the solution of a forward well-posed problem with a **given** land-sea interface [3, 4]. However, many deep coastal aquifers extend far under the sea-bed and, generally, little is known about the extension of these aquifers beyond the shoreline. When studying and modeling these aquifers, researchers are often led to fixing an arbitrary limit to which a null piezometric level is assigned. This statement represents the hydraulic contact between the aquifer and the ocean. It is clear that the position of this limit influences the piezometric distribution of the entire aquifer as well as the exchanges of water between the aquifer and the ocean.
In this work we consider the problem of estimating SGE quantities as an **inverse problem** in which the unknown is the location of the interface between the land and the sea, whereas overspecified boundary conditions are available on another part of the domain boundary.
We consider a fictitious domain Ω_f larger than the real one Ω. Ω_f has the same overspecified and prescribed boundaries as Ω, but is extended beyond the zone where the unknown interface could be located. The aim is to solve a data completion problem for Ω_f, by exploiting the over-specified

*LAMSIN-ENIT & INAT, BP37, 1002 Tunis-Belvedere, Tunisie, tlatli@topnet.tn,
†Université de Lyon, CNRS, Université Lyon1, LaMCoS UMR5259, Villeurbanne, F-69622, France, thouraya.baranger@univ-lyon1.fr
‡LMHE-ENIT, BP37, 1002 Tunis-Belvedere, Tunisie, bouhlila.rachida@enit.rnu.tn

data. Then, the land-sea interface is located where the zero hydraulic head isovalue line occurs. The method and numerical tools used in this paper have already been presented in [1, 2], our contribution in this work is based on the application aspect.

2 Land-sea interface identification

2.1 The model

The mathematical model of the forward problem is given by equation (1), where the hydraulic head is denoted by h, T is the given transmissivities field and $\overline{q_s}$ is the source term. Γ_m is the portion of the boundary where both piezometric level H_m and hydraulic flux Φ_m are given (i.e. over-specified conditions), Γ_b is the boundary where a condition is known. Depending on the values taken by parameters λ and μ this condition can be a prescribed hydraulic flux or head. Γ_{ls} is the unknown land-sea interface corresponding to a null hydraulic head.
To identify the unknown land-sea interface Γ_{ls} we introduce a **fictitious domain** with all known boundaries. Thus we shift the difficulty of finding the unknown interface to that of identifying the boundary conditions on the boundaries of the fictitious domain. We consider an extended domain Ω_f, such that $\Omega_f = \Omega \cup \Omega_e$, $\Gamma_{ls} = \Omega \cap \Omega_e$ and q_s the extension of $\overline{q_s}$ to Ω_e. $\partial\Omega_e$ has two parts, one with the same known conditions as Γ_b and one, noted by Γ_u, where the boundary conditions are unknown. The over-specified data (Φ_m, H_m) are given on Γ_m. The data completion problem is defined by equation (2).

$$\begin{cases} div(-T\nabla h) = \overline{q_s} & \text{in } \Omega, \\ h = H_m & \text{on } \Gamma_m, \\ -T\frac{\partial h}{\partial n} = \Phi_m & \text{on } \Gamma_m, \\ -\lambda T\frac{\partial h}{\partial n} + \mu h = \phi & \text{on } \Gamma_b, \\ h = 0 & \text{on } \Gamma_{ls}, \end{cases} \quad (1)$$

$$\begin{cases} div(-T\nabla h) = q_s & \text{in } \Omega_f, \\ h = H_m & \text{on } \Gamma_m, \\ -T\frac{\partial h}{\partial n} = \Phi_m & \text{on } \Gamma_m, \\ -\lambda T\frac{\partial h}{\partial n} + \mu h = \phi & \text{on } \Gamma_b, \\ h = H_u & \text{on } \Gamma_u, \\ -T\frac{\partial h}{\partial n} = \Phi_u & \text{on } \Gamma_u. \end{cases} \quad (2)$$

2.2 The Data Completion Problem and Identification Procedure

Let us consider the above Cauchy problem (2) defined in the fictitious domain Ω_f . Provided that data H_m are compatible with flux Φ_m, solving the Cauchy problem can be stated as that of solving problem (2) and finding (H_u,Φ_u) which are the hydraulic head and the flux on Γ_u respectively.

To solve this problem, we resort to a method based on the minimization of a constitutive law gap functional. Here, we focus on the use of the dual form of the method, presented in [2]. The dual approach in the constitutive law gap functional method follows two steps. First, we consider, for a given unknown flux η, two mixed well-posed problems and in the second step, we minimize a constitutive law gap functional on the unknown data η. For more details, see [2].
We use an iterative process based on the data completion method to perform the interface identification : we consider an initial fictitious domain Ω_f^o ; the data completion problem is then solved using this fictitious domain. This procedure is repeated by changing the fictitious domain at each iteration until the interface Γ_{ls} is identified (see figure 1).
When the optimization problem is solved we obtain the hydraulic head throughout the extended domain Ω_f. The land-sea interface is then determined as the geometric support of the **isoline** $h = 0$. Since the piezometry over the entire initial domain Ω is available, we can compute the hydraulic flux across any internal boundary and evaluate the quantity of water exchanged between the land and the sea. If this quantity is negative, we are in the presence of seawater intrusion, if not, then of submarine discharge.

3 Conclusion

For numerial trials, we study different cases : in the discharge situation as well as the intrusion situation, with fictitious domain larger the real one, as well as smaller and with noisy data. On all these tests obtained results were satisfactory and errors acceptable.
Therefore this procedure could be applied as the first step in coastal aquifer studies and modeling in order to specify the extension of the domain and the position of the aquifer-ocean border. It could also be a stage in a larger iterative procedure including domain geometry and extension, and the calibration of physical parameters.

Références

[1] S. Andrieux, T. N. Baranger, and A. Ben Abda. Solving Cauchy problems by minimizing an energy-like functional. *Inverse Problems*, 22(1) :115–133, FEB 2006.

[2] T. N. Baranger and S. Andrieux. Constitutive law gap functionals for solving the cauchy problem for linear elliptic pde. *Applied Mathematics and Computation*, 218(5) :1970 – 1989, 2011.

[3] J. Bear and S. Sorek. *Seawater intrusion in costal aquifers - concepts methods and practices.* Kluwer Academic Publisher, 1999.

[4] M. Bonnet and J.P. Sauty. Un modele simplifie pour la simulation des nappes avec intrusion saline. In Int. Assoc. Sci Hydrology, editor, *Application of Mathematical Models in Hydrology and Water Resources Systems. Proc. Bratislava Symposium*, pages 45–56, 1975.

[5] W. C. Burnett, P. K. Aggarwal, A. Aureli, H. Bokuniewicz, J. E. Cable, M. A. Charette, E. Kontar, S. Krupa, K. M. Kulkarni, A. Loveless, W. S. Moore, J. A. Oberdorfer, J. Oliveira, N. Ozyurt, P. Povinec, A. M. G. Privitera, R. Rajar, R. T. Ramassur, J. Scholten, T. Stieglitz, M. Taniguchi, and J. V. Turner. Quantifying submarine groundwater discharge in the coastal zone via multiple methods. *Science of the Total Environment*, 367(2-3) :498–543, AUG 31 2006.

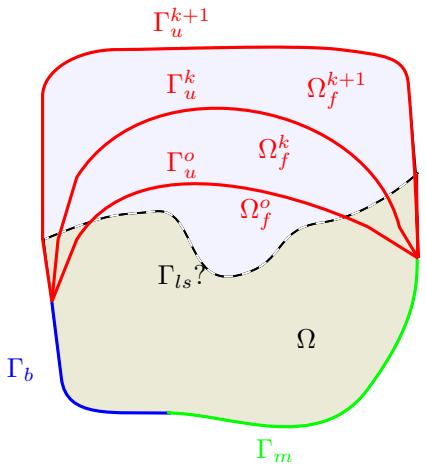

FIGURE 1 – Evolution of the fictitious domain.

Identification de fissures interfaciales en élasticité tridimensionnelle par une méthode d'optimisation.

Mohamed Larbi KADRI* Jalel Ben Abdallah †

Résume : On s'intéresse au problème d'identification de fissures interfaciales dans un solide élastique tridimentionnel. On utilise des données surabondantes et disponibles sur une partie de la frontière. Le problème ainsi posé est un problème de Cauchy connu pour être mal-posé au sens de la stabilité. Nous ramenons la résolution du problème de Cauchy à un problème de minimisation sous contraintes d'une fonction coût. Le gradient de la fonction coût est effectué par la méthode de l'état adjoint.
Mots clés : Problème inverse, identification de fissures interfaciales, élasticité, optimisation.

1 Introduction

Ce travail traite de l'identification de fissures interfaciales dans un solide élastique tridimensionnel. Les données du problème sont les déplacements et les efforts mesurés sur une partie accessible du bord du solide. Ce problème appartient à la famille des problèmes de Cauchy, connus pour être mal posé au sens de la continuité de la solution vis à vis des données [1]. L'idée qu'on propose est de combiner les techniques d'optimisation et de la décomposition de domaine pour résoudre ce problème de Cauchy. Nous ramenons la résolution du problème de Cauchy à un problème de minimisation sous contraintes d'une fonction coût. Le gradient de la fonction coût est effectué par la méthode de l'état adjoint. La technique de l'état adjoint permet de transformer le problème de minimisation sous contraintes en la recherche du point de stationnarité d'un Lagrangien associé. L'idée de cet algorithme est inspirée des méthodes de décomposition de domaine appliquées aux problèmes de contrôle optimal, qui ont été introduites initialement par Ellabib [2], Bensoussan et al. [3] et reprise plus tard par Benamou [4] et Lions [5].

2 Position du problème

Nous cherchons à identifier des fissures localisées sur une surface à priori connue dans un solide élastique tridimentionnel (décollement de surface) à partir de données surabondantes sur seulement une partie de la frontière externe. La littérature sur la détection de fissures est très abondantes, nous citons [6] et [7] où l'identification est faite moyennant des conditions aux limites surabondantes. Le premier est dans le cadre de l'élastostatique alors que le deuxième utilise des mesures qui dépendent du temps. L'exemple suivant est inspiré du cas étudié dans [6]. Le domaine fissuré est un parallélépipède de dimensions $70 \times 25 \times 15$ constitué d'un matériau homogène, élastique et isotrope ($E = 200GPa, \nu = 0.3$). Deux fissures elliptiques : S_1 d'axes principaux $a_1 = 13$ et $b_1 = 5$ parallèles aux axes x et y, et S_2 d'axes principaux $a_2 = 7$ et $b_2 = 2.5$ faisant un angle de $^\circ 45$ avec l'axe des x. Le centre de la fissure $S1$ se situe au point de coordonnées ($x = 45$, $y = 15$), celui de S_2 au point de coordonnées ($x = 15$, $y = 15$) sur la surface plane $\Gamma_i = \{(x, y, z)^t \in \Gamma / z = 10\}$ (voir figure 1). La facette gauche du cube est encastrée, la facette droite est bloquée seulement selon les directions y et z . Le chargement exercée sur le solide est un effort de traction $t_0 = 2kPa$ appliqué sur la totalité des surfaces supérieures et inférieures agissant sur le plan xz avec un angle

*ENIT–lamsin, medlarbi.kadri@lamsin.rnu.tn,
†ENIT–MAI, jalel.benabdallah@enit.rnu.tn

de 45^0. Les autres facettes sont libres. Le domaine est discrétisé par des éléments finis quadratiques tridimensionnels avec trois degrés de liberté (8012 éléments finis). $\Gamma_c = \Gamma_c^+ \cup \Gamma_c^-$ est discrétisée en 999 noeuds. Les fissures S_1 et S_2 sont des frontières avec une condition de Neumann homogène *i.e* les contraintes sont nulles, alors que sur le reste du plan interne $\Gamma_i \setminus S_1 \cup S_2$ les conditions de continuités des déplacements et contraintes usuelles sont admises. La simulation est faite en utilisant des données synthétiques, générées par la résolution du problème direct.

3 Le Problème de Cauchy en élasticité

Le problème d'identification de fissures à partir de mesures partielles et surabondantes est un problème de Cauchy en élasticité qui consiste à chercher un champ de déplacement $\boldsymbol{u}$ vérifiant le problème aux limites suivant :

$$\left\{\begin{array}{rl} -div\boldsymbol{\sigma}(\boldsymbol{u}(x)) & = \boldsymbol{f} \ \text{ dans } \Omega \\ \boldsymbol{u} & = \tilde{\boldsymbol{u}}(x) \ \text{ sur } \Gamma_c \\ \boldsymbol{\sigma}(\boldsymbol{u}(x)).\boldsymbol{n} & = \tilde{\boldsymbol{t}}(x) \ \text{ sur } \Gamma_c \end{array}\right. \tag{1}$$

Où $\boldsymbol{\sigma}(\boldsymbol{u})$ est le champ de contraintes relié au champ de déformations $\boldsymbol{\varepsilon}(\boldsymbol{u})$ par la relation de comportement $\boldsymbol{\sigma}(\boldsymbol{u}) = C\boldsymbol{\varepsilon}(\boldsymbol{u})$ (C est le tenseur de rigidité). Pour localiser les défauts, deux problèmes de Cauchy sont résolus. Le premier P_+ est défini sur le sous-domaine supérieur Ω_+ où les données surabondantes sont considérées uniquement sur la facette supérieure Γ_c^+ et les inconnus à identifier sont considérés sur l'interface Γ_i. Le second problème de Cauchy P_- est défini sur le sous-domaine inférieur où les données surabondantes sont localisées sur la facette inférieure et les inconnus seront identifiés sur Γ_i. Nous nous n'intéressons qu'aux inconnus de déplacements. En fait, désignant par $\boldsymbol{u}^+$ (resp. $\boldsymbol{u}^-$) les déplacements sur Γ_i issues de la résolution de P_+ (resp. P_-), les fissures apparaîtront comme les parties de Γ_i où le vecteur de saut des déplacements $[\boldsymbol{u}^+ - \boldsymbol{u}^-]$ n'est pas nul.

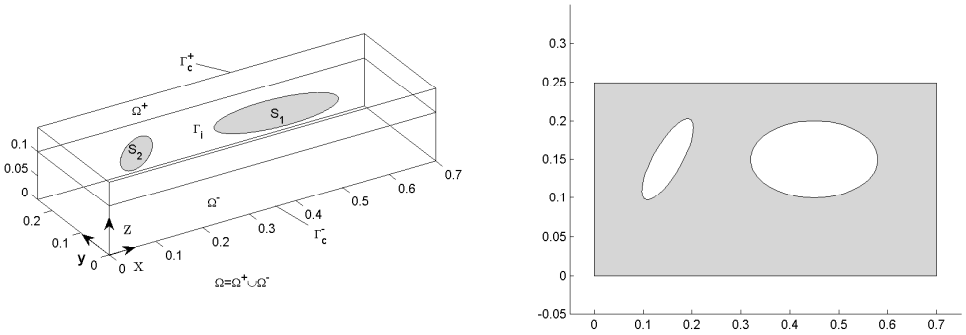

FIGURE 1 – Géométrie du domaine fissuré

4 Le Problème d'optimisation

On considère les deux problèmes suivants (issus de la duplication fictive du problème de Cauchy (1), dont les solutions sont notées $\boldsymbol{u}_D$ et $\boldsymbol{u}_N$:

$$\left\{\begin{array}{rl} -div\boldsymbol{\sigma}(\boldsymbol{u}_D) & = \boldsymbol{f} \ \text{ dans } \Omega \\ \boldsymbol{u}_D & = \tilde{\boldsymbol{u}} \ \text{ sur } \Gamma_c \\ \boldsymbol{\sigma}(\boldsymbol{u}_D).\boldsymbol{n} & = \boldsymbol{\mu} \ \text{ sur } \Gamma_i \end{array}\right. \quad \text{et} \quad \left\{\begin{array}{rl} -div\boldsymbol{\sigma}(\boldsymbol{u}_N) & = \boldsymbol{f} \ \text{ dans } \Omega \\ \boldsymbol{\sigma}(\boldsymbol{u}_N)).\boldsymbol{n} & = \tilde{\boldsymbol{t}} \ \text{ sur } \Gamma_c \\ \boldsymbol{\sigma}(\boldsymbol{u}_N).\boldsymbol{n} & = \boldsymbol{\mu} \ \text{ sur } \Gamma_i \end{array}\right. \tag{1}$$

Pour formuler le problème de contrôle optimal relatif au problème (1) nous introduisons une fonction coût $s\boldsymbol{u} = \boldsymbol{u}_D - \boldsymbol{u}_N$ qui minimise l'écart entre les solutions $\boldsymbol{u}_D$ et $\boldsymbol{u}_N$ au sens de la norme L^2, et ceci sans ajouter aucun terme qui assure la régularité du contrôle.

On considère le problème d'optimisation suivant :

$$\left\{\begin{array}{ll} \text{Minimiser} & J(\boldsymbol{u}_D(\boldsymbol{\mu}), \boldsymbol{u}_N(\boldsymbol{\mu})) \ \ \forall \boldsymbol{\mu} \in H^{-\frac{1}{2}}(\Gamma_i) \\ \text{où} & J = \frac{1}{2}\displaystyle\int_\Omega (\boldsymbol{u}_D - \boldsymbol{u}_N).(\boldsymbol{u}_D - \boldsymbol{u}_N) d\Omega \\ \text{avec} & \boldsymbol{u}_D(\boldsymbol{\mu}) \text{ et } \boldsymbol{u}_N(\boldsymbol{\mu}) \text{ solutions de (1)} \end{array}\right. \tag{2}$$

C'est un problème d'optimisation d'une fonctionnelle convexe.

On considère les espaces de déplacements admissibles $V = \{\boldsymbol{u} \in H^1(\Omega), \boldsymbol{u}_{|\Gamma_c} = \tilde{\boldsymbol{u}}\}$ et $V_0 = \{u \in V, \boldsymbol{u}_{|\Gamma_c} = 0\}$. Les formulations faibles de (1) s'ecrivent :
Trouver $\boldsymbol{u}_D \in V$ telle que : $\forall \boldsymbol{v} \in V_0(\Omega)$

$$a_D(\boldsymbol{u}_D, \boldsymbol{v}) = \int_\Omega \boldsymbol{\sigma}(\boldsymbol{u}_D) : \boldsymbol{\varepsilon}(\boldsymbol{v}) = \int_\Omega \boldsymbol{f}\boldsymbol{v} dx + \int_{\Gamma_i} \boldsymbol{\mu}\boldsymbol{v} d\Gamma \tag{3}$$

Trouver $\boldsymbol{u}_N \in V$ telle que $\forall \boldsymbol{v} \in V(\Omega)$

$$a_N(\boldsymbol{u}_N, \boldsymbol{v}) = \int_\Omega \boldsymbol{\sigma}(\boldsymbol{u}_N) : \boldsymbol{\varepsilon}(\boldsymbol{v}) = \int_\Omega \boldsymbol{f}\boldsymbol{v} dx + \int_{\Gamma_c} \tilde{\boldsymbol{t}}\boldsymbol{v} d\Gamma + \int_{\Gamma_i} \boldsymbol{\mu}\boldsymbol{v} d\Gamma \tag{4}$$

On défini l'espace des solutions admissibles $\mathcal{U}_{ad}$ par :

$$\mathcal{U}_{ad} = \{(\boldsymbol{u}_D(\boldsymbol{\mu}), \boldsymbol{u}_N(\boldsymbol{\mu})) \text{ solutions de (3) et (4) } \forall \boldsymbol{\mu} \in H^{-\frac{1}{2}}(\Gamma_i)\}$$

Le problème d'optimisation (2) peut être reformulé comme suit :

$$\text{Minimiser} \quad J(\boldsymbol{u}_D(\boldsymbol{\mu}), \boldsymbol{u}_N(\boldsymbol{\mu})) \ \ \forall \ \ (\boldsymbol{u}_D(\boldsymbol{\mu}), \boldsymbol{u}_N(\boldsymbol{\mu})) \in \mathcal{U}_{ad} \tag{5}$$

Soit $\boldsymbol{u}_D$, $\boldsymbol{\lambda}_D$, $\boldsymbol{u}_N$, $\boldsymbol{\lambda}_N \in H^1(\Omega)$, $\boldsymbol{\mu} \in H^{-\frac{1}{2}}(\Gamma)$, on introduit le champs de multiplicateurs de Lagrange afin de relaxer la contrainte sur les déplacements :

$$\begin{aligned} \mathcal{L}(\boldsymbol{u}_D, \boldsymbol{u}_N, \boldsymbol{\mu}, \boldsymbol{\lambda}_D, \boldsymbol{\lambda}_N) \quad &= J(\boldsymbol{\mu}, \boldsymbol{u}_D, \boldsymbol{u}_N) - \int_\Omega \boldsymbol{\sigma}(\boldsymbol{u}_D) : \boldsymbol{\varepsilon}(\boldsymbol{\lambda}_D) + \int_\Omega \boldsymbol{f}\boldsymbol{\lambda}_D dx \\ &+ \int_{\Gamma_i} \boldsymbol{\mu}\boldsymbol{\lambda}_D d\Gamma - \int_\Omega \boldsymbol{\sigma}(\boldsymbol{u}_N) : \boldsymbol{\varepsilon}(\boldsymbol{\lambda}_N) dx \\ &+ \int_\Omega \boldsymbol{f}\boldsymbol{\lambda}_N dx + \int_{\Gamma_c} \tilde{\boldsymbol{t}}\boldsymbol{\lambda}_N d\Gamma + \int_{\Gamma_i} \boldsymbol{\mu}\boldsymbol{\lambda}_N d\Gamma \end{aligned} \tag{6}$$

$\boldsymbol{\lambda}_D$, $\boldsymbol{\lambda}_N \in H^1(\Omega)$ sont les multiplicateurs de Lagrange associés à la contrainte :

$$\boldsymbol{\sigma}(\boldsymbol{u}_N).\boldsymbol{n} = \boldsymbol{\sigma}(\boldsymbol{u}_D).\boldsymbol{n} \ \text{ sur } \ \Gamma_i$$

Grâce à la convexité, le problème d'optimisation (5) est équivalent au problème de recherche de point-selle :

$$\mathcal{L}(\boldsymbol{u}_D, \boldsymbol{u}_N, \boldsymbol{\mu}, \boldsymbol{\eta}_D, \boldsymbol{\eta}_N) \leq \mathcal{L}(\boldsymbol{u}_D, \boldsymbol{u}_N, \boldsymbol{\mu}, \boldsymbol{\lambda}_D, \boldsymbol{\lambda}_N) \leq \mathcal{L}(\boldsymbol{v}_D, \boldsymbol{v}_N, \boldsymbol{\mu}, \boldsymbol{\lambda}_D, \boldsymbol{\lambda}_N), \ \ \forall (\boldsymbol{v}, \boldsymbol{\eta}_D, \boldsymbol{\eta}_N) \in V \times H^{\frac{1}{2}}(\Gamma_i) \tag{7}$$

L'étude du point de stationnarité de ce Lagrangien conduit à un problème adjoint défini par la différentiation du Lagrangien par rapport aux champs décrivant le problème direct.

Nous allons calculer l'expression du gradient de la fonctionnelle J à partir de l'état adjoint. En annulant les dérivées de $\mathcal{L}$ par rapport à $\boldsymbol{\lambda}_D$ et $\boldsymbol{\lambda}_N$, on obtient les équations (3) et (4). En annulant les dérivées de $\mathcal{L}$ par rapport à $\boldsymbol{u}_D$ et $\boldsymbol{u}_N$ on obtient les équations adjointes suivantes :

$$a_D(\boldsymbol{v}, \boldsymbol{\lambda}_D) = (\boldsymbol{u}_D - \boldsymbol{u}_N, \boldsymbol{v})_{\Gamma_i}, \ \ \forall \boldsymbol{v} \in V_0 \tag{8}$$

et

$$a_N(\boldsymbol{v}, \boldsymbol{\lambda}_N) = -(\boldsymbol{u}_D - \boldsymbol{u}_N, \boldsymbol{v})_{\Gamma_i}, \quad \forall \boldsymbol{v} \in V \tag{9}$$

respectivement.

D'où les equations adjointes sont données par :

$$\left\{ \begin{array}{rl} -div\boldsymbol{\sigma}(\boldsymbol{u}_D) & = 0 \text{ dans } \Omega \\ \boldsymbol{u}_D & = 0 \text{ sur } \Gamma_c \\ \boldsymbol{\sigma}(\boldsymbol{u}_D).\boldsymbol{n} & = (\boldsymbol{u}_D - \boldsymbol{u}_N) \text{ sur } \Gamma_i \end{array} \right. \quad \text{et} \quad \left\{ \begin{array}{rl} -div\boldsymbol{\sigma}(\boldsymbol{u}_N) & = 0 \text{ dans } \Omega \\ \boldsymbol{\sigma}(\boldsymbol{u}_N)).\boldsymbol{n} & = 0 \text{ sur } \Gamma_c \\ \boldsymbol{\sigma}(\boldsymbol{u}_N).\boldsymbol{n} & = -(\boldsymbol{u}_D - \boldsymbol{u}_N) \text{ sur } \Gamma_i \end{array} \right. \tag{10}$$

Les multiplicateurs de Lagrange $\boldsymbol{\lambda}_D$ et $\boldsymbol{\lambda}_N$ assurent donc la continuité des déplacements à travers Γ_i.

Soit $\mathcal{J}(\boldsymbol{\mu}) = J(\boldsymbol{\mu}, \boldsymbol{u}_D, \boldsymbol{u}_N)$. Le problème de minimisation est equivalent au problème de détermination de $\boldsymbol{\mu} \in H^{-\frac{1}{2}}(\Gamma_i)$ telle que $\mathcal{J}(\psi)$ soit minimisée. Maintenant, la derivée première de $\mathcal{J}$ est définie à travers son action sur les variations $\boldsymbol{\mu}$:

$$< \frac{dJ}{d\boldsymbol{\mu}} >= (\boldsymbol{u}_D - \boldsymbol{u}_N, \tilde{\boldsymbol{u}}_D - \tilde{\boldsymbol{u}}_N)_{\Gamma_i} \quad \forall \tilde{\boldsymbol{\mu}} \in (L^2(\Gamma_i))^2 \tag{11}$$

Où $\tilde{\boldsymbol{u}}_D$ et $\tilde{\boldsymbol{u}}_N$ sont solutions de :

$$a_D(\tilde{\boldsymbol{u}}_D, \boldsymbol{v}) = (\tilde{\boldsymbol{\mu}}, \boldsymbol{v})_{\Gamma_i} \quad \forall \boldsymbol{v} \in V(\Omega) \tag{12}$$

et

$$a_N(\tilde{\boldsymbol{u}}_N, \boldsymbol{v}) = -(\tilde{\boldsymbol{\mu}}, \boldsymbol{v})_{\Gamma_i} \quad \forall \boldsymbol{v} \in V(\Omega) \tag{13}$$

Soit $\boldsymbol{v} = \boldsymbol{\lambda}_D$ dans (12), $\boldsymbol{v} = \boldsymbol{\lambda}_N$ dans (13) et $\boldsymbol{v} = \boldsymbol{u}_N$ dans (9). En combinant les résultats on obtient :

$$\frac{d\mathcal{J}}{d\boldsymbol{\mu}} = \boldsymbol{\lambda}_D - \boldsymbol{\lambda}_N \quad \text{sur } \Gamma_i. \tag{14}$$

4.1 L'algorithme de minimisation

Pour résoudre le problème de contrôle optimal, on a besoin d'un algorithme efficace de minimisation. La fonctionnelle à minimiser, étant quadratique, nous optons pour un algorithme de descente efficace qui est l'algorithme du Gradient Conjugué.

Schéma de la minimisation

La résolution du problème de minimisation est présentée sur la figure 2. Chaque itération comporte schématiquement trois phases :

- La résolution des problèmes directs (1) (le calcul de $\boldsymbol{u}_D$ et $\boldsymbol{u}_N$ permet le calcul de J).
- La résolution des états adjoints (10) permet le calcul de ∇J.
- Le pas d'optimisation proprement dit permet la calcul de la nouvelle estimation de $\boldsymbol{\mu}$.

5 Résultats Numérique

Le Calcul du gradient ne dépend que des résultats des problèmes directs et adjoints. On obtient donc toutes les composantes du gradient au prix d'un seul calcul auxiliaire. L'utilisation de l'état adjoint est donc particulièrement efficace pour des problèmes avec un grand nombre d'inconnues. Les problèmes adjoints dépendent des problèmes directs ils seront toujours résolus après ceux-ci.

L'identification des fissures par la méthode d'optimisation permet l'identification de la position et l'allure des fissures. l'algorithme converge en 27 itérations pour des données bruitées à 10%. Il peut être intéressant de régulariser le problème d'optimisation en ajoutant un terme régularisant à la fonctionnelle coût.

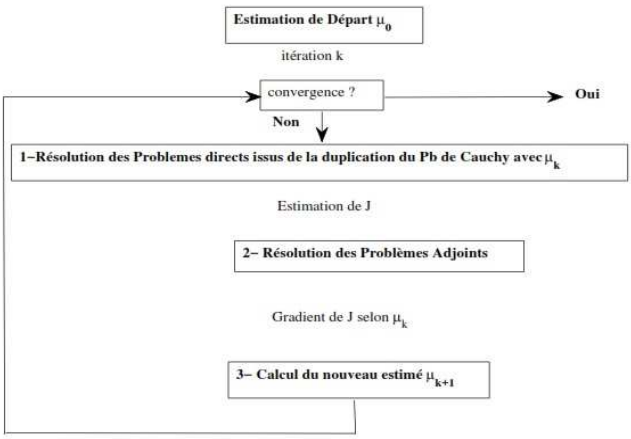

FIGURE 2 – Etapes de la minimisation de la fonctionnelle coût J.

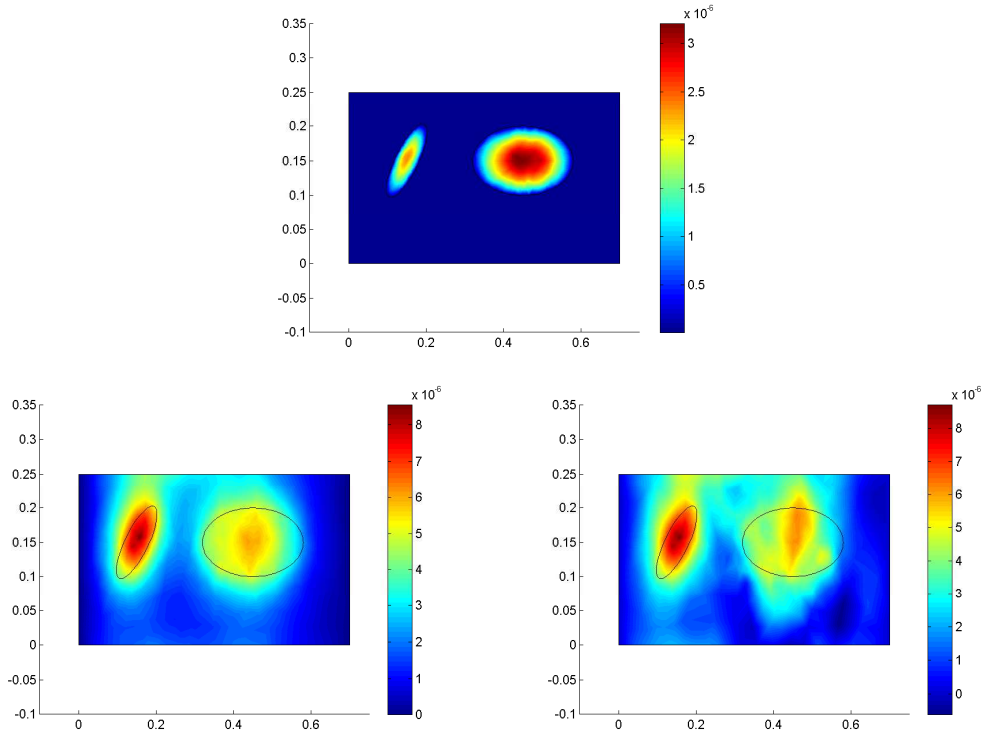

FIGURE 3 – $[\boldsymbol{u}^+ - \boldsymbol{u}^-]$ haut : exact à travers Γ_i, en bas à gauche : données non bruitées. (N.B.=0%), en bas à droite : données bruitées (N.B.=10%)

Références

[1] J. Hadamard, *Lectures on Cauchys problem in linear partial differential equation. Dover, New York, 1953.*

[2] A. Ellabib, *Contribution a l'approximation de probleme d'identification et decomposition de domaine en elasticite. Habilitation universitaire (2008)*

[3] A. Bensoussan, R. Glowinski, J. Lions, *Méthode de décomposition appliquée au contrôle optimal de systèmes distribués, Lecture Notes in Computer Science, 5. In the fifth IFIP Conference on Optimization Techniques, 1973.*

[4] J. Benamou, *A domain decomposition method with coupled transmission condi- tions for the control of systems governed by elliptic partial differential equations, SIAM J. Numer. Anal. 33 (1996)* 2401-2416.

[5] P. Lions, *On the Schwarz alternating method III A variant for nonoverlapping sub- domains. Proc. 3rd Conference on Domain Decomposition Methods, Philadelphia. SIAM. (1990)* 202-223.

[6] W. Weikl, H. Andrãa, E. Schnack, *An alterning iterative algorithm for the recons- truction of internal cracks in a three-dimensional solid body, Inverse Problems 17 (2001)* 1957-1975.

[7] C. Bellis, M. Bonnet, *Crack identification by 3D time-domain elastic or acoustic topological sensitivity, C. R. Mécanique 337 (2009)* 124 -130.

A free boundary prolem for the stokes operator

F. Bouchon* G. Peichl † M. Sayeh ‡ R. Touzani§

Abstract: A free boundary problem for the Stokes equations governing a viscous flow with over-determined condition on the free boundary is investigated. This free boundary problem is transformed into a shape optimization one which consists in minimizing a Kohn Vogelius energy cost functional. Existence of the shape derivative of the cost functional is also proven and the analytic expression of the shape derivative is given in the Hadamard structure form. The gradient information is combined with the level set method in a steepest descent algorithm to solve the shape optimization problem. The efficiency of this approach is illustrated by numerical results.
Keyworlds: Bernoulli problem, Shape derivative, free boundary problems, level set method.

1 Formulation of the problem

We consider a problem derived from a two-dimensional magnetic shaping process which can be viewed as an analog of the Bernoulli free boundary problem [1], where the Laplace operator is replaced by the Stokes operator. Typically, a fluid is subject to Lorentz forces. The shape of the fluid is determined by the pressure balance equations and the fluid flow is governed by the incompressible Navier-Stokes equations. Consider a bounded $C^{2,1}$ domain $A \subset \mathbb{R}^2$ with boundary Γ_f. The fluid is considered in levitation around A and occupies then the domain $\Omega = B \backslash \overline{A}$, where B is a bounded domain with boundary Γ that contains $\overline{A}$. Let u and p stand for the fluid velocity and pressure respectively. Let $f \in H^1_{\text{loc}}(\mathbb{R}^2)^2$ denote the density of a given Lorentz force and $g \in H^{1/2}(\Gamma_f)^2$. For a given vector field λ we consider the free boundary problem of determining the domain Ω occupied by the fluid, the fluid velocity u and its pressure p such that:

$$\begin{aligned} &-2\text{div}(\sigma(u)) + \nabla p = f && \text{in } \Omega, \\ &\text{div} u = 0 && \text{in } \Omega, \\ &u = g && \text{on } \Gamma_f, \\ &u = 0 \text{ and } 2\sigma(u)\nu - p\nu = \lambda && \text{on } \Gamma. \end{aligned} \tag{1}$$

Above, ν is the out normal unit vector to the boundary Γ respectively and $\sigma(u) = \frac{1}{2}(\nabla u + \nabla u^T)$ is the symmetric deformation tensor. For given Ω let (u_D, p_D) and (u_N, p_N) be the functions defined on Ω satisfying both the first three relations in (1) and

$$u_D = 0 \text{ and } 2\sigma(u_N)\nu - p_N\nu = \lambda \qquad \text{on } \Gamma, \tag{2}$$

respectively.

Let us define the functional J on a suitable class of domains Ω by

$$J(\Omega) = 2\int_\Omega \sigma(u_D - u_N)^{:2},$$

where $\sigma(u)^{:2} = \sum_{i,j=1}^2 \sigma(u)_{ij}^2$. The problem (1) is equivalent to the following shape optimization problem: find (u, Ω) such that

*Blaise Pascal university Frence, francois.bouchon@math.univ-bpclermont.fr
†University of Graz Austria, gunther.peichl@uni-graz.at
‡ENIT–lamsin, Mohamed.Sayeh@ipein.rnu.tn
§Blaise Pascal university Frence, rachid.touzani@math.univ-bpclermont.fr

$$J(\Omega) = \min_{\tilde{\Omega}} J(\tilde{\Omega}) = 0. \tag{3}$$

2 Shape derivative and numerical results

In order to define the shape derivative [3] of J we perturb the reference domain Ω by a transformation of type $F_t = id + th$, where h is C^2 vector field on $\mathbb{R}^2$ vanishing on Γ_f and t is sufficiently small such that F_t defines a family of C^2-diffeomorphisms from Ω onto its image. For such t one sets $\Omega_t = F_t(\Omega)$, $\Gamma_t = F_t(\Gamma)$. Then the Eulerian derivative of J at Ω in the direction h is defined as the limit, when it exists,

$$J'(\Omega; h) = \lim_{t \to 0} \frac{1}{t}(J(\Omega_t) - J(\Omega)).$$

The functional J is called shape differentiable at Ω if $J'(\Omega; h)$ exists for all $h \in C^2(\mathbb{R}^2, \mathbb{R}^2)$ and defines a continuous linear functional on $C^2(\mathbb{R}^2, \mathbb{R}^2)$. We use the level set method [2] and the shape gradient information in a steepest descent algorithm to solve numerically the shape optimization problem. The following numerical test illustrates the efficiency of this approach. The dashed line is the fixed boundary and the solid black one is the exact solution and the solid red line is the numerical solution which converges to the exact one, for (U,p) is given in polar coordinate by,

$$U(r,\theta) = \begin{pmatrix} u(r,\theta) \\ v(r,\theta) \end{pmatrix} = \begin{pmatrix} u_r(r)\cos^2(\theta) + u_\theta(r)\sin^2(\theta) \\ (u_r(r) - u_\theta(r))\cos(\theta)\sin(\theta) \end{pmatrix}, \quad p(r,\theta) = (\alpha r + \frac{\beta}{r})\cos(\theta),$$

where $u_r(r) = A + \frac{B}{r^2} + \frac{\alpha}{8}r^2 - \frac{\beta}{2}lnr$, $u_\theta(r) = A - \frac{B}{r^2} + \frac{3\alpha}{8}r^2 - \frac{\beta}{2}(1 + lnr)$, and $A,\ B,\ \alpha, \beta$ are real constants chosen in an appropriate way.

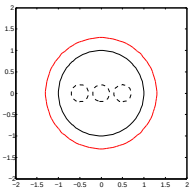
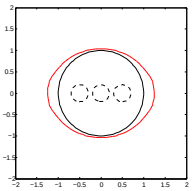
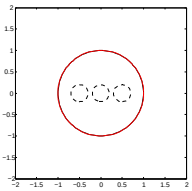

References

[1] A. Ben Abda, F. Bouchon, G. H. Peichl, M. Sayeh and R. Touzani, 2012, *A Dirichlet-Neumann cost functional approach for the Bernoulli problem*, J. Eng. Math.

[2] Osher S, Fedkiw R, 2002, *Level Set Methods and Dynamic Implicit Surfaces*, Springer-Verlag, New York.

[3] Sokolowski J, Zolésio J P, 1992, *Introduction to Shape Optimization: Shape Sensitivity Analysis*, Springer.

3.2 Data completion (DC)

Two step observer approach to solve Cauchy problem for Laplace equation

Muhammad Usman Majeed* Taous Meriem Laleg-Kirati†

Keyworlds: Inverse problem, Laplace equation, State observer

Abstract

In this paper a two step state observer approach is developed to solve severely ill-posed Cauchy problem for Laplace equation on an annulus domain. Cauchy data is available only on the outer boundary and objective is to find solution on the inner boundary. For this purpose a two step observer is designed with a forward and a reverse step and results of both steps are combined to get full solution. Numerical results are presented.

Problem statement

Let Ω be the annulus domain in $\mathbb{R}^2$ with two boundaries Γ_{in} and Γ_{out} respectively, the cauchy problem for Laplace equation on this domain is given by (1).

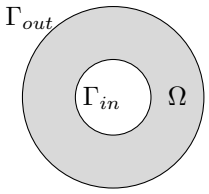

Figure 1: Annulus domain Ω with inner boundary Γ_{in} and outer boundary Γ_{out}.

Find $u|_{\Gamma_{in}}$:

$$\begin{cases} \triangle u = r^2\dfrac{\partial^2 u}{\partial r^2} + r\dfrac{\partial u}{\partial r} + \dfrac{\partial^2 u}{\partial \theta^2} = 0 & in\ \Omega, \\ u = f(r,\theta) & on\ \Gamma_{out}, \\ \dfrac{\partial u}{\partial r} = g(r,\theta) & on\ \Gamma_{out}. \end{cases} \tag{1}$$

Two step state observer approach is developed to solve this problem as follows.

Methodology

In control systems theory, a state observer provides an estimate of the observable internal states of a real system from measurements of inputs and outputs (i.e. data, in inverse problem terminology). In order to solve the inverse problem, first of all Laplace equation is written as first order state equation in variable θ by introducing new variables as follows,

$$\dot{\xi} = \mathcal{A}\xi \quad where\ \mathcal{A} = \begin{pmatrix} 0 & 1 \\ -r^2\dfrac{\partial^2}{\partial r^2} - r\dfrac{\partial}{\partial r} & 0 \end{pmatrix} \ and\ \xi = \begin{pmatrix} \xi_1 = & u \\ \xi_2 = & \dfrac{\partial u}{\partial \theta} \end{pmatrix}, \tag{2}$$

where dot represents partial derivative with respect to θ. Given the abstract formulation (2), following theorem provides the algorithm for the two step state observer to solve problem (1).

*M. U. Majeed is a PhD Student in Computer, Electrical and Mathematical Sciences and Engineering (CEMSE), King Abdullah University of Science and Technology (KAUST), K.S.A muhammadusman.majeed@kaust.edu.sa,

†T. M. Laleg-Kirati is an Assistant Professor in CEMSE, KAUST, K.S.A taousmeriem.laleg@kaust.edu.sa

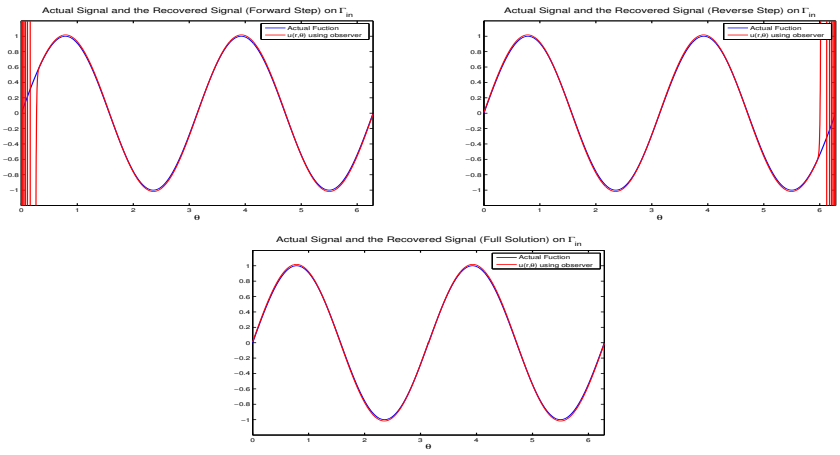

Figure 2: Initial simulation results on Γ_{in}: blue: true solution obtained by solving a well-posed forward problem, red: computed using observer (left: forward step, right: reverse step, bottom: Half of the well constructed solution taken from each step).

MAIN RESULTS

Theorem 1. *Let $\hat{\xi}$ be the estimate of true state ξ, $\mathcal{A}$ be the state operator matrix and $\mathcal{K}$ be the gain operator in proper sobolev spaces respectively, then solution $\hat{\xi}_1|_{\Gamma_{in}}$ found by combining the two solutions, obtained from one forward $(\theta = 0 \to \theta = 2\pi)$ and one reverse $(\theta = 2\pi \to \theta = 0)$ implementation of the following algorithm converges to the true solution of the inverse problem (1).*

$$\begin{cases} \dot{\hat{\xi}} = \mathcal{A}\hat{\xi} - \mathcal{K}(\hat{f} - f) & in\ \ \Omega, \\ \hat{\xi}_1 = \hat{f}(r,\theta) & on\ \ \Gamma_{out}, \\ \dfrac{\partial \xi_1}{\partial r} = g(r,\theta) & on\ \ \Gamma_{out}, \\ \dfrac{\partial^2 \hat{\xi}_1}{\partial \theta^2} = -r^2 \dfrac{\partial^2 \hat{\xi}_1}{\partial r^2} - r\dfrac{\partial \hat{\xi}_1}{\partial r} - \mathcal{K}(\hat{f} - f) & on\ \ \Gamma_{in}. \end{cases} \tag{3}$$

Initial guess at the start of the observer algorithm is zero, that is, $\hat{\xi} = 0$ over the whole domain $\Omega \cup \Gamma_{in} \cup \Gamma_{out}$ except $\hat{\xi}_1 = \hat{f}$ on Γ_{out} as given above. Last equation in (3) is the assumption that Laplace equation is valid on the inner boundary Γ_{in} [1]. Proof of the above theorem will be provided in full version of the paper using concepts of semigroup theory and observability for infinite dimensional systems [2] [3].

Numerical Results

Above two step observer is implemented numerically using second order accurate centered finite difference schemes in r and forward Euler in variable θ. Fictitious point method is used on the inner boundary Γ_{in} to tackle the boundary condition [1]. True solution and the one obtained using observer approach is presented in Figure(2) on the inner boundary Γ_{in}. Convergence of observer (3) in very small θ guarantees the accuracy of two step approach.

References

[1] M. U. Majeed, C. Zayane-Aissa and T. M. Laleg-Kirati, *Cauchy problem for Laplace equation: An observer based approach*, 3rd International Conference on Systems and Control, Algiers Algeria 2013.

[2] M. Tucsnak and G. Weiss, *Observation and control for operator semigroups*, Birkhauser Advanced Texts 2009.

[3] K. Ramdani, M. Tucsnak and G. Weiss, Recovering the initial state of an infinite-dimensional system using observers, Automatica 46 (2010) 1616-1625.

Recovering boundary data from incomplete Cauchy data: The Cauchy-Stokes system

Elyes Ahmed [*], Amel Ben Abda [†]

December 15, 2013

Abstract: We are interested in this paper with the ill-posed Cauchy-Stokes problem. We consider a data completion problem in which we aim recovering lacking data on some part of a domain boundary, from the knowledge of not-complete Cauchy data on the other part. The inverse problem is formulated as an optimization one using an energy-like functional. We gives the first order optimality condition in term of an interfacial operator. Displayed numerical results highlight its accuracy.
Keyworlds:Cauchy-Stokes problem, data completion, Shear stress, Interfacial equation.

We are interested in the Cauchy-Stokes problem that consists of solving the Stokes problem on a domain from a given-data on a part of its boundary, which known as data completion problem. The more common problem in such inverse problem type consists in recovering the missing boundary conditions on the inaccessible part of the boundary from known-cauchy data that are over-specified on accessible boundary: assuming velocity field and the normal stress are given over the accessible region of the boundary [1]. However, in many engineering applications, or essentialy in biomedical applications, these data are often not complete,i.e. that on the accessible boundary Γ_c available data often refer to the velocity field u and only one component of the normal stress. From haemodynamics applications, which inspires this work, where for special geometries only the tangential component of the normal stress could be known from medical measurements, whilst in other situations one knows the normal component.(we refer in the sequel to this data as less-known data). The problem we are dealing with is to reconstruct the velocity v and the pressure p that fits the less-known data on the accessible boundary. Giving a velocity Φ and the corresponding shear stress component T, we would like to recover the corresponding velocity and the normal stress on Γ_i.

Then, the Cauchy problem is written as :

$$\begin{cases} -\nu\Delta u + \nabla p = 0 & \text{in} \quad \Omega \\ \nabla \cdot u = 0 & \text{in} \quad \Omega \\ (\sigma(u)n)_\tau = T & \text{on} \quad \Gamma_c \\ u = \Phi, & \text{on} \quad \Gamma_c. \end{cases} \tag{1}$$

[*]ENIT–lamsin, elyes_ahmed@yahoo.com,
[†]ENIT–lamsin, amel.benabda@enit.rnu.tn

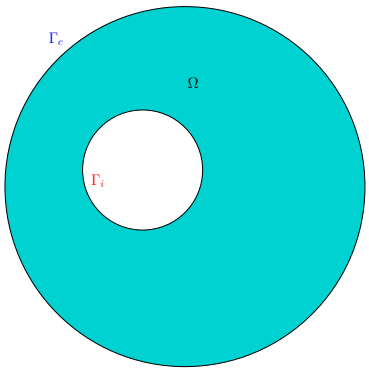

where ν is the viscosity of the fluid, σ denotes the stress tensor $\sigma(u) = 2\nu D(u) - pI$, where $D(u)$ is the strain tensor defined by : $D(u) = \frac{1}{2}(\nabla u + \nabla u^T)$, and I is the identity matrix in $\mathbb{R}^2$. We consider two mixed well-posed problems: the first one is a classical Dirichlet problem (with Dirichlet condition on Γ_c), and the second one is Stokes problem with non classical boundary condition. We attribute to each of them one unknown on Γ_i. Then to reformulate the inverse problem as a minimization one, we consider the energy-like error functional [2]:

$$E(g, \eta) = \frac{1}{2} \int_\Omega \sigma(u_1^\eta - u_2^g) : \nabla(u_1^\eta - u_2^g) \tag{2}$$

The first order optimality condition is rephrased in terms of an interfacial problem using the Steklov-Poincaré operator, and we propose a numerical procedure for solving the resulting interface problem.

References

[1] A. Ben Abda, I. Ben Saad, M. Hassine, *Recovering boundary data: The Cauchy Stokes system*, Applied Mathematical Modelling 37 (2013) 1-12.

[2] S. Andrieux, A. Ben Abda, T.N. Baranger, *Data completion via an energy error functional*, C.R. Mecanique 333 (2005) 171-177.

[3] A.V. Fursikov, *Optimal control of distributed systems: theory and applications*, Translations of mathematical Monograph 187 (2000).

An inverse boundary problem for the heat equation in the presence of small inhomogeneities

Abstract

For the heat equation in a bounded domain, we consider the inverse problem of identifying locations and certain properties of the shapes of small heat-conducting inhomogeneities from dynamic boundary measurements on part of the boundary and for finite interval in time. The key ingredient is an asymptotic method based on appropriate averaging of the partial dynamic boundary measurements. Our approach is expected to lead to very effective computational identification algorithms.

Let Ω be a bounded, smooth subdomain of $\mathbb{R}^d$, $d = 2, 3$. For simplicity we take $\partial\Omega \in \mathcal{C}^\infty$. We suppose that Ω contains a finite number of inhomogeneities, the total collection of inhomogeneities thus takes the form $\mathcal{B}_\alpha = \bigcup_{j=1}^m (z_j + \alpha B_j)$. The points $z_j \in \Omega, j = 1 \dots m$, determine the location of the inhomogeneities. We assume that $\alpha > 0$, the common order of magnitude of the diameters of the inhomogeneities, is sufficiently small that these inhomogeneities are disjoint.

Let u the solution of the heat equation :

$$\begin{cases} \partial_t u - c_0 \Delta u = 0, & (x,t) \in \Omega \times [0,T] \\ u(x,0) = \varphi(x), & x \in \Omega \\ u(x,t)|_{\partial\Omega\times[0,T]} = u(x,t)|_{\Gamma\times[0,T]} = f(x,t) \end{cases}$$

Where $\varphi \in \mathcal{C}^\infty(\overline{\Omega})$ and $f \in \mathcal{C}^\infty([0,T] \times \mathcal{C}^\infty(\partial\Omega))$.

geneities :

$$\begin{cases} \partial_t u_\alpha - (\nabla \cdot c_\alpha \nabla) u_\alpha = 0, & (x,t) \in \Omega \times [0,T] \\ u_\alpha(x,0) = \varphi(x), & x \in \Omega \\ u_\alpha(x,t)|_{\Gamma \times [0,T]} = f(x,t) \end{cases}$$

To obtain the localization of the inhomogeneities centers we need to apply a Fourier inversion transform to a function $\aleph_\alpha(\eta)$. We have to recall also that the function $e^{2i\eta \cdot z_j}$ is exactly the Fourier Transform (up to a multiplicative constant) of the Dirac function δ_{-2z_j} (a point mass located at $-2z_j$), where the set of the points $z_j,\ j = 1, \ldots, m$ represents the centers of the inclusions to be detected. As well, if we consider that we have already constructed numerically the $\aleph_\alpha(\eta)$, after applying the IFFT (Inverse Fast Fourier Transforms) algorithm over $\aleph_\alpha(\eta)$, we obtain the linear combination of the Dirac functions δ_{-2z_j}. So that, after rescaling, we obtain the total collection of the points $z_j,\ j = 1, \ldots, m$.

We had also applied the result obtained in the first part in numerical examples Using Matlab and Fortran.

Managing Disasters Consequences on the Fitness of Environmental Resources for Population Survival

Fethi Ben Belgacem*

Abstract: In this presentation we will attempt to give an illustration of mathematical models describing population dispersal and persistence in environments that are "fit" for them. We will characterize this "Fitness" through the said models, and show how it may be effected pursuant to natural and manmade disasters, which may warrant interventions to save the population(s) considered. This means that before direct intervention, the situation must be studied and the new fitness parameters must be estimated beforehand to predict the best outcome for the population after the intervention. This may save a lot of money and resources that may be lost in vain if the problem were treated ad-hoc. We illustrate the conceptual and mathematical aspects of the fitness through the mead fish kill of 2002 in kuwait, and other similar occurrences around the world.

Keyworlds: Population dispersal, fitness.

*Department of Mathematics, Faculty of Basic Education, PAAET, Aardhia, Kuwait, fbmb1007@gmail.com,

3.3 Inverse problems for electromagnetics (IPE)

A new approach to solve the inverse scattering problem for the wave equation

Maya de Buhan* Marie Kray†

Abstract: We propose a new approach to solve the inverse scattering problem: the aim is to recover the location, the shape and the physical properties of an unknown obstacle surrounded by a known ambient medium. Our approach works directly with the wave equation in the time-dependent domain and combines two methods recently developed by the authors. The first method is the Time-Reversed Absorbing Condition (*TRAC*) method which allows us to reconstruct and regularize the signal from boundary measurements and then reduces the computational domain. The second method is the Adaptive Inversion (AI) method which relies on a mesh-adaptation and basis-adaptation process, that increases the accuracy of the reconstruction. We propose some numerical results in two-space dimensions.

Keyworlds: Inverse problems, wave equation, time reversed absorbing boundary condition, mesh and basis adaptation.

Résumé : Nous proposons une nouvelle approche pour résoudre le problème de la diffraction inverse : le but est de retrouver la position, la forme et les propriétés physiques d'un obstacle entouré d'un milieu ambiant dont on connaît les caractéristiques. Notre approche fonctionne directement dans le domaine temporel, à partir de l'équation des ondes, et combine deux méthodes développées récemment par les auteurs. La première est la méthode *TRAC* (Time-Reversed Absorbing Condition) qui permet de reconstruire et de régulariser le signal à partir des données mesurées au bord et de réduire ainsi la taille du domaine de calcul. La deuxième est une méthode d'inversion (Adaptive Inversion method) qui repose sur un processus d'adaptation de base et de maillage pour augmenter la précision de la reconstruction. Nous présentons plusieurs résultats numériques en deux dimensions.

Mots clés : Problèmes inverses, équation des ondes, condition aux limites absorbante retournée en temps, adaptation de base et de maillage.

1 Our approach: Combination of the *TRAC* and AI methods

In paper [1], we propose a new method to solve the following inverse problem: we aim at reconstructing, from boundary measurements, the location, the shape and the wave propagation speed of an unknown inclusion surrounded by a medium whose properties are known.

Our strategy combines two methods recently developed by the authors:

1. the Time-Reversed Absorbing Condition method (*TRAC*) first introduced in [2]:
   It combines time reversal techniques and absorbing boundary conditions to reconstruct and regularize the signal in a truncated domain that encloses the inclusion. This enables one to reduce the size of computational domain where we solve the inverse problem, now from virtual internal measurements.

*CNRS, UMR 8145, MAP5, Université Paris Descartes, France, maya.de-buhan@parisdescartes.fr
†Department of Mathematics and Informatic, University of Basel, Switzerland, marie.kray@unibas.ch

2. the Adaptive Inversion (AI) method initially proposed for the viscoelasticity equation in [3]: The originality of this method comes from the parametrization of the problem. Instead of looking for the value of the unknown parameter at each node of the mesh, it projects the parameter into a basis composed by eigenvectors of the Laplacian operator. Then, the AI method uses an iterative process to adapt the mesh and the basis of eigenfunctions from the previous approximation to improve the reconstruction.

The novelty of our work is threefold. Firstly, we present a new study on the regularizing power of the *TRAC* method. Secondly, we adapt the Adaptive Inversion method to the case of the wave equation and we propose a new anisotropic version of the iterative process. Finally, we present numerical examples to illustrate the efficiency of the combination of both methods. In particular, our strategy allows (i) to reduce the computational cost, (ii) to stabilize the inverse problem and (iii) to improve the precision of the results.

2 Numerical Results

On Figure 1, we display our results for a penetrable pentagon. We compare the exact propagation speed (a) to the reconstruction by using both methods, first without noise on the recorded data (b), then with 20% level of noise (c). We denote by *20%-noisy TRAC data*, the virtual data obtained after the *TRAC* process from 20%-noisy external boundary measurements.

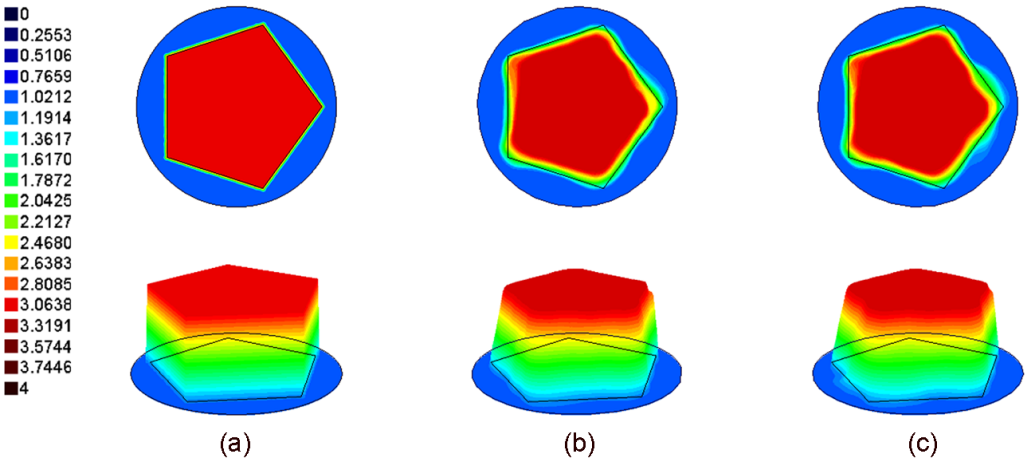

Figure 1: Shape and properties reconstruction of a penetrable pentagon by using both *TRAC* and AI methods: (a) Propagation speed profile inside and outside the inclusion. (b) Result obtained with 0%-noisy *TRAC* data, relative L^2-error = 1.72%. (c) Result obtained with 20%-noisy *TRAC* data, relative L^2-error = 1.92%.

References

[1] Maya de Buhan and Marie Kray. *A new approach to solve the inverse scattering problem for waves: combining the* TRAC *and the Adaptive Inversion methods.* Inverse Problems, 29 (8), 085009, 2013.

[2] Franck Assous, Marie Kray, Frédéric Nataf, and Eli Turkel. *Time Reversed Absorbing Condition: Application to inverse problem.* Inverse Problems, 27 (6), 065003, 2011.

[3] Maya de Buhan and Axel Osses. *Logarithmic stability in determination of a 3D viscoelastic coefficient and a numerical example.* Inverse Problems, 26 (9), 95006, 2010.

Formulation of the emission sources localization problem in the case of a selftriggered radio-detection experiment: Between Ill-posedness and Regularization

AHMED Rebai[1], TAREK Salhi[2,3]

November 30, 2013

[1] Subatech IN2P3-CNRS/Université de Nantes/cole des Mines de Nantes, Nantes, France.
[2] Ecole des Mines de Nantes, Nantes, France.
[3] now at: Département de mathématiques Université de Rennes, France.
ahmed.rebai@subatech.in2p3.fr, tarek.salhi@gmail.com

Abstract

In the field of radio detection in astroparticle physics, the transition from small-scale prototype experiments, triggered by particle detectors, to large-scale antenna array experiments based on standalone detection, has emerged new problems. These problems are related to the localization, recognition and the suppression of the noisy background sources induced by human activities (such as high voltage power lines, electric transformers, cars, trains and planes) or by stormy weather conditions (such as lightning). In this talk, we focus on the localization problem which belongs to a class of more general problems usually termed as "inverse problems". Based on a detailed analysis of some already published results of experiments like : CODALEMA 3 in France AERA in Argentina and TREND in China, we demonstrate the ill-posed character of this problem. This work is organized into three specific points: the existence of a solutions degeneration, the bad conditioning of the problem and also we add a new criteria linked to the non-existence of a global solution. We show, however, that this ill-posed problem is manageable through two kind of regularizations: an empiric algorithm and a Tikhonovs regularization. On the other hand, we also propose an exploitation of the lit antennas convex-hull concept for introducing a new generation of 3D antennas array. This last part is discussed as new preliminary results.

Keywords: UHECR, radio-detection, inverse problem, ill-posed problem, regularization.

3D direct and inverse solver for eddy current tests of SG tubes

P.-L Filiot[*], H. Haddar[†], M.-K Riahi[‡] and Z. Jiang[§]

Abstract: We consider the inverse problem of estimating the shape profile of an unknown deposit on the exterior of stream generator (SG) tubes from a set of eddy current impedance measurements due to coils located in the interior of the tubes. We shall address the problem in a 3D setting to treat the case where the deposits are located in the vicinity of the support plates. Numerical validating experiments on synthetic deposits with different shapes will be presented.
Keyworlds: inverse problems, shape identification, eddy current testing.

1 Industrial problem

We are interested in the direct and inverse simulation of eddy current testing (ECT) experiments of SG tubes using monostatic probes composed of two coils introduced in the interior of the tubes. The generator coil creates an electromagnetic field which in turn induces a current flow in the conductive material nearby. The presence default distorts the flow and change the current in the receiver coil, which is measured as ECT signals. Our goal is to estimate the shape of deposits with known electromagnetic parameters from these ECT signals. Although the tube and coils are axisymmetric, one has to address the problem in a 3D setting since in practice the deposits are located in the vicinity of the (non axi-symmetric) support plates (see Figure 1).

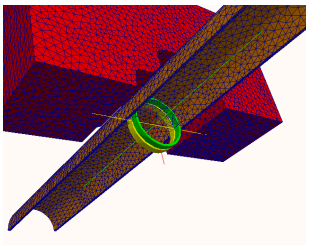

Figure 1: Sketch of the tube + coils + supporting plates.

2 The direct eddy current problem

The eddy current approximation of the harmonic Maxwell's equations reads: $\mathbf{curl}\mathbf{H} - \sigma\mathbf{E} = \mathbf{J}$ on Ω and $\mathbf{curl}\mathbf{E} - i\omega\mu\mathbf{H} = 0$ on Ω, where $\mathbf{H}$ and $\mathbf{E}$ are the magnetic and the electric field respectively. $\mathbf{J}$ is the the source term representing the current density (in the coils) and σ, ω and μ are respectively the conductivity, frequency and magnetic permeability. In order to solve the eddy current problem we use the mixed formulation on $(\mathbf{A}, \mathbf{V}_c)$, where $\mathbf{A}$ represents the magnetic vector potential and $\mathbf{V}_c$ the scalar electric potential only defined on Ω_c : the region where $\sigma \neq 0$. We have $\mathbf{E} = i\omega\mathbf{A} + \nabla\mathbf{V}_c$ on Ω and $\mu\mathbf{H} = \mathbf{curl}\mathbf{A}$ on Ω (see for instance [1]). We are thus concerned with

[*]EDF-R&D STEP, pierre-louis.filiot@edf.fr,
[†]Inria-Saclay and Ecole polytechnique, haddar@cmap.polytechnique.fr,
[‡]Inria-Saclay and Ecole polytechnique, riahi@cmap.polytechnique.fr,
[§]Inria-Saclay and Ecole polytechnique, zixian.jiang@polytechnique.edu.

the strong formulation (where $\Omega_I := \Omega \setminus \bar{\Omega}_c$),

$$\begin{cases} \mathbf{curl}\big(\frac{1}{\mu}\mathbf{curl}\,\mathbf{A}\big) - \frac{1}{\tilde{\mu}}\nabla\mathbf{div}\mathbf{A} - \sigma i\omega\mathbf{A} - \sigma\nabla\mathbf{V}_c = \mathbf{J} & \text{on } \Omega, \\ \mathbf{div}\big(i\omega\sigma\mathbf{A} + \sigma\nabla\mathbf{V}_c\big) = \mathbf{div}\mathbf{J} = 0 & \text{on } \Omega_c, \\ \big(\sigma i\omega\mathbf{A} + \sigma\nabla\mathbf{V}_c\big)\,.\,\boldsymbol{\nu} = \mathbf{J}\,.\,\boldsymbol{\nu} & \text{on } \partial\Omega_I \cap \partial\Omega_c, \\ \mathbf{A}\,.\,\boldsymbol{\nu} = 0 \text{ and } \big(\frac{1}{\mu}\mathbf{curl}\,\mathbf{A}\big) \times \boldsymbol{\nu} = 0 & \text{on } \partial\Omega. \end{cases} \tag{1}$$

The ECT is based on the analysis and processing of impedance signal $\mathbf{Z}(\Omega_d)$ measured during a scan procedure of SG tube. Numerically, the impedance measured for the coil k in the electromagnetic field induced by the coil l is computed as follows:

$$\Delta\mathbf{Z}_{kl} = \frac{1}{|\mathbf{J}|}\left(\frac{\mu_0 - \mu_d}{i\omega\mu_d\mu_0}\int_{\Omega_d}\big(\mathbf{curl}\,\mathbf{E}_k\,.\,\mathbf{curl}\,\mathbf{E}_l^0\big)\,\delta v + (\sigma_0 - \sigma_d)\int_{\Omega_d}\mathbf{E}_k\,.\,\mathbf{E}_l^0\,\delta v\right). \tag{2}$$

In industrial applications one uses different combinations of $\Delta\mathbf{Z}_{kl}$ for a given frequency ω.We give in Figure 2 a validation of the direct 3D vs 2D solvers (in the axisymmetric case) by comparing two frequently used combinations $\mathbf{Z}_{FA} = \Delta\mathbf{Z}_{11} + \Delta\mathbf{Z}_{21}$ and $\mathbf{Z}_{F3} = \Delta\mathbf{Z}_{11} - \Delta\mathbf{Z}_{22}$.

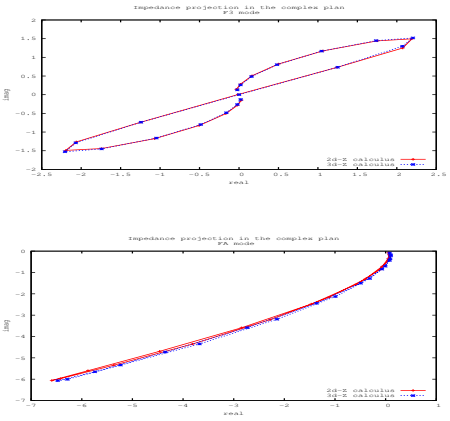

Figure 2: Complex-plane 3D-vs-2D comparison of the Impedance $\mathbf{Z}_{F3}$ and $\mathbf{Z}_{FA}$.

3 The inverse problem

The inverse problem aims at minimizing the misfit cost function $\mathcal{J}(\Omega_d) = \int_{z_{\min}}^{z_{\max}} |\mathbf{Z}(\Omega_d;\zeta) - \mathbf{Z}_{mes}(\zeta)|^2 d\zeta$, where $\mathbf{Z}$ is either $\mathbf{Z}_{FA}$ or $\mathbf{Z}_{F3}$ and Ω_d denotes the deposit domain. We shall present an inversion algorithm based on steepest gradient descent. Prior to this we shall rigorously define and characterize the shape gradient $\mathcal{J}'(\Omega_d)$. Using the adjoint technique this derivative is then expressed as $\mathcal{J}'(\Omega_d)(\boldsymbol{\theta}) = -\frac{\omega}{I^2}\int_{\Gamma_0}(\boldsymbol{\nu}^t\boldsymbol{\theta})g\,\delta s$ where the computation of the the function g involves the solution of the direct and the adjoint problem. In the shape gradient formulae, θ represents the transformation field and $\boldsymbol{\nu}$ stands for the outward normal. The solutions of the adjoint problem is expressed with P and W as the magnetic vector potential and the scalar electric potential respectively. The function g may have the form $g = g_{11} + g_{21}$ in the absolute mode or $g = g_{11} - g_{22}$ in the differential mode, with

$$\begin{aligned} g_{kl} = \int_{z_{\min}}^{z_{\max}} \Re\Big(& (\overline{\mathbf{Z}(\Omega_D;\zeta) - \mathbf{Z}_{mes}(\zeta)})\Big\{ \Big[\tfrac{1}{\mu}\Big]_{\pm}(\boldsymbol{\nu}\cdot\mathbf{curl}\,A_k)(\boldsymbol{\nu}\cdot\overline{P_l} - \boldsymbol{\nu}\cdot\mathbf{curl}\,\mathbf{A}_l^0) \\ & -[\mu]_{\pm}\Big(\boldsymbol{\nu}\times(\tfrac{1}{\mu}\mathbf{curl}\,\mathbf{A}_k\times\boldsymbol{\nu})\Big)\cdot\Big(\boldsymbol{\nu}\times(\tfrac{1}{\mu}\mathbf{curl}\,\overline{P_l}\times\boldsymbol{\nu}) - \boldsymbol{\nu}\times(\tfrac{1}{\mu^0}\mathbf{curl}\,\mathbf{A}_l^0\times\boldsymbol{\nu})\Big) \\ & +\tfrac{1}{i\omega}[\sigma]_{\pm}(i\omega\mathbf{A}_{k\tau} + \nabla_\tau\mathbf{V}_k)\cdot(\overline{i\omega P_{l\tau} + \nabla_\tau W_l} + i\omega\mathbf{A}_{l\tau}^0 + \nabla_\tau\mathbf{V}_l^0)\Big\}\Big)\,d\zeta. \end{aligned}$$

We shall present and compare two inversion strategies : the first one is based on a parametrized regularization of the shape and the second one is based on a regularized descent direction.

References

[1] Ana Alonso Rodriguez and Alberto Valli.Eddy current approximation of Maxwell equations, volume 4 of MS&A. Modeling, Simulation and Applications. Springer-Verlag Italia, Milan, 2010.Theory, algorithms and applications.

Inside-Outside-Duality and Interior Eigenvalues of Impenetrable Scatterers

Stefan Peters
ZeTeM, Zentrum für Technomathematik, Universität Bremen, Germany
Email: Stefan.Peters@math.uni-bremen.de

Abstract: Direct and inverse scattering problems for impenetrable scatterers are connected to the interior eigenvalues of scattering objects. Reconstruction methods like the linear sampling method or the factorization method for example can fail at interior eigenvalues [1]. Therefore we introduce a method to rigorously characterize the interior eigenvalues for either Dirichlet or Robin boundary conditions, using the far field data of corresponding exterior scattering problems.
Keywords: Dirichlet/Neumann/Robin eigenvalues, Inside-Outside-Duality.

1 The Determination of Interior Eigenvalues from Far Field Data

In our model the scatterer $D \subset \mathbb{R}^3$ is a bounded Lipschitz-domain with connected complement. We want to determine positive wave numbers $k > 0$ such that k^2 is an interior eigenvalue of the negative Laplacian, i.e. there exists a non-trivial solution of

$$\Delta u + k^2 u = 0 \quad \text{in } D, \qquad \mathcal{B}(u) = 0 \quad \text{on } \partial D,$$

where $\mathcal{B}(u)$ represents either Dirichlet conditions $\mathcal{B}(u) = u$ or Robin-boundary conditions $\mathcal{B}(u) = \partial u/\partial n + \tau u$ for a real-valued function $\tau \in L^\infty(D)$. Since we do not exclude the special case $\tau = 0$, the case of Neumann-boundary conditions is included in the following discussion. To determine the interior eigenvalues we consider corresponding exterior scattering problems

$$\Delta u + k^2 u = 0 \quad \text{in } \mathbb{R}^3 \setminus \overline{D}, \qquad \mathcal{B}(u) = 0 \quad \text{on } \partial D.$$

The total wave field u can be split into a sum of an incident incoming plane wave $u^i(x, \theta) = \exp(\mathrm{i}k\,\theta \cdot x)$ with direction $\theta \in \mathbb{S}^2 = \{x \in \mathbb{R}^3,\ |x| = 1\}$ and a scattered field $u^s(\cdot, \theta)$ that satisfies Sommerfeld's radiation condition. The scattered wave $u^s(\cdot\theta)$ behaves like an outgoing spherical wave, such that it can be represented by its far field $u^\infty(\hat{x}, \hat{\theta})$. In particual the far field operator can now be defined as

$$F : L^2(\mathbb{S}^2) \to L^2(\mathbb{S}^2), \qquad Fg(\hat{x}) := \int_{\mathbb{S}^2} u^\infty(\hat{x}, \theta) g(\theta)\, \mathrm{d}S(\theta), \qquad \hat{x} \in \mathbb{S}^2.$$

The farfield operator is compact and normal [1] and its eigenvalues λ_j lie on a circle of radius $8\pi^2/k$ with center $8\pi^2\mathrm{i}/k$ in the complex plane. We represent the eigenvalues in polar coordinates such that

$$\lambda_j = r_j \exp(\mathrm{i}\vartheta_j), \qquad r_j > 0, \quad \vartheta_j \in (0, \pi).$$

It can be shown that the eigenvalues λ_j converge to zero from the left for Dirichlet boundary condition and from the right for Robin boundary conditions. Therefore the eigenvalue λ_* with the smallest phase ϑ_* is well-defined for Dirichlet boundary conditions and the eigenvalue λ^* with the largest phase ϑ^* is well defined for Robin boundary conditions.
Our main result in the following: k_0^2 is an interior Dirichlet eigenvalue if and only if the smallest phase ϑ_* of the eigenvalue λ_* of F converges to zero as k approaches k_0 from below. Crucial tools we use in the process are the eigenvalue decemposition of the far field operator F, its well-known factorization $F = -G^* S^* G$, the denseness of the range of G in $H^{1/2}(\partial D)$ and the behaviour of the kernel of $S = S(k)$ with varying wave number k. In the case of Robin-eigenvalues k_0^2 is interior Robin eigenvalue if and only if the largest phase ϑ^* of the eigenvalue λ^* converges to π as k approaches k_0 from above. To proof this assertion, we use a more complex factorization of the far field operator and adapt the preceding arguments accordingly.

2 Numerical Results

In order to verify our theoretical results, we created far field data using the software package BEM++ (see [2]) to solve the arising boundary integral equations. As domains of computation we chose the unit ball $B_1(0)$ and the unit cube $C := [0,1]^3$. As a result we obtained a matrix F_N as a numerical approximation to the far field operator F. In particular we obtained numerical approximations λ_j^N and ϑ_j^N to the eigenvalues λ_j and its corresponding phases ϑ_j. Since we are interested in the behaviour of the smallest phase ϑ_* in the case of Dirichlet-boundary conditions and the behaviour of the largest phase ϑ^* in the case of Neumann-boundary conditions with varying wavenumber k, we plottet the phases ϑ_j^N against the wavenumber k. The results can be seen in the following graphs.

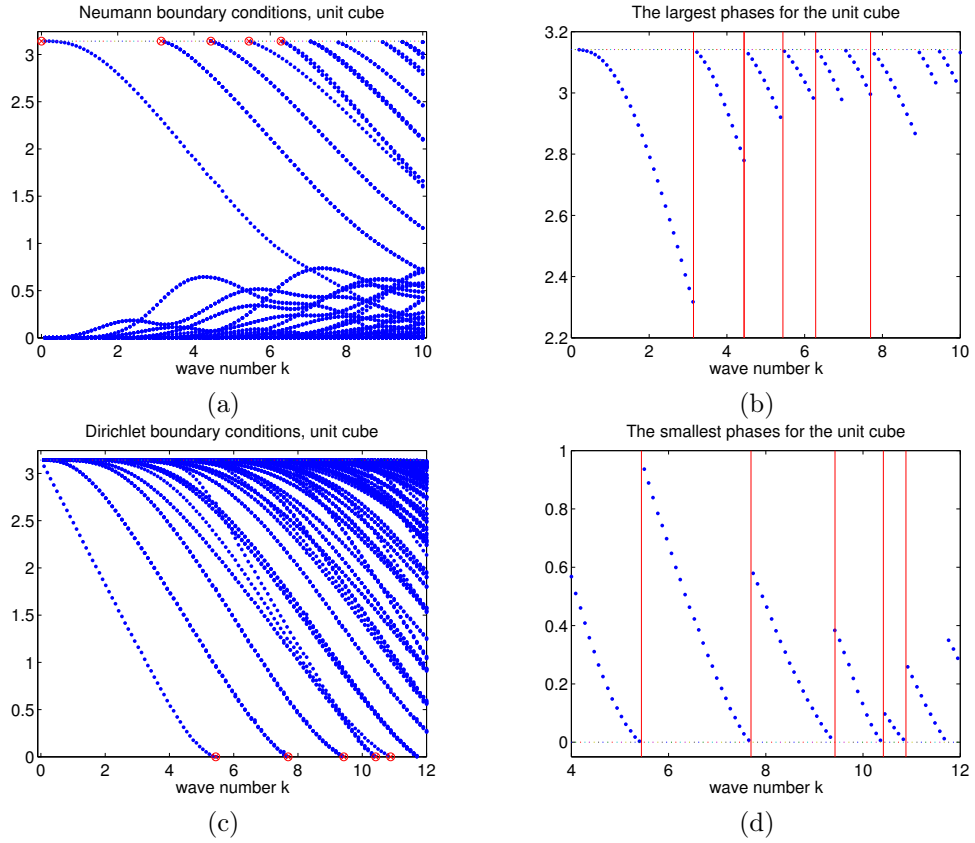

Figure 1: Blue dots mark the phases ϑ_j^N of the numerical eigenvalues $\lambda_j^N(k)$. Red circles on the k-axis mark the exact positions of the smallest five interior eigenvalues. (a) Phases of the numerical eigenvalues for the unit cube C and Neumann boundary conditions. (b) Only the largest phase from (a) was plotted. Vertical red lines mark the smallest five interior Dirichlet eigenvalues. (c) Phases of the numerical eigenvalues for the unit cube C and Dirichlet boundary conditions. (d) Only the smallest phase from (c) was plotted. Vertical red lines mark the smallest five interior Dirichlet eigenvalues.

This method of determining interior eigenvalues can be used especially well in those cases, where either the shape of the scattering object or the boundary condition of the scattering process is unknown. Furthermore the multiplicity of the interior eigenvalues can be determined as well without any additional expenses.

References

[1] A. Kirsch and N. I. Grinberg. *The Factorization Method for Inverse Problems.* Oxford Lecture Series in Mathematics and its Applications 36. Oxford University Press, 2008.

[2] Betcke T. Arridge S. Phillips J. Smigaj, W. and Schweiger. Solving boundary integral problems with BEM++. *Submitted to ACM Trans. Math. Softw*, 2013.

3.4 Mathematics for structure mechanics (MSM)

Estimation de paramètres dans une EDP elliptique $1D$

Lahcène Chorfi*

Résumé : On étudie un problème inverse d'identification de deux coefficients dans une équation elliptique 1D à partir de données sur la solution. On étudira l'opérateur direct qui associe aux coefficients la solution du problème aux limites. Cet opérateur n'est pas injectif (lorsque les coefficients sont variables), on étudiera alors son inverse au sens des moindres carrés. Pour reconstruire les coefficients nous proposons l'algorithme de Gauss-Newton régularisé. A chaque itération l'équation linéarisée est résolue par la méthode du gradient conjugué. Nous montrerons des résultats numériques qui illustrent les difficultés rencontrés dans un problème non linéaire mal posé.
Mots clés : Problèmes Inverses, Identification de paramètres, Moindres carrés non linéaires.

1 Problème direct

Considérons le problème aux limites elliptique $1D$ suivant : Trouver $u \in H^2(0,1)$, vérifiant :

$$(P) \quad \begin{cases} Lu := -b(x)u'' + c(x)u' = f(x) & \text{pour } x \in]0,1[\\ u(0) = 0, \quad u'(1) = 0. \end{cases}$$

Les fonctions b, c sont supposées continues sur $[0,1]$ telles que $b(x) \geq b_0 > 0$ et $c(x) \geq 0$. Le second membre $f \in L^2(0,1)$. Ce problème admet une solution unique donnée par l'intégrale

$$u(x) = \int_0^1 K(x,y) f(y) dy \tag{1}$$

avec

$$K(x,y) = \begin{cases} \left[\frac{1}{\lambda(y)} - \frac{\exp(\Lambda(0)-\Lambda(y))}{\lambda(0)}\right] \frac{1}{b(y)} & si \quad 0 \leq y \leq x \\ \left[\frac{1}{\lambda(x)} \exp(\Lambda(x)) - \frac{\exp \Lambda(0)}{\lambda(0)}\right] \frac{\exp(-\Lambda(y))}{b(y)} & si \quad x \leq y \leq 1 \end{cases}$$

où $\lambda(x) = \frac{c(x)}{b(x)}$ et $\Lambda(x) = \int_1^x \lambda(y) dy$.
Considérons l'opérateur direct $\Phi : U \mapsto H^1$ qui associe au couple $p \in U = \{(b,c) \in C^1[0,1] \times C[0,1],\ b(x) \geq b_0 > 0,\ c(x) \geq 0\}$ la solution u de (P). U est équipé de la norme $\|p\| = \|b\|_{C^1} + \|c\|_\infty$. On a le résultat de stabilité suivant.

Proposition 1.1 *(i) $\Phi : U \to H^2(0,1)$ est bornée sur chaque ensemble borné de U.*
(ii) Φ est localement Lipschitzienne : si $u_1 = \Phi(p_1)$ et $u_2 = \Phi(p_2)$, alors

$$\|u_1 - u_2\|_{H^1} \leq \frac{C}{b_0} \|p_1 - p_2\|_\infty \tag{2}$$

Remarquons que l'opérateur Φ n'est pas injectif (sauf si les coefficients (b,c) sont constants) comme le montre l'exemple suivant. En effet, si $u(x) = x - \frac{x^2}{2}$ et $f(x) = 2 - x$ alors pour tout $\alpha \in \mathbf{R}$ on a :

$$-u'' + u' = (1 - \alpha + \alpha x)u'' + (1 + \alpha)u' = f(x).$$

*Univ. B.M. Annaba–LMA, l_chorfi@homail.com

2 Problème inverse

Etant donné le terme source f, il s'agit d'identifier les coefficients b et c d'après des observations d sur la solution u. Considérons le cas d'une observation distribuée $d = u$. Si $u \in H^1(0,1)$ cela revient à inverser l'équation $\Phi(b,c) = u$. Cette équation est mal posée d'après l'exemple suivant. Soit la suite de fonctions $u_n = \frac{x}{n} + \frac{1}{n^2}(e^{-n} - e^{n(x-1)})$, alors, pour tout $n \geq 1$, on a $-u_n'' + nu_n' = 1$. On voit que u_n converge vers zéro dans H^1 alors que $c_n = n$ tend vers l'infini. Supposons maintenant que la donnée n'est pas exacte i.e $d = u^\delta \in L^2(0,1)$ avec $\|u - u^\delta\| \leq \delta$. On cherche alors une solution au sens des moindres carrés, c'est à dire trouver $p = (b,c) \in U$ qui minimise la fonction coût $J(a,b) = \dfrac{1}{2}\displaystyle\int_0^1 (u-d)^2 dt, \quad u = \Phi(a,b).$

2.1 Algorithme de Gauss-Newton

Le problème d'optimisation : $p_{min} = \text{argmin } J(p), \quad p = (b,c) \in U$, est résolu par la méthode de Gauss-Newton qui consiste à itérer la procédure suivante : p_0 étant une approximation initiale, $p_{n+1} = p_n + h_n$ où h_n est solution de l'équation

$$\Phi'^*(p_n)\Phi'(p_n)h_n = -\nabla J(p_n) = -\Phi'^*(p_n)(\Phi(p_n) - d)$$

Cette équation est mal conditionnée, on l'a résout par gradient conjugué ([2],[1]). On montre que la dérivée est donnée par $\Phi'(p;h,k) = (v,w)$ où (v,w) est solution du système :

$$\{-bv'' + cv' = hu''; \quad -bw'' + cw' = -ku'\} \text{ avec } u = \Phi(p).$$

2.2 Discrétisation et résultats numériques

La solution numérique du problème direct est obtenu par quadrature et collocation basée sur l'intégrale (1), d'où $u = R(p)f$ et $u' = S(p)f$ et $u'' = T(p)f$ avec des matrices du type $(2n,n)$, n étant le nombre de points de l'intervalle $(0,1)$. La matrice de $\Phi'(p)$ est donnée par :
$A(p) = [R(p)\ o\ \text{diag}(u''); -R(p)\ o\ \text{diag}(u')]$. Dans la figure 1, on montre les résultats de la simulation avec les données exactes suivantes : $b(x) = 1 + 0.5\sin(\pi x)$; $\quad c(x) = 1 + x - x^2$ et $f(x) = x - x^2$, $(d = u = R(b,c)f)$. Nous montrerons aussi des résultats lorsque la donnée est perturbée $(d = u^\delta)$. On vérifiera que l'algorithme est stable, par contre il est sensible à l'approximation initiale p_0.

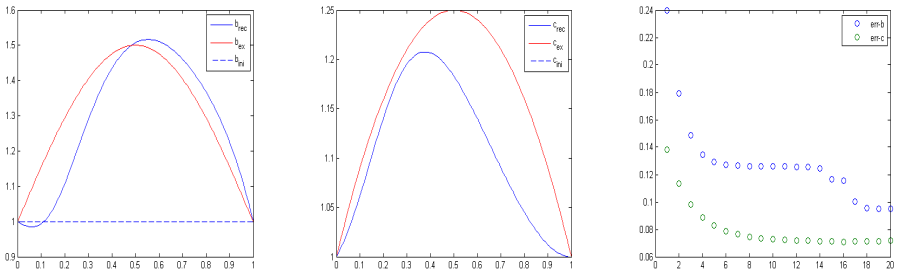

FIG. 1 – Reconstruction de b et c avec une donnée non bruitée $(n = 100)$

Références

[1] H. W. ENGL, M. HANKE, AND A. NEUBAUER., *Regularization of Inverse Problems.*, Kluwer Academic Publishers, 1996.

[2] M. HANKE, *Regularizing properties of a truncated Newton CG algorithm for nonlinear inverse problems*, Numer. Funct. Anal. Optim. 18 (1997), p.p. 971-93

Improving the mechanical performances of a multilayered plate with the orientations of its layers of fibers

Mekki Ayadi* Asma Gdhami† Abderrahmane Habbal‡
Maroua Mokni§ Boutheina Yahyaoui¶

Abstract: We consider a symmetric composite multilayered plate whose fibers orientation varies from one layer to another. The plate model used is that of Mindlin. We are interested in determining the optimal fiber orientations that maximize, in the same time, two criterions: the smallest eigenfrequency of vibration and the compliance or the smallest eigenfrequency of vibration and the smallest buckling critical load. In order to only maximize one criterion of the preceding ones, a metaheuristic algorithm of Simulated Annealing type is used. While, in the case of maximizing two objective functions, the Pareto frond method is used. Numerical results for a rectangular plate composed of four layers are presented.
Keywords: bending, free vibration, linear buckling, optimal orientations, compliance.

1 Introduction

We consider a multilayered composite plate which is symmetric with respect to its mid-plane, of thickness 2ε, and composed of $2m$ layers of fibers whose orientation varies from one layer to another, see figure 1. Every layer of fibers is assumed to be homogeneous and orthotropic with respect to its local coordinate system consisting of the fiber axis and its perpendicular. Hence, the multilayered plate is homogeneous but anisotropic. It is desirable that the composite plate should be very resistant and very light, but it should also be well suited to parametric optimization [1]. Indeed, in order to avoid the resonance of a structure under a given excitation, its eigenfrequencies have previously been controlled by its mass (location of some masses in adequate places on the plate). For a multilayered composite plate, we can also control the eigenfrequencies by its rigidity: find the optimal orientations of the layers of fibers, $\theta^* = (\theta_1^*, \theta_2^*, ..., \theta_m^*) \in [0, \pi]^m$, for which the spectrum of eigenfrequencies does not intercept the set of excitation frequencies (such as those corresponding to wind, earthquake, etc). The problem of maximizing the first eigenfrequency has been tackled by many authors [2], [6] by using the topological optimization method. However, in certain structure designs, such as the deck of a bridge, we are not allowed to create holes. In that case, one can recourse to parametric optimization. Moreover, the multilayered plate should be very resistant to buckling phenomenon, besides having a good bending rigidity. To do this, we must maximize the smallest critical buckling load and minimize the compliance: the work of uniform transverse load p, applied to the upper surface of the plate, in the vertical displacement. Therefore, we are faced with a compromise.

In this paper, we deal with the three following problems. First, we maximize the smallest eigenfrequency with respect to the orientations of layers of fibers. Second, we minimize the compliance. Finally, we look for minimizing, in the same time, the compliance and the opposite of the smallest buckling critical load since the smallest eigenfrequency and the compliance are not competitive. For these purposes, Mindlin's plate model is considered, the six-node triangular finite

*ENIT–lamsin, mekki.ayadi@enis.rnu.tn,
†ENIT–lamsin, asmagdhami@yahoo.fr,
‡Univ, Nice Sophia Antipolis–CNRS, LJAD, habbal@polytech.unice.fr,
§ENIT–lamsin, mokni.maroua@hotmail.com,
¶ENIT–lamsin, boutheinayahyaoui@hotmail.fr

element is used and the Simulated Annealing algorithm as well as the Pareto front method are implemented.

2 Mathematical setting

Let

$$W_M = \{v = (v_3, r_1, r_2) \in H^1(\omega)^3; v_3 = 0 \quad \text{on} \quad \partial\omega\}, \tag{1}$$

be the space of kinematically admissible bending displacements, where v_3 denotes the deflection of the plate, r_1 and r_2 denote the rotations of its mid plan, and $H_M = L^2(\omega)^3$. Let

$$V = \{v = (v_1, v_2) \in H^1(\omega)^2; v_1 = 0 \quad \text{on} \quad \gamma_0\}, \tag{2}$$

be the space of kinematically admissible membrane displacements, where v_α, $\alpha = 1, 2$, denote the displacements in the plane of the plate, and γ_1 is a portion of the boundary whose measure is not zero.
Let us now define the bilinear form $a_M(R(\theta).,.)$ by: $\forall u = (u_3, \eta_1, \eta_2), v = (v_3, r_1, r_2) \in W_M$,

$$a_M(R(\theta)u, v) = \int_\omega D_{\alpha\beta\mu\nu}(\theta)\partial_\nu\eta_\mu\partial_\beta r_\alpha d\omega + \int_\omega G_{\alpha\beta}(\theta)(\partial_\beta u_3 + \eta_\beta)(\partial_\alpha v_3 + r_\alpha)d\omega, \tag{3}$$

and the bilinear form $a(R(\theta).,.)$ by: $\forall u = (u_1, u_2), v = (v_1, v_2) \in V$,

$$a(R(\theta)u, v) = \int_\omega E_{\alpha\beta\mu\nu}(\theta)\partial_\nu u_\mu\partial_\beta v_\alpha d\omega, \tag{4}$$

The uniform W_M-ellipticity of a_M and the uniform V-ellipticity of a are shown in [3]. On the space H_M, we define the inner product:

$$(u, v) = \int_\omega (\frac{2\varepsilon^3}{3}\eta_\alpha r_\alpha + 2\varepsilon u_3 v_3)d\omega, \quad \forall u = (u_3, \eta_1, \eta_2), v = (v_3, r_1, r_2) \in H_M, \tag{5}$$

whose associated norm is equivalent to that of $L^2(\omega)^3$.
The free vibration problem is governed by the the following eigenvalue problem ($\lambda(\theta) = \varpi^2(\theta)$).

$$a_M(R(\theta)w(\theta), v) = \lambda(\theta)(w(\theta), v) \quad \forall v \in W_M. \tag{6}$$

The maximizing problem of the smallest eigenfrequency is

$$\max_{\theta\in[0,\pi]^m} \lambda_1(\theta) \quad \text{where} \quad \lambda_1(\theta) = \min_{v\in W_M\setminus\{0\}} \frac{a_M(R(\theta)v, v)}{(v, v)} = a_M(R(\theta)w_1(\theta), w_1(\theta)). \tag{7}$$

The maximizing problem of bending rigidity is

$$\min_{\theta\in[0,\pi]^m} \int_\omega pu_3(\theta)d\omega \quad \text{where} \quad a_M(R(\theta)u(\theta), v) = \int_\omega pv_3 d\omega \quad \forall v \in W_M. \tag{8}$$

The plate being submitted to a plane load $g_\alpha, \alpha = 1, 2$, the membrane problem is

$$a(R(\theta)u^g, v) = \int_{\gamma_1} g_\alpha v_\alpha d\gamma \quad \forall v \in V \quad \text{with membrane effort tensor} \quad n^g_{\alpha\beta} = E_{\alpha\beta\mu\nu}(\theta)\partial_\nu u^g_\mu. \tag{9}$$

The linear buckling problem is governed by the following eigenvalue problem [3].

$$a_M(R(\theta)w(\theta), v) = \delta(\theta)b(w(\theta), v) \quad \forall v \in W_M \quad \text{where} \quad b(w, v) = \int_\omega \frac{1}{2}n^g_{\alpha\beta}(\partial_\alpha w_3\partial_\beta v_3 + \eta_\alpha r_\beta)d\omega. \tag{10}$$

The maximizing problem of buckling rigidity is

$$\max_{\theta\in[0,\pi]^m} \delta_1(\theta) \quad \text{where} \quad \delta_1(\theta) = \min_{v\in W_M\setminus\{0\}} \frac{a_M(R(\theta)v, v)}{b(v, v)} = a_M(R(\theta)w_1(\theta), w_1(\theta)). \tag{11}$$

3 Numerical results

We consider a rectangular plate of thickness 8 mm, occupying a two dimensional domain $\overline{\omega} = [-0.1, 0.1] \times [-0.05, 0.05]$ and composed of four layers of carbon fibers assumed to be orthotropic. The material has density $\rho = 1000$ kg/m^3 and the following mechanical properties: $E_1 = 14.000e + 010$ Pa is the Young's modulus in the direction of fibers, $E_2 = 1.000e + 010$ Pa is the Young's modulus in the perpendicular direction, $\nu_{12} = 0.31$ is the Poisson's coefficient, and $G_{12} = G_{13} = G_{23} = 57.000e + 08$ Pa are the coefficient of plane shear and the transversal shear coefficients, respectively.
Using the simulated annealing algorithm [5], we obtain the following results.

-Smallest eigenfrequency
Also reached in$(\theta_1, \theta_2, \theta_2, \theta_1) = (\frac{\pi}{2}, \frac{\pi}{2}, \frac{\pi}{2}, \frac{\pi}{2})$, the maximum is equal $6.7785e + 8 \quad N/m^4$.

-Compliance
Reached in $(\theta_1, \theta_2, \theta_2, \theta_1) = (\frac{\pi}{2}, \frac{\pi}{2}, \frac{\pi}{2}, \frac{\pi}{2})$, the minimum compliance is equal $2.6071e - 12 \quad N.m$.

-Smallest buckling critical load
Reached in $(\theta_1, \theta_2, \theta_2, \theta_1) = (0.4443, 0.4443, 0.4443, 0.4443)$, the maximum is equal $5.8587e{+}6 \quad m$, while the minimum is reached in $(\frac{\pi}{2}, \frac{\pi}{2}, \frac{\pi}{2}, \frac{\pi}{2})$.
We observed that the two first criteria are not competitive, while the two last criteria are competitive as exemplify the Pareto front [4] given by figure 2.

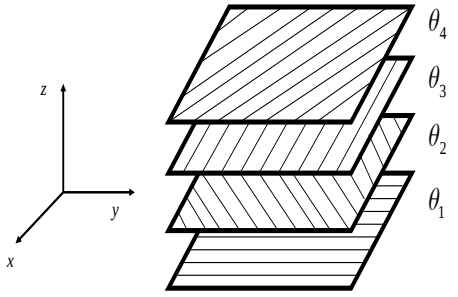

Figure 1: A multilayered rectangular plate with different orientations of layers of fibers.

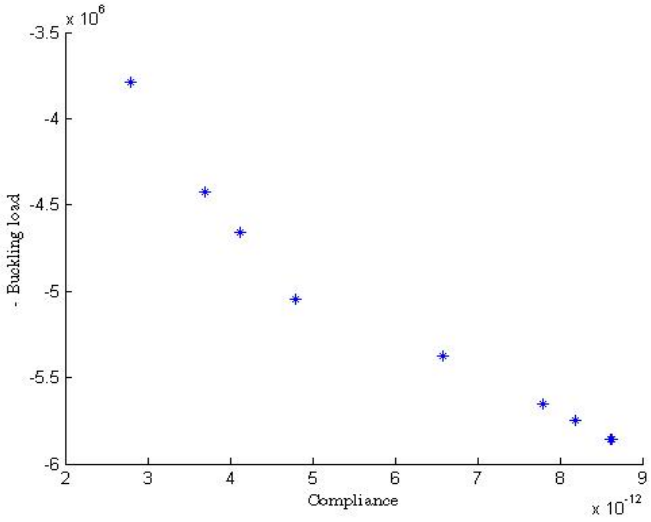

Figure 2: Pareto front for the compliance and the opposite of the smallest buckling critical load.

4 Bibliography

References

[1] Allaire G., Conception optimale de structures, Editions de l'Ecole Polytechnique, (2005).

[2] Allaire G., Jouve F., level-set method for vibrations and multiple loads in structural optimization, Comp. Meth. Appl. Mech. Engrg., 194 : 3269-3290, (2005).

[3] Ayadi M., Error estimates for the unilateral buckling load of a plate involving the membrane efforts consistency error, Euro. Jour. Comp. Mech., 17/8 : 1003-1038, (2008).

[4] Deb K., Evolutionary Algorithms for Multi-Criterion Optimization in Engineering design, pp. 135-161.1999.

[5] Kirkpatrick S., Gelatt C.D., Vecchi M.P, optimization by simulated annealing, Science, tome 220 $n°4598$, 671-680, 1983.

[6] Pedersen L.P., Optimization of holes in plates for control of eigenfrequencies, Struct Multidisc Optim, Vol. 28, 1-10. (2004).

Stabilized finite elements for curved fibred plates

Aymen Mannai*

Abstract: The solution of the most problems in thin structures using the classical finite elements methods isn't robust, since it is a subjected to numerical loking phenomenon. It was proved in [1] that it is the case for fibred plates.
An analysis was done to avoid this phenomenon in the plane plates case. We want to extend this work to the case of curved plates.

Keyworlds: Stabilized finite elements,

1 Energetic model :

The system energy is, in the general case, the sum of three energy contributions, namely

Gum energy : characterised by the energy's density w_{gum}, fiber energy characterised by the energy's density w_{cab} and coupling energy characterised by the energy's density w_{coup}. The expresion of total energy is

$$\begin{array}{l} \mathbf{E}_{plate} = \mathbf{E}_{gom} \ + \ \mathbf{E}_{cab} \ + \ \mathbf{E}_{coup} \\ \quad = \mathbf{E}_{gom} \ + \ \mathbf{E}_{mb}{}^{1} + \mathbf{E}_{fl} \ + \ \mathbf{E}_{coup} \\ \quad = \mathbf{E}_{gom} \ + \ \mathbf{E}_{coup} \int_{\overline{P}} \omega_{cab}(u,v) \ + \ \int_{\overline{P}} \omega_{coup}(d_3) \end{array} ,$$

where $\mathbf{E}_{mb}$ is the menmbrane part energy and $\mathbf{E}_{fl}$ is the flexion part energy of the fibres. The potential energy is:

$$\mathbf{J}(x,r,d_i) = \mathbf{E}_{plate} - \int_{\overline{P}} f \cdot r d\xi_\alpha,$$

where f is the external load, x is the 3D mouvement of plate, r is the fibers centerlines and and $d_{i\{i=1,2,3\}}$ the directors defined both at each point m of the plate's midsurface.

The main problem is to find the minimum of the potential energy in the space $\mathbf{K}^{ort}$ given by:

$$\mathbf{K}^{ort} = \left\{ \begin{array}{l} (x,r,d_i) \in \ \mathbf{K};\ \forall (\xi_1,\xi_2) \in \overline{P}, r(\xi_1,\xi_2) = x(\xi_1,\xi_2,0)\ ,\ d_i(\xi_1,\xi_2)\cdot d_j(\xi_1,\xi_2) - \delta_{j,j} = 0 \\ ,\ (x,r,d_i) \ \ \textit{verifies the boundary conditions selected} \end{array} \right\}, \tag{1}$$

where

$$\mathbf{K} = \left\{ (x,r,d_i) \in ((H^1(\overline{\Omega}))^3 \times (H^1(\overline{P}))^3 \times ((H^1(\overline{P}))^3)^3 \ \forall (\xi_1,\xi_2) \in \overline{P}, r(\xi_1,\xi_2) = x(\xi_1,\xi_2,0) \right. \tag{2}$$

where $\overline{P}$ is an open set of $\mathbb{R}^2$ and $\overline{\Omega}$ is an open set of $\mathbb{R}^3$

2 2D problem

In order to simplify our analysis, the 3D-problem is approached by a 2D-problem posed on the mid surface of the plate has discribed by the fonctional energy:

$$\mathbf{E}_{plate}(r,d_i) \ = \ \int_{\overline{P}} \sum_{i,j} \alpha_{i,j}(d_{i,1}\cdot d_j)^2 \ + \ \int_{\overline{P}} \sum_{i,j} \beta_{i,j}(d_{i,2}\cdot d_j)^2 \ + \ \int_{\overline{P}} \theta_i (r'\cdot d_i)^2 \ + \int_{\overline{P}} \omega^{2D}_{gom}(r,d_i), \tag{3}$$

where $\alpha_{i,j},\ \beta_{i,j}$ and θ_i are positive integrable and bounded coefficients.

*FST, mann3i86@yahoo.fr,

2.1 Classical finite elements method :

The problem of non-inhibited flexion fibered plate is non linear. By usig Newton method, the final problem is reduced to find:

$$\begin{array}{l} U_h^{\tilde{\varepsilon}} \;=\; (\delta r_h^{\tilde{\varepsilon}}, \delta d_{i,h}^{\tilde{\varepsilon}}) \in d\tilde{\mathbf{K}}_h^{ort} \;\; such\; that \\ \\ \mathbf{A}(U_h^{\tilde{\varepsilon}}, U_h) + \tilde{\varepsilon}^{-2}\mathbf{A}_{mb}(U_h^{\tilde{\varepsilon}}, U_h) = \mathbf{F}^0(U_h) \\ \forall \;\; U_h \;\in\; d\tilde{\mathbf{K}}_h^{ort} \end{array} \tag{4}$$

Here the orthogonal condition is limited to nodes of mesh,

$$d\tilde{\mathbf{K}}_h^{ort} = \left\{(\delta r, \delta d_i) \;\in (\mathbf{H}^1(\overline{P}))^2 \quad such\; that \quad \forall\, e \;\in\; [1, NE_h]\; (\delta r^i, \delta d_j^i) \;\in (\mathbf{Q}_2(I_h^e))^2 \right. \quad . \tag{5}$$

A_{mb} is the linerized membrane energy portion and A is the linerized remaining term of the total energy.

The error estimate is given by:

$$\exists \mathbf{C} \;>\; 0,\; \forall\, \tilde{\varepsilon} \;>\; 0,\; ||\; U^{\tilde{\varepsilon}} \;-\; U_h^{\tilde{\varepsilon}} \;||_{\tilde{\mathbf{K}}} \;\leq\; \mathbf{C}\tilde{\varepsilon}^{-2} \inf_{U^* \in d\tilde{\mathbf{K}}_h} ||U^{\tilde{\varepsilon}} \;-\; U^*\;||_{\tilde{\mathbf{K}}}$$

2.2 Stabilized finite elements for curved fibred plates

In order to obtain a uniform error estimate independent of $\tilde{\varepsilon}$, we will introduce, like in [1], a mixed formulation. We will choose a suitable finite elements spaces and build an orthogonal projection operator. The mixed formulation is given by:

$$\begin{array}{l} Find\; \{(\delta r, \delta d_i); p\} \;\in\; d\tilde{\mathbf{K}}_h \times (\mathbf{L}_h^2(\overline{P}))^3 \; such\; that \; \forall\; [(r, d_i); p] \;\in\; d\tilde{\mathbf{K}}_h \times (\mathbf{L}_h^2(\overline{P}))^3 \; we\; have \\ \\ \begin{array}{l} \mathbf{A}[(\delta r, \delta d_i); (r, d_i)] \;+\; \mathbf{B}[p; (r, d_i)] \;=\; L(\; r, d_i)\;) \\ \mathbf{B}[p; (\delta r, \delta d_i)] \;-\; \varepsilon^2\mathbf{C}[p; (r, d_i)] \;=\; \mathbf{M}(\; p\;) \end{array} \quad , \end{array} \tag{6}$$

where

$$\begin{array}{lll} \mathbf{A}:\; d\tilde{\mathbf{K}}_0 \times d\tilde{\mathbf{K}}_0 & \to & \mathbb{R} \\ \\ ((\delta r, \delta d_i), (r, d_i)) & \mapsto & (\delta r, \delta d_i)\frac{\partial^2 \tilde{\mathbf{E}}_0}{\partial (r, d_i)^2}(r, d_i) \;\; + c_0 \int\int_{\overline{P}} (\delta r' \cdot d_i \;+ r' \cdot \delta d_i) K_{i,i}^0 (r' \cdot d_i \;+\; r' d_i) \\ & & + \; c_0 \int\int_{\overline{P}} r' \cdot d_i \; K_{ii}^0 (r' \cdot \delta d_i \;+\; \delta r' \cdot d_i) \\ \\ \mathbf{B}:\; (\mathbf{L}^2(\overline{P}))^3 \times d\tilde{\mathbf{K}}_0 & \to & \mathbb{R} \\ (p; (r, d_i)) & \mapsto & \int_{\overline{P}} p_i (r_i' \cdot d_i \;+\; r_i' \cdot d_i)\; d\xi_\alpha \\ \\ \mathbf{C}:\; (\mathbf{L}^2(\overline{P}))^3 \times (\mathbf{L}^2(\overline{P}))^3 & \to & \mathbb{R} \\ (\; \delta p\;, p) & \mapsto & \int_{\overline{P}} (\; p_i \mathbf{K}_{ii}^{-1} \delta p_i)\; d\xi_\alpha \\ \\ \mathbf{L}:\; d\tilde{\mathbf{K}}_0 & \to & \mathbb{R} \\ (r, d_i) & \mapsto & \int_{\overline{P}} r \cdot f \;+\; \frac{\partial \tilde{E}_0(r, d_i)}{\partial (r, d_i)} \cdot (r, d_i) \;-\; p_i (r' \cdot d_i \;+\; r' \cdot d_i) d\xi_\alpha \\ \\ \mathbf{M}:\; (\mathbf{L}^2(\overline{P}))^3 & \to & \mathbb{R} \\ p & \mapsto & \varepsilon^2 \int_{\overline{P}} p_i \mathbf{K}_{ii}^{-1} p_i \;+\; \int_{\overline{P}} \; p_i (r' \cdot d_i \;-\; v_{i0}\;) d\xi_\alpha. \end{array}$$

and c_0 is positive constant.

The finite elements spaces in which we discretize δr and δd_i are given successively by:

$$\mathcal{V}_h \;=\; \left\{\delta r \;\in \mathbf{H}^1(\overline{P}) \;\; tel\; que \;\; \forall\, e \;\in\; [1, NE_h]\; \delta\, r^i \;\in \mathbf{Q}_2 + \;\bar{\mathbf{B}}_2(I_h^e) \;+ \mathbf{B}_2^0(I_h^e) \right. \quad . \tag{7}$$

$$\mathcal{W}_h \;=\; \big\{\delta d_i \;\in \mathbf{H}^1(\overline{P}) \;\; tel\ que \;\; \forall\, e \;\in\; [1, NE_h]\; \delta\, d_i^i \;\in \mathbf{Q}_2 + \;\mathbf{B}^0{}_2(I_h^e) \quad . \tag{8}$$

We obtain the following error estimate:

$$\begin{array}{l} ||\delta r \;-\; \delta r_h||_{\mathcal{V}_h} \;+\; ||\delta d_i \;-\; \delta d_{ih}||_{\mathcal{W}_h} \;+\; |||p \;-\; p_h|||_{\mathbf{W}} \;+\varepsilon||p \;-\; p_h||_{\mathbf{W}} \\ \leq\; C\inf_{\{\delta r \,\in\, \mathcal{V}_h,\; \delta d_i \in \mathcal{W}_h\; q \,\in\, (\mathbf{L}_h^2(\overline{P}))^3\}}(||\delta r \;-\; \delta r_h||_{\mathcal{V}_h} \;+\; |||p \;-\; q|||_{\mathcal{W}} \;+\; \varepsilon||p \;-\; q||_{\mathbf{W}} \end{array} \tag{9}$$

References

[1] Eric ligon , Modélisation multi-échelles de nappes fibrées en compression, Phd, Ecole polytechnique, LMS.

[2] Arnold, Douglas N. and Brezzi, Franco. Looking-free finite element methods for shells, Mathematics of Computation, vol 66 1997 N217 , pages :1-14.

3.5 Optimization and data assimilation (ODA)

Assimilation d'un déplacement de dunes de type Barkhane

Lamia Jaafar Belaid* Walid Mourou†

Abstract: This paper deals with a new application of data assimilation for a moving sand dunes of Barchans kind. Observations are derived from a series of satellite images using a segmentation approach based on watersheds. The simulations were made using a nudging technique.
Keywords: Barchans, nudging, segmentation, watersheds.

Résumé : Une application d'assimilation de données pour le déplacement de dunes de type Barkhanes est proposée. Les observations dérivent d'une série d'images satellites suivant une approche de segmentation basée sur la technique de la ligne de partage des eaux. Les simulations ont été réalisées en utilisant une technique de nudging.
Mots clés : Barkhanes, nudging, segmentation, ligne de partage des eaux.

1 Les dunes Barkhanes

Dans la nature, plusieurs formes de dunes de sable se présentent. On peut citer les dunes en étoiles, en rides, en vagues, nebka, ect. Nous nous intéressons dans notre travail aux dunes de type Barkhanes, voir Figure 1. Les Barkhanes se forment dans des milieux désertiques où le vent souffle en moyenne dans une seule direction tout au long de l'année avec une faible présence de sable. Ces formes sont assez présentes au sud des pays du Maghreb.

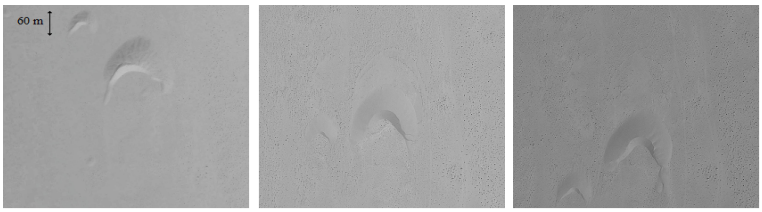

FIGURE 1 – Serie d'images satellites de deux Barkhanes à Tarfaya, Maroc (Google Earth).

Soit $h(x, y, t)$ le relief de la dune qui varie en temps et en espace selon l'équation de conservation de masse [3]. En notant par q le flux de matière emportée et par q_s le flux saturé après une distance parcourue l_s, on donne les équations d'évolution suivantes

$$\begin{cases} \dfrac{\partial h}{\partial t} = -\dfrac{1}{\rho_{sable}} \dfrac{\partial q}{\partial x} \\ \dfrac{\partial q}{\partial x} = \dfrac{q_s - q}{l_s} \\ \dfrac{q_s}{q} = 1 + A\dfrac{1}{\pi} \displaystyle\int_{-\infty}^{+\infty} \dfrac{h_e^{'}}{x - \xi} d\xi + B h_e^{'}, \end{cases} \tag{1}$$

où ρ_{sable} désigne la densité moyenne du sable et A, B sont des constantes liées au modèle. Le calcul des perturbations du vent est fait à travers une surface $h_e(x, y)$. Cette enveloppe prolonge le profil de la dune en amont de façon à satisfaire les conditions de régularité C^1.

*Université de Dammam, Ljaafar@ud.edu.sa,
†LAMSIN–ENIT, walid.mourou@gmail.com

2 Segmentation d'images

On considère une série d'images satellites de dunes. En général, ce type d'observations satellites permet d'identifier le type de dunes de sable (des Bakhanes dans notre cas), et de suivre leur évolution durant une période donnée. La dimension des dunes est extraite à partir d'une technique de segmentation d'images, comme le montre la figure 2. Cette technique est basée sur l'approche de la ligne de partage des eaux, combinée à une méthode de restauration d'images par gradient topologique, [4].

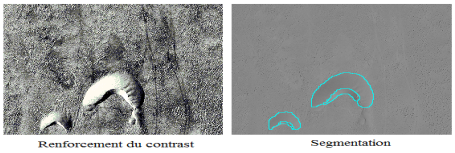

FIGURE 2 – Extraction des dunes à partir de l'image satellite.

Pour l'étape d'assimilation, les observations sont les reliefs 3D (h_{obs}) des dunes pour des différentes dates $\{\tau_1, .., \tau_p\}$. Nous utiliserons une approximation morphologique déduites des études des Barkhanes pour estimer leur hauteur $H = a\frac{W}{L} + b$. Les paramètres a et b dépendent essentiellement de l'endroit géographique et de la nature des grains de sable.

3 Assimilation

L'assimilation des données consiste à combiner de façon optimale toutes les sources d'informations disponibles sur un système dynamique pour en faire la prévision. Trois grandes classes de méthodes d'assimilation se présentent dans la littérature scientifique : l'assimilation séquentielle [1], l'assimilation variationnelle et le nudging [2]. Le nudging consiste à rajouter à l'équation du problème initial, un terme de régularisation $K(h_{obs} - h)$ (un terme de rappel aux observations).

$$\begin{cases} \dfrac{dh}{dt} = Ah + K(h_{obs} - h)\delta_{t\tau},\ 0 < t < T,\ \tau \in \{\tau_1, .., \tau_p\}, \\ h(t = 0) = h_0, \end{cases} \tag{2}$$

où K désigne la matrice de nudging. On donne dans la figure 3, l'assimilation de l'évolution d'une Barkhane suite à deux observations.

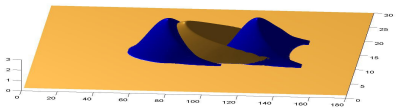

FIGURE 3 – Assimilation du déplacement d'une Barkhane selon deux observations.

Références

[1] D. Auroux, *Etude de différentes méthodes d'assimilation de données pour l'environnement.* Décembre, 2003. Thèse de Doctorat, Université de Nice, Sophia-Antipolis.

[2] D. Auroux, M. Nodet, *The back and forth nudging algorithm for data assimilation problems : theoretical results on transport equations.* 2012, 18(2) :318-342. ESAIM Control Optim. Calc. Var.

[3] P. Hersen, *Morphogenèse et Dynamique des Barchanes.* Juin, 2004. Thèse de Doctorat, Université Paris Diderot.

[4] L. Jaafar Belaid, W. Mourou, *Image segmentation : A Watershed Transformation Algorithm.* 2009, 28 :93-102. Image Anal Stereol.

VARIATIONAL DATA ASSIMILATION WITH YAO PLATFORM FOR THE CALIBRATION OF A HYDROLOGICAL MODEL

Amara ABBARIS[1], Hammouda DAKHLAOUI[2,3],
Sylvie THIRIA[1], Zoubeida BARGAOUI[2]

Abstract In this study a data assimilation based on Variational assimilation was implemented with HBV Rainfall-Runoff model by the mean of YAO platform of University Pierre and Marie Curie (France). The principle of the Variational assimilation is to consider the model state variables and/or model parameters as control variables and optimise them by minimizing a cost function measuring the disagreement between observations and model simulations. The Variational assimilation is used for the calibration of the HBV hydrological model. In this case the 14 model parameters are considered as control variables and optimised by minimizing the Nash criterion as cost function. Results are compared to those obtained by the well known powerful optimisation algorithm SCE-UA. To draw the calibration, parameters were divided into different sensitivity groups. A multistep calibration strategy was implemented beginning by the calibration of the most sensitive parameters and ending by the less sensitive. Two basins that belong under different climate: Sejnène from Tunisia, and Serein from France are studied. A Very good comparison is obtained with SCE-UA results in terms of Nash performance.

Key words: Variational assimilation, YAO, HBV model, Hydrological forecasting, optimisation, SCE-UA

1. Methods and Tools:

1.1 The HBV Rainfall-Runoff Model

The HBV model (Begström, 1976) is one of the most successful conceptual rainfall-runoff models that has been applied in more then 30 countries (Lindstrom et al., 1997). In the current study, a lumped modelling is adopted. The main model outputs are daily mean flows (m3/s) as well as daily actual evapotranspiration (mm/day). The principal water balance components of the HBV model are snow accumulation and melt, actual evapotranspiration and infiltration evaluation, soil humidity evolution, and water transfer through soil (Fig. 1). Further description of HBV model version used in this study could be found in Dakhlaoui & Bargaoui (2013). The model includes several state variables evolving continuously and that decide the flows values.

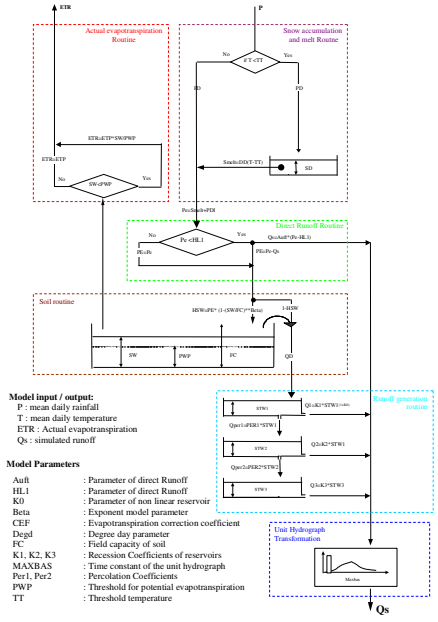

Fig. 1 HBV Model Structure

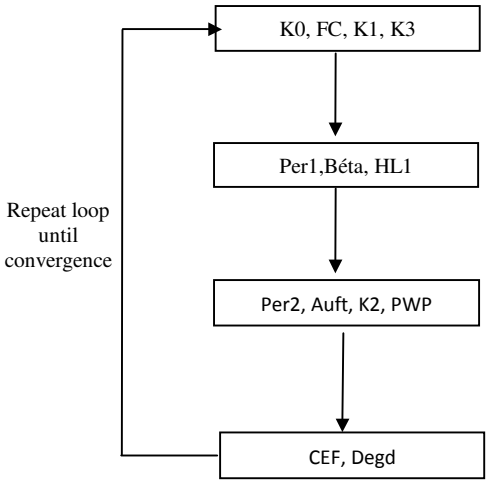

Fig. 2 Strategy of calibration of HBV model by Variational Assimilation,*In each box are mentioned the parameters to be calibrated in the step, the other parameters are fixed*

1.2 Variational assimilation

Variational assimilation (4D-VAR) (Le Dimet et al., 1986) considers a physical phenomenon described in space by one, two or three dimensions and its time evolution. It thus requires the knowledge of a direct dynamical model M, which describes the time evolution of the physical phenomenon.

(1) LOCEAN, Sylvie.Thiria@locean-ipsl.upmc.fr, amara.abbaris@gmail.com
(2) LMHE, zoubeida.bargaoui@laposte.net
(3) ENAU, hammouda.dakhlaoui@laposte.net Tel: (+216) 97534137

M allows connecting the geophysical variables studied with observations. By varying some geophysical variables (model parameters), assimilation seeks to infer the physical variables that led to the observation values. The basic idea is to determine the minimum of a cost function J that measures the misfits between the observations and the model estimations. Due to the complexity related to the non-linearity of this function, the desired minimum is classically obtained by using gradient methods, which implies the use of the tangent linear and the adjoint models of M. The latter and the former are derived from the equations of the direct model M. The adjoint model estimates changes in the control variables in response to a disturbance of the output values calculated by M (here HBV equations). It is therefore necessary to proceed in the backward direction to tangent linear calculations, which means to use the transpose of the Jacobian matrix. When observations are available, the adjoint allows to minimize the function J, and to find the values of the control variables.

1.3 YAO

YAO provides a framework helping the implementation of the adjoint model using a programming based on a general formalism decomposition of complex systems into modular graph (Nardi et al., 2009, http://www.locean-ipsl.upmc.fr/~yao/). The graph is composed of modules connected together by nodes and representing the numerical model. Each module is composed of an elementary function specific to the dynamic model, which is differentiable. YAO compiles and generates an executable that can compute the direct model M, the tangent linear model M and the adjoint model Mt. An interface with a quasi Newton optimiser is used to minimize the cost function.

2. Methodology

2.1 Calibration of HBV model with SCE-UA-KNN

The calibration consists on determining suitable model parameters values that give the best reconstitution of observed runoff by the model giving the observed rainfall data and air temperature data as inputs. The calibration of rainfall-runoff model could be considered as an optimization problem stated as follows:

$$\min_{\theta} \{FO(qoi, qci, \theta), i=1,n\} \quad (1)$$

with: n : number of time steps or observations qoi : observed runoff at time step i; i=1,… n.
qci : simulated runoff at time step i; i=1,… n. θ: model parameters FO: objective function.

It minimizes over θ, several performance model criteria that reflect the degree of similarity between observed and simulated runoff series. Generally distance based measures are involved also taking account for model errors heteroscedasticity. In this paper we selected the Nash-Suttclife as calibration criterion (Nash and Sutcliffe, 1970).

$$\text{Nash}=1-\frac{\sum_{i=1}^{n}(q_{ci}-q_{oi})^2}{\sum_{i=1}^{n}(q_{oi}-\bar{q}_o)^2} \quad (2)$$

With $\bar{q}_0$: mean observed runoff:

The Shuffled Complex Evolution of the University of Arizona (SCE-UA) (Duan et al., 1993) global optimisation method is recognised as one of the most effective optimisation algorithms applied to achieve rainfall runoff model calibration (Gupta et al., 1999; Thyer et al., 1999). Despite the fact that it is efficient and effective, the SCE-UA is time consumer when applied to the calibration of rainfall-runoff models. In fact it needs a great number of objective function evaluations to reach the optimal solution (Tolson and Shoemaker, 2007) especially in the case of a huge number of parameters to be calibrated. Dakhlaoui et al. (2012) proposed a hybrid version of SCE-UA that adopts the K-Nearest Neighbours (KNN) to approximate the objective function: SCE-UA-KNN. This enhanced optimisation algorithm was found to be two to three times faster than original SCE-UA with conserving the same rate of effectiveness. It was adopted in this study to calibrate HBV model.

2.2 Calibration of HBV model with variational assimilation :

The HBV model has a huge number of parameters to be calibrated. The calibration of all these parameters simultaneously can give a high dimension problem which is not evident to be resolved. We propose in this study a specific strategy to calibrate the model parameters by dividing them into 4 groups with respect to their sensitivity to the objective function (Nash). The calibration is performed separately for each group beginning by the most sensitive parameters and finishing by the less sensitive. This loop is repeated until convergence (Fig. 5).

3. Results and Discussion

3.1 Calibration with SCE-UA-KNN and validation

The HBV model was calibrated, firstly with the hybrid SCE-UA-KNN optimisation algorithm (Dakhaloui et al., 2012) for two catchments (Sejnène and Serein). The calibration period was from September 1964 to August 1967 for Sejnène and from January 1998 to December 2002 for Serein. The validation periods were from January 2008 to Mars 2010 for Serein and from September 1967 to August 1969 for Sejnène (Table 2). The 14 model parameters were considered simultaneously in the calibration process. It is concluded that satisfactory model performances are achieved. In fact, the Nash-Suttclife criterion is about 0.85 for Serein, 0.80 for Sejnène. The plots of the time series of observed and simulated runoff illustrate the good quality reconstitution of flows

(Fig. 3 and 4). There is little difficulty for the model to reconstitute the peak flows. The disparity found in parameter values within studied catchments may reflect the difference in climate, geology, soil and vegetation specific conditions. It may also be due to scaling effects of basin area. For the validation period model conserves a high performance in the case of Serein, with similar Nash criterion values as found in calibration period. For Sejnène there is an important deterioration of Nash criterion that decrease to 0.61 (which is still acceptable).

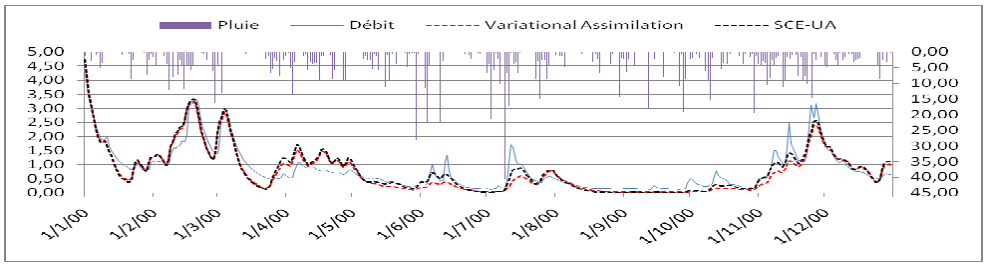

Fig 3. Evolution of streamflow at the outlet of the **Serein** for calibration period (2000). Solid line corresponds to measured streamflow, dash dotted line to simulated streamflow.

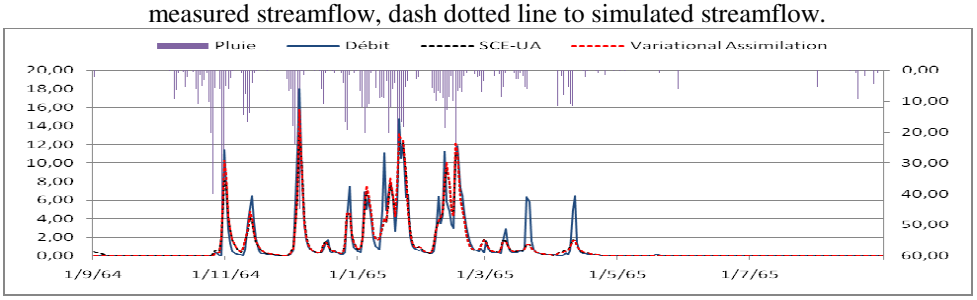

Fig 4. Evolution of streamflow at the outlet of the **Sejnène** for calibration periond (1964-1965). Solid line corresponds to measured streamflow, dash dotted line to simulated streamflow.

3.2 Calibration with Variational assimilation and validation

The HBV model was calibrated with the Variational assimilation for the two studied catchments. The plots of the time series of observed and simulated runoff reflect the high quality of the reconstitution of flows (Fig.3 and 4). The Nash-Suttclife criterion is about 0.85 for Serein, and 0.80 for Sejnène. As in the case of SCE-UA, there is also little difficulty for the model to reconstitute the peak flows. For both methods, it is found that, in the validation period, the model conserves its high performance for Serein while deteriorates for Sejnène (with the same Nash=0.61). For Serein catchment, the Nash quality is not deteriorated in validation.

4. Conclusion

YAO is a very flexible and powerful tool for developing assimilation procedures; it allowed us to apply Variational assimilation for calibrating HBV model. The calibration of HBV model was not an easy exercise for Variational assimilation. We were constrained to use a specific strategy to calibrate the 14 parameters of HBV model. The model parameters were adjusted separately group by group. The parameters groups were selected according their sensitivity to Nash. In term of performance, similar results were obtained by SCE-UA and 4D-Var. However, some (optimal) model parameters were very different. In term of efficiency, the variational assimilation seems to be less time consumer then SCE-UA.

Acknowledgments

Authors would like to thank IRSTEA and DGRE for data. This work is part of the Tunisia – France scientific cooperation 2011-2014 program CMCU number 10G1102.

5. References

Dakhlaoui H., Bargaoui Z et Bárdossy A., 2012. Toward a more efficient Calibration Schema for HBV Rainfall-Runoff Model . Journal of hydrology. Volumes 444–445, 11 June 2012, Pages 161-179.

Dakhlaoui H. et Bargaoui Z., 2013. A hybrid SCE-UA-KNN Optimisation Algorithm applied to the calibration of Rainfall-Runoff Model. In : Calibration Theory and Application. Edited by : Ikumatsu Fujimoto and Kunitoshi Nishimura. Nova Publication. ISBN: 978-1-62618-808-2

Duan Q., Gupta V. K., and Sorooshian S., 1993. A Shuffled complex evolution approach for effective and efficient global minimization. Journal of optimisation Theory Application, 76 (3) , 501-521.

Gupta H.V. , Sorooshian S. and Yapo P.O., 1999. Status of automatic calibration for hydrologic models: comparison with multilevel expert calibration. Journal of hydrologic Engineering, April 1999 , 135-143

Johnston P. R., and Pilgrim D., 1976. Parameter optimisation for watershed models. Water Resources Research,

Le Dimet, F.-X., Talagrand, O. Variational Algorithms for Analysis and Assimilation of Meteorological Observations: Theoretical Aspects. Dynamic Meteorology and Oceanography 38. 1986.

Nardi L., C. Sorror, F. Badran, and S. Thiria. 2009. YAO: a Software for Variational Data Assimilation using Numerical Models, International Conference on Computational Science and its Applications, ICCSA 2009, Seul, South Korea, June 2009, pp.Part II, 621-636, Series LNCS 5593,

Nash, J. E., and J. V. Sutcliffe, 1970. River flow forecasting through conceptual models. 1. A discussion of principles. J. Hydrol., 10 (3), 282–290.

YAO: Home Page http://www.locean-ipsl.upmc.fr/~yao/

Proper orthogonal decomposition in cardiac electrophysiology

Lassoued jamila * Mahjoub moncef † Zemzemi néjib ‡

Abstract:

A reduced-order model based on Proper Orthogonal Decomposition (POD) is proposed for the monodomain equations of cardiac electrophysiology. In this work we propose to evaluate the accuracy of this method while changing different parameters in the model. We first build the reduced order model using a set of parameters, afterwards, we evaluate the accuracy of the reduced model by changing the parameters of the ionic model model. The main goal of this study is to evaluate the usefulness or the unusefulness of the POD in the parameter estimation problem.

Keyworlds: Cardiac electrophysiology, reduced-order model, POD, ionic parameters.

1 Modelling

1.1 Electric model

We use the moodomain model to describe the propagation of the electrical wave in the heart. The model consists of a reaction-diffusion PDE, where the reaction term is linked to a dynamic system representing the cell activity. The heart is supposed to be isolated from the external environement. The coupled PDE/ODE system is described by the following equations [4]:

$$\begin{cases} \chi_m \dfrac{\partial V_m}{\partial t} + I_{ion}(V_m, w) - div(\sigma \nabla V_m) = I_{app} & \text{in } \Omega_H \times (0,T) \\ \dfrac{\partial w}{\partial t} + G(V_m, w) = 0 & \text{in } \Omega_H \times (0,T) \\ \sigma \nabla V_m . n = 0 & \text{on } \Sigma. \end{cases} \tag{1}$$

where Ω_H and Σ denote respectively the heart field and heart thorax interface. The time domain is given by $[0,T]$. And χ_m the membrane capacitance per area unit. The variable V_m denote the action potential, and σ is the bulk conductivity. The term I_{app} is a given external current stimulus, w represents the concentrations of different chemical species, and variables representing the openings or closures of some gates of the ionic channels. And the ionic current I_{ion} and the function $G(V_m, w)$ depends on the considered ionic model.

*ENIT–lamsin, lassoued.jamila@gmail.com,
†ENIT–lamsin, moncef.mahjoub@lamsin.rnu.tn ,
‡INRIA Bordeaux Sud-Ouest, nejib.zemzemi@inria.fr,

1.2 Numerical results

To solve numerically the simplified model in the heart given by (1) we follow the procedure explained in [1] , After a variational formulation and a time discretization, we obtain:

$$\begin{cases} w^{n+1} = w^n - \delta t G(V_m^n, w^{n+1}) = 0 & \text{in } \Omega_H \\ \chi_m \int_{\Omega_H} V_m^{n+1}\phi + \delta t \int_{\Omega_H} \sigma \nabla V_m^{n+1} \nabla \phi = \chi_m \int_{\Omega_H} V_m^n \phi & \\ \qquad + \delta t \int_{\Omega_H} (I_{app}^{n+1} - I_{ion}(V_m^n, w^{n+1}))\phi & \forall\ \phi \in H^n(\Omega_H) \end{cases} \tag{2}$$

Using the finite element method, we obtain the space discretization of the variational formulation follows:

$$\begin{cases} w^{n+1} = w^n - \delta t G(V_m^n, w^{n+1}) & \text{in } \Omega_H \\ \chi_m M V_m^{n+1} + \delta t K V_m^{n+1} = \chi_m M V_m^n + \delta t M (I_{app}^{n+1} - I_{ion}(V_m^n, w^{n+1})) & \end{cases} \tag{3}$$

$$M = (\int_{\Omega_H} e_i e_j)_{i,j=1,\cdots,n} \quad \text{and} \quad K = (\int_{\Omega_H} \sigma \nabla e_i \nabla e_j)_{i,j=1,\cdots,n}$$

where M is the Mass matrix, and K is the stifness matrix, and $I_{ion}(V_m, w)$, $G(V_m, w)$ depends on the ionic model used.

In this study, the dynamics of w and I_{ion} are described by the phenomenological two-variable model introduced by Mitchell and Schaeffer [2]. then The dynamics of w and I_{ion} are described by:

$$I_{ion}(v, w) = \frac{w}{\tau_{in}} v^2 (v - 1) - \frac{w}{\tau_{out}}$$

$$G(v, w) = \begin{cases} \dfrac{w - 1}{\tau_{open}} & \text{si } \ v > v_{gate} \\ \dfrac{w}{\tau_{close}} & \text{si } \ v > v_{gate} \end{cases} \tag{4}$$

2 Reduced order method

The proper orthogonal decomposition (POD)(see [3, 5]) is a linear process aiming to determine an optimal orthogonal basis in the sense of energy. This means that there is no base capable to capture higher amount of energy with the same number of modes. The POD basis is computed using the Truncated Singular Value Decomposition (SVD) procedure performed on a precomputed solution. This solution is computed for a given set of parameters. We are concerned about what happens when this POD basis is used to solve the same problem but with different parameters. Our investigation is restricted to the characteristic times of gate opening and closing respectively τ_{close}, τ_{open} and the constants time τ_{in}, τ_{out} respectively related to the length of the depolarization and repolarization (final stage) phases.

3 Numerical results

We constructed a POD basis using the original values of the ionic model parameters. Then, we variate each of the parameters between half and three halfs its original value. We look at the error between the reduced order solution and the full finite element solution. The figures below show the L2 relative error in time and space between the full finite element solution and the reduced order solution for different set of parameters.

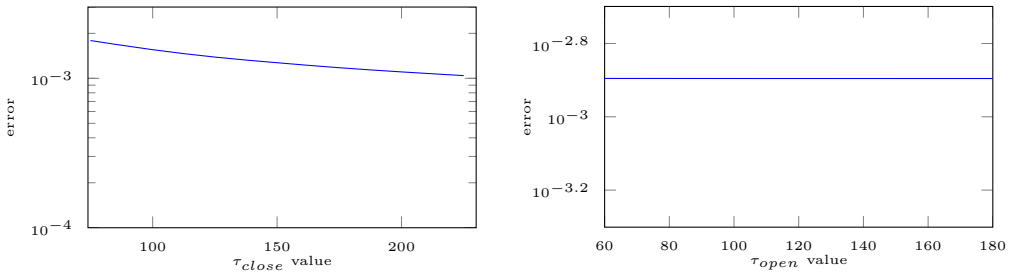

Figure 1: Left: The error between the finite elements solution and the POD solution when the value of the paramerter τ_{close} vary . Right: The error between the finite elements solution and the POD solution when the value of the paramerter τ_{open} vary.

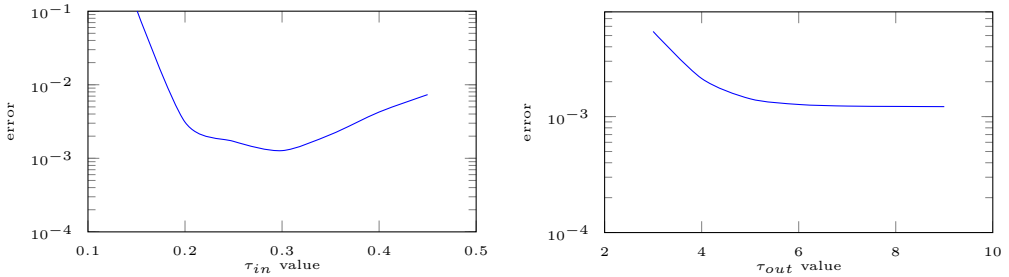

Figure 2: Left: The error between the finite elements solution and the POD solution when the value of the paramerter τ_{in} vary. Right: The error between the finite elements solution and the POD solution when the value of the paramerter τ_{out} vary.

From these figures, we remark that the error remains too small (less than 1%) when changing τ_{close}, τ_{open} and τ_{out}. While, for τ_{in}, the relative error increase considerably when the distance between the value of parameters and the original value increases. The main conclusion of this study is that in case of parameter estimation framework it is recommended to use the POD in order to estimate τ_{close}, τ_{open} and τ_{out}. But to estimate τ_{in}, the data from which the POD basis is computed should be sufficiently rich in order to maintain a good accuracy of the results.

References

[1] N. Zemzemi, Etude théorique et numérique de l'activité électrique du coeur: applications aux électrocardiogrammes, PhD thesis, 2009.

[2] C. C. Mitchell and D. G. Schaeffer, A Two-Current Model for the Dynamics of Cardiac Membrane. Department of Mathematics,Duke University and Center for Nonlinear and Complex Systems,Durham NC 27708,Box 90320,U.S.A.

[3] Muruhan Rathinam and Linda R. Petzold – A new look at proper orthogonal decomposition . SIAM J. NUMER. ANAL. c 2003 Society for Industrial and Applied Mathematics Vol. 41, No. 5, pp. 1893-1925

[4] P. C. Franzone, L. F. Pavarino, and B. Taccardi, Simulating patterns of excitation, repolarization and action potential duration with cardiac bidomain and monodomain models. Math. Biosci., 197(1):35-66, 2005.

[5] S. Volkwein. Model reduction using proper orthogonal decomposition.

Continuation methods and Nesterov optimisation techniques for general structured sparse learning

Hadj Selem Fouad *
(joint with Tommy Löfstedt, Edouard Duchesnay, Vincent Frouin and Vincent Guillemot)

Keyworlds: convex nonsmooth optimisation; structured learning.

1 Introduction

Machine Learning methods applied to the analysis of high-dimensional data are often required to use complex penalties either inducing sparse models or making possible to take the structure of the variables into account. Such penalties help to regularise the optimisation problem and at the same time yield models that are more interpretable. We present a framework to combine one or several non-smooth convex penalties, such as for example the ℓ_1-norm or a Total Variation penalisation, with a smooth convex objective function, such as the ordinary least squares loss.

2 Method

Let us consider the constrained optimisation problem

$$\min_{\beta \in \mathbb{R}^p} f(\beta) = \min_{\beta \in \mathbb{R}^p} \left\{ g(\beta) + \gamma s(\beta) + \kappa h(\beta) \right\}, \tag{1}$$

where g is a differentiable convex function with a Lipschitz continuous gradient, h is a convex non-differentiable function with a known proximal operator, s is an additional convex non-differentiable structured penalty whose proximal operator is not necessarily known or is difficult to express or compute, and κ and γ are regularisation parameters belonging to $\mathbb{R}^+$. This class of optimisation models is very general and includes classical models such as LASSO, Ridge and Elastic Net, the less common TV and group LASSO. In the general case, when the functions are not separable, the computation of the proximal operator is difficult if possible at all. We therefore propose to apply Nesterov's smoothing technique to approximate s and consequently be left with the remaining non-differentiable part of the function g with a known and easy to compute proximal operator. From this regularisation arises a new optimisation problem, closely related to the one given in Eq. (1), namely

$$\min_{\beta \in \mathbb{R}^p} \widetilde{f}(\mu, \beta), \text{ with } \widetilde{f}(\mu, \beta) = g(\beta) + \kappa h(\beta) + \gamma s_\mu(\beta), \tag{2}$$

problems like those in Eq. (2) can be solved by iterative methods such as FISTA (Beck and Teboulle 2009) which is chosen because of its fast convergence rate governed by:

$$\widetilde{f}(\mu, \beta^{(k)}) - \widetilde{f}(\mu, \beta^*_\mu) \leq \frac{2}{t_\mu (k+1)^2} \|\beta^{(0)} - \beta^*_\mu\|_2^2, \tag{3}$$

where $k \geq 0$ is the iteration number and t_μ is the time step that must be chosen smaller or equal to the inverse of $L(\nabla g + \gamma \nabla s_\mu)$:

$$t_\mu = \frac{1}{L(\nabla(g)) + \gamma \frac{\|A_s\|_2^2}{\mu}}. \tag{4}$$

It should be noticed that μ and t_μ are linked to one another and vary in the same way, although they drive different aspects of the algorithm convergence. Indeed, if μ is small the algorithm will converge with a high precision and if t_μ is large it will converge rapidly. There is thus a trade-off between speed and accuracy.

that allows us to smooth a part of the non-smooth function while retaining a maximum speed of convergence towards the minimum of the original function (and not that of the approximation). In particular, this will allow us to take into account the ℓ_1 penalty explicitly, since it induces the desired sparsity of the solution. Our method, called CONESTA.

3 Application and Results

Now, we place ourselves in the context of linear regression models. Let $X \in \mathbb{R}^{n \times p}$ be a matrix of n samples, where each sample lies in a p-dimensional space; and let $y \in \mathbb{R}^n$ denote the n-dimensional response vector. In the linear regression model $y = X\beta + e$, where e is an additive normally distributed noise, β represents the unknown vector of length p containing the regression coefficients. The ordinary least squares regression, constrained with both an Elastic Net and a "group" penalty, will be considered in this work as an application example of such optimisation problems. The function we wish to minimise is

$$f(\beta) = \underbrace{\frac{1}{2}\|X\beta - y\|_2^2 + \frac{1-\kappa}{2}\|\beta\|_2^2}_{\text{smooth}} + \underbrace{\gamma \sum_{G \in \mathcal{G}} (\|A_G\beta\|_2) + \kappa\|\beta\|_1}_{\text{non-smooth}}, \tag{5}$$

where $s(\beta) = \sum_{G \in \mathcal{G}} (\|A_G\beta\|_2)$ is a constraint on the structure of the variables, with $\mathcal{G}$ a set of groups of variables and A_G a linear operator on $\mathbb{R}^p$. TV and group $\ell_{1,2}$ are two good examples of such "group" penalties.

We show on both simulated data and realistic simulated data that CONESTA compares favorably in terms of execution time and precision to the reference method we considered, namely the Excessive Gap method (see Figure 2). One particularly interesting result of our application on linear regression with an ℓ_1-norm and a Total Variation penalties is that we recover more meaningful groups of variables in the estimated model with CONESTA than with state-of-the-art methods (see Figure 1).

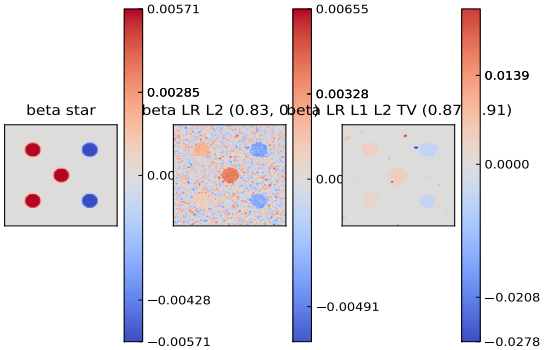

Figure 1: Maps of weights. β^* is the ground truth, β^{EN+TV} the map found with Elastic Net and TV penalties found by CONESTA and β^{EN} is the map found with just the Elastic Net penalty.

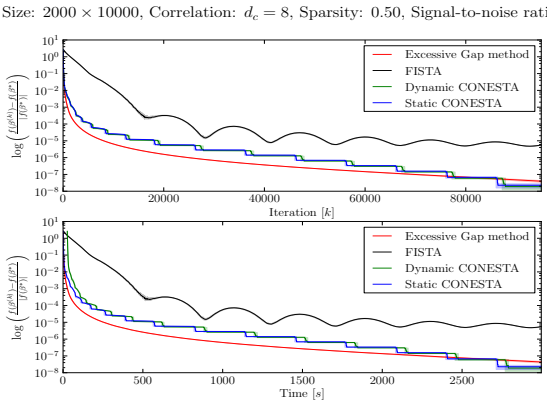

Figure 2: The logarithmic relative error as a function of the number of iterations (upper plot) and the computational time (lower plot).$p = 10000$, $n = 2000$, $d_c = 8$, sparsity $= 0.50$ and SNR $= 20$.

Acknowledgments

This work was supported by grants from the French National Research Agency: ANR GENIM (ANR-10-BLAN-0128), ANR IA BRAINOMICS (ANR-10-BINF-04), ANR Karametria (ANR-09-BLAN-0332-01) and a European Commission grant: MESCOG (FP6 ERA-NET NEURON 01 EW1207).

References

[1] Hadj Selem F., Löfstedt T., Duchesnay E., Frouin V. and Guillemo V.; Continuation methods and Nesterov techniques for general structured sparse learning (submitted).

3.6 Stochastic optimization and non linear problems (SONL)

Étude de la performance de l'hybridation d'une méthode d'optimisation avec une formule de représentation de l'optimum global

M. Chemkhi, M. Jebalia, A. Makhlouf, and M. Moakher

LAMSIN - École Nationale d'Ingénieurs de Tunis - Université Tunis El-manar
BP37, Le Belvédère 1002, Tunis
majed_chemkhi@hotmail.fr
mohamed.jebalia@enit.rnu.tn
azmi.makhlouf@gmail.com
maher.moakher@enit.rnu.tn

Abstract. Dans ce travail, nous nous intéressons à l'amélioration de la performance de certaines méthodes d'optimisation lors de la recherche de l'optimum global d'une fonction objectif multimodale. Nous regardons en particulier la possibilité d'améliorer la performance de la méthode de quasi-Newton "BFGS", méthode locale, de point de vue recherche globale.
Pour ce faire, notre idée est de coupler une méthode de recherche stochastique dérivée d'une formule de représentation [1] avec la méthode déterministe BFGS. La méthode numérique est basée sur écriture, en méthode de Monté-Carlo, de la formule de représentation.
Tout d'abord, nous étudions théoriquement et numériquement la convergence de la méthode numérique issue de la formule de représentation. Dans l'étude théorique, nous établissons la convergence de la méthode et regardons sa vitesse de convergence en utilisant des outils de probabilités tels que la loi des grands nombres. L'étude numérique est faite sur des fonctions objectifs tests bien connues dans la littérature [3]. La méthode est d'abord validée en la comparant à des méthodes de Monte-Carlo basiques tels que la méthode de recherche aléatoire adaptative [4]. Les résultats numériques montrent que la méthode issue de la formule de représentation donne de meilleurs performances par rapport aux méthodes références et ceci en termes de vitesse de convergence et de robustesse.
Par la suite, on couple la méthode stochastique avec la méthode de BFGS. Le nouveau procédé donne de meilleurs résultats que la méthode de BFGS sur l'ensemble de fonctions testées.
En outre, un résultat trés intéressant est le fait que les résultats numériques montrent une robustesse du nouveau procédé par rapport à la dimension de l'espace de recherche.

Mots clés
Optimisation numérique - Méthodes de Monté-Carlo - BFGS - Probabilités - Loi des grands nombres.

2

Reférnces

[1] J. E. Souza de Cursi. Une formule de représentation pour le point d'optimum global d'une fonctionnelle régulière en dimension finie. Note de recherche 061/02, LMR, Rouen.

[2] H. Zidani, R. Ellaia, and J. E. Souza de Cursie. A hybrid Nelder Mead search with representation formula for global optimization. TAMTAM, Sousse, Tunisia, 2011.

[3] S. Finck, N. Hansen, R. Ros, and A. Auger. Real-parameter black-box optimization benchmarking 2010. Presentation of the noiseless functions, 2010.

[4] Z. B. Zabinsky and R. L. Smith. Pure adaptive search in global optimization. Mathematical programming, 53(3) :323-338, 1992.

RUNGE KUTTA APPROACH FOR OPTION PRICING WITH CONSTANT ELASTICITY OF VARIANCE (CEV) MODEL

Abdelilah Jraifi* Rajae Aboulaich†

Abstract: In this talk we consider a constant elasticity of variance (CEV) diffusion model for pricing of an European option. We prove firstly the existence and uniqueness of the solution in weighted Sobolev spaces, then we suggest the finite difference method using runge Kutta technique to solve the associated parabolic partial differential equation (PDE). Therefore, we compare the results with those given by the Monte Carlo method in Broadie and Kaya [4], using two simulations techniques : the exact method and the Euler discretization. Further, we demonstrate the faster convergence rate of the error obtained by this approach.

Keyworlds: CEV model, Stochastic volatility, Option pricing, Finite difference method.

1 Introduction

The approximation numerical ("estimation") of continuous time models has recently received increasing attention by both financial economists and macro economists. The Black & Scholes formula [3] who considered the volatility as a constant. It's clear that such assumption does not reflect the reality of the market. Empirical studies show that volatility is random and depends on the time, where the modeling of options is made by a system of stochastic differential equations (SDE), one for the underlying and the other for its volatility, taking into account the correlation coefficient between the two noise sources. Hull-White [6], Stein & Stein [7], Heston [5] proposed analytical solvable models that have stochastic volatility. In Aboulaich et al [1] we studied the general extension of this model with jumps. The constant elasticity of variance model (CEV) is an other extension of the stochastic volatility diffusion model (see [2]). It can estimate the change in asset prices in continuous time. In this work, we focus on the problem for the option valuation where underlying price is modeled by a diffusion system of stochastic volatility, the volatility follows another distribution which variance is a polynomial of degree greater than 1. We use the finite difference method, to calculate the values of these options.

References

[1] R. Aboulaich, F. Baghery and A. Jraifi. *Option pricing for a stochastic volatility jump-diffusion model.* International Journal of Mathematics and Statistics. 13 (1) (2013), 1 – 19.

[2] R. Aboulaïch, L.Hadji, A.Jraifi. *Option pricing with constant elasticity of variance (CEV) model.* Applied Mathematical Sciences. 7(109), 5443-5456, 2013.

[3] F. Black and M.Scholes. *The princing of options and corporate liabilities.* Journal of Political Economy. 81 (1973), 635–654.

*EMI–LERMA, jraifi.abdelilah@gmail.com,
†EMI–LERMA, aboulaich@gmail.com

[4] M. Broadie and O. Kaya. *Exact simulation of stochastic volatility and other affine jump diffusion processes.* Operations Research. 54 (2) (2006), 217 - 231.

[5] S. Heston. *A Closed-Form solution for Options with stochastic volatility with applications to bond and currency options.* Review of Financial Studies. 6 (2) (1993), 327 - 343.

[6] J. Hull and A. White *The pricing of options on assets with stochastic volatilities.* Journal of Finance. 42 (1989), 281 - 300.

[7] E.M. Stein and J. C. Stein. *Stock Price Distributions with Stochastic Volatility: An Analytic Approach.* Review of Financial Studies. 4 (1991), 727 - 752.

A family of estimators for the solution of a non-linear inverse problem

Federico Benvenuto * Houssem Haddar †

Abstract: A strategy for the derivation of a fast, accurate and stable algorithm for solving a non-linear ill-conditioned problem is presented. It is divided into two steps. First, the transformation of the non-linear forward model by an invertible map for non-negative data, which allows the use of a well-known family of estimators for the regularization of the generalized inverse operator. Second, the choice of a suitable estimator of this family according to some statistical criterion. This strategy allows for simpler methods than algorithms derived by the non-linear model and better results than estimates provided by model linearization.

Keyworlds: non-linear inverse problem, Poisson noise, variance stabilizing transform, biased estimators, regularization

1 A non-linear inverse problem

The inverse problem considered consists of retrieving a vector of unknown positive parameters x from a vector of indirect measures z with a model given by

$$\left| \sum_{j=1}^{M} A_{ij} x_j \right|^2 = z_i \ , \tag{1}$$

where A is a ill-conditioned $N \times M$ matrix with non-negative elements, between finite dimensional normed spaces ($N \geq M$), and each data vector component z_i is a realization of an independent Poisson variable.

1.1 Variance stabilizing transformation

. We introduce a transformation of the non-linear problem by taking the square root of both sides of equation (1). The advantage is two-fold:

1. the problem becomes piecewise linear.
2. the sampling variance associated with observation $y_i = \sqrt{z_i}$ for all $i = 1, \ldots, N$ will be nearly constant, as the square root is a variance-stabilizing transform for each Poisson variable z_i.

In practice, when A is a non-negative matrix, we transform the problem (1) in a linear problem

$$Ax = y \quad \text{where} \quad y \sim p(Y) \quad , \tag{2}$$

where $p(Y)$ is approximately a multivariate Gaussian with covariance matrix $\Sigma := \sigma^2 I$ and $\sigma \simeq 1$.

A family of estimators for the solution of the linear inverse problem (2) can be defined as

$$X_k := R_k \ Y \ , \tag{3}$$

*INRIA Saclay Ile de France and Ecole Polytechnique (CMAP) Route de Saclay, 91128, Palaiseau, France federico.benvenuto@inria.fr,

†INRIA Saclay Ile de France and Ecole Polytechnique (CMAP) Route de Saclay, 91128, Palaiseau, France houssem.haddar@inria.fr

where

$$R_k := \tau \sum_{n=1}^{k-1} (I - \tau A^* A)^n A^* \tag{4}$$

is the series expansion of the generalized inverse operator $(A^*A)^{-1}A^*$ which converges when $0 < \tau < 2/\|A\|^2$ and A has maximum rank.

1.2 Family of biased estimators

We propose a method which provides regularized solutions of the problem (1) by studying the properties of the family (3), i.e. expectation, covariance and bias of its elements and its asymptotic properties. In particular, starting from the computation of expectation and covariance

$$\mathbb{E}(X_k) = R_k \, \mathbb{E}(Y) \quad \text{and} \quad \mathrm{Cov}(X_k) = R_k \Sigma R_k^* \, , \tag{5}$$

and the expected value and the covariance of the predicted signal

$$\mathbb{E}(AX_k) = AR_k \, \mathbb{E}(Y) \quad \text{and} \quad \mathrm{Cov}(AX_k) = AR_k \Sigma R_k^* A^* \, , \tag{6}$$

we notice that the covariance of X_k is definitely increasing as $k \to \infty$ where a positive increment is understood to mean that the difference matrix is positive semidefinite. It is easy to show that, while the covariance of the predicted signal is bounded by the Cramer-Rao bound, the covariance of the unknowns, although it is bounded, begins with being small and becomes very large when $k \to \infty$ as the matrix A is ill-conditioned.

Because of this, we propose to achieve regularization by choosing the $k-$estimator of the family X_k such that the unknown signal x_k has a given signal-to-noise ratio (SNR). Other choices can be considered and in this work we provide a motivation for this one. To approximate the SNR, we define the *integrated covariance*

$$(s_k)_j = \sum_{i=1}^{M} \mathrm{Cov}(X_k)_{ij} \tag{7}$$

and we compute it as the amount of reconstructed signal versus its uncertainty, i.e $SNR(x_k) := \|x_k/s_k\|_1$. According to this criterion, when the best meaningful SNR approximation is obtained, the corresponding reconstruction x_k is a reliable estimate of the solution of problem (1).

2 SAXS application

We apply the method described above in the determination of the size and shape of colloidal particles by small angle X-ray scattering (SAXS). A good approximation of the model describing the scattered X-ray distribution is equation (2) where the matrix columns of A represent the so-called *form factor* of a given particle shape by varying the radius x_j of the particle j, and y_i is the amount of detected photon-count in each charged-coupled-device pixel i. We show the reliability and efficiency of the proposed method with simulated data.

3 Acknowledgements

This work was carried out during the tenure of an ERCIM "Alain Bensoussan" Fellowship Programme. The research leading to these results has received funding from the European Union Seventh Framework Programme (FP7/2007-2013) under grant agreement n° 246016.

3.7 Shape and topological derivatives (STD)

THE TOPOLOGICAL DERIVATIVE FOR ANISOTROPIC ELASTICITY OF A STRESS-DISPLACEMENT TYPE CRITERION

Gabriel Delgado Keeffe* Marc Bonnet†

Abstract: A comprehensive treatment of the topological derivative for anisotropic elasticity is presented, with both the background material and the trial small inhomogeneity assumed to have arbitrary anisotropic elastic properties. A formula for the topological derivative of any cost functional defined in terms of regular volume depending on the displacement and its gradient is established, by combining small-inhomogeneity asymptotics and the adjoint solution approach. A numerical experiment on the application of the topological derivative to non-destructive testing are reported.
Keyworlds: Topological derivative; Anisotropic Elasticity; Elastic Moment Tensor.

1 Setting of the problem

Consider an elastic body occupying a smooth bounded domain $\Omega \subset \mathbb{R}^n, n = 2, 3$. The anisotropic elastic properties of the background material (against which the effect of small inhomogeneities will be considered), assumed to be homogeneous, are characterized by the fourth-order elasticity tensor $\boldsymbol{\mathcal{C}}$. The boundary $\partial\Omega$ is split according to $\partial\Omega = \Gamma_{\mathrm{D}} \cup \Gamma_{\mathrm{N}}$ (where $\Gamma_{\mathrm{D}} \cap \Gamma_{\mathrm{N}} = \emptyset$ and $|\Gamma_{\mathrm{D}}| \neq 0$), so that a given force density $\boldsymbol{g} \in L^2(\Gamma_{\mathrm{N}}; \mathbb{R}^n)$ is applied on Γ_{N} while a given displacement $\bar{\boldsymbol{u}} \in H^{1/2}(\Gamma_{\mathrm{D}}; \mathbb{R}^n)$ is prescribed on Γ_{D}. Additionally, a body force density $\boldsymbol{f} \in L^2(\Omega; \mathbb{R}^n)$ is applied to Ω. Let be a single small elastic inhomogeneity located at $\boldsymbol{z} \in \Omega$, of characteristic linear size a, occupying the domain

$$B_a = \boldsymbol{z} + a\mathcal{B},$$

where $\mathcal{B}$ is a bounded smooth domain of $\mathbb{R}^n$ and a is small enough so that $\bar{B}_a \Subset \Omega$. The inhomogeneity is endowed with anisotropic elastic properties characterized by the elasticity tensor $\boldsymbol{\mathcal{C}}^\star$, so that the elastic properties of the whole solid are defined by the tensor-valued field $\boldsymbol{\mathcal{C}}_a$ such that

$$\boldsymbol{\mathcal{C}}_a = (1 - \chi(B_a))\boldsymbol{\mathcal{C}} + \chi(B_a)\boldsymbol{\mathcal{C}}^\star = \boldsymbol{\mathcal{C}} + \chi(B_a)\Delta\boldsymbol{\mathcal{C}}, \tag{1}$$

$\chi(D)$ being the characteristic function of the domain D and $\Delta\boldsymbol{\mathcal{C}} := \boldsymbol{\mathcal{C}}^\star - \boldsymbol{\mathcal{C}}$ denoting the elastic tensor perturbation. Let be $W(\bar{\boldsymbol{u}})$ the space of kinematically admissible displacement with respect to arbitrary prescribed Dirichlet data

$$W(\bar{\boldsymbol{u}}) := \left\{\boldsymbol{v} \in H^1(\Omega; \mathbb{R}^n),\, \boldsymbol{v} = \bar{\boldsymbol{u}} \text{ on } \Gamma_{\mathrm{D}}\right\}. \tag{2}$$

Then the displacement field $\boldsymbol{u}_a \in W(\bar{\boldsymbol{u}})$ arising in the solid containing the small inhomogeneity due to the prescribed excitations $(\boldsymbol{f}, \boldsymbol{g}, \bar{\boldsymbol{u}})$ solves the transmission problem

$$\mathrm{div}(\boldsymbol{\mathcal{C}}_a : \boldsymbol{\varepsilon}[\boldsymbol{u}_a]) + \boldsymbol{f} = \mathbf{0} \text{ in } \Omega, \quad \boldsymbol{\mathcal{C}}_a : \boldsymbol{\varepsilon}[\boldsymbol{u}_a] \cdot \mathbf{n} = \mathbf{g} \text{ on } \boldsymbol{\Gamma}_{\mathrm{N}}, \quad \mathbf{u} = \bar{\mathbf{u}}_{\mathbf{a}} \text{ on } \boldsymbol{\Gamma}_{\mathrm{D}}. \tag{3}$$

We also introduce the auxiliary problem of a perfectly-bonded inhomogeneity $(\mathcal{B}, \boldsymbol{\mathcal{C}}^\star)$ embedded in an infinite elastic medium $\Omega = \mathbb{R}^n$ subjected to a uniform remote stress equal to the background stress at $\boldsymbol{z}$. The problem thus consists in finding the displacement field $\boldsymbol{u}_{\mathcal{B}}$ such that

$$\mathrm{div}(\boldsymbol{\mathcal{C}}_{\mathcal{B}} : \boldsymbol{\varepsilon}[\boldsymbol{u}_{\mathcal{B}}]) = \mathbf{0} \text{ in } \mathbb{R}^n, \qquad \boldsymbol{u}_{\mathcal{B}}(\boldsymbol{\xi}) - \boldsymbol{u}_\infty(\boldsymbol{\xi}) = O(|\boldsymbol{\xi}|^{-2}), \;\; |\boldsymbol{\xi}| \to \infty, \tag{4}$$

*CMAP–Ecole Polytechnique, delgado@cmap.polytechnique.fr,
†ENSTA, mbonnet@ensta.fr

where the background displacement $\boldsymbol{u}_\infty$ is defined by $\boldsymbol{u}_\infty(\boldsymbol{\xi}) = \boldsymbol{\nabla u}(\boldsymbol{z})\cdot\boldsymbol{\xi}$ and with $\boldsymbol{\mathcal{C}}_\mathcal{B} := \boldsymbol{\mathcal{C}} + \chi(\mathcal{B})\Delta\boldsymbol{\mathcal{C}}$.

2 Elastic moment tensor

The *elastic moment tensor* (EMT) [1, 3] plays an important role in the small-inhomogeneity asymptotics. The EMT $\boldsymbol{\mathcal{A}}$ is the fourth-order tensor defined for any value of the constant tensor $\boldsymbol{\nabla u}(\boldsymbol{z}) \in \mathbb{R}^{n,n}$ by

$$\boldsymbol{\mathcal{A}} : \boldsymbol{\nabla u}(\boldsymbol{z}) = \int_\mathcal{B} \Delta\boldsymbol{\mathcal{C}} : \boldsymbol{\nabla u}_\mathcal{B} \, \mathrm{d}V. \tag{5}$$

The EMT has the same lower and mayor symmetry properties of the elasticity tensor $\boldsymbol{\mathcal{C}}$. Furthermore let be $\boldsymbol{G}_\infty$ the elastostatic full-space Green's tensor. Then the following asymptotic development stands

$$\boldsymbol{u}_\mathcal{B} = \boldsymbol{u}_\infty + \boldsymbol{\nabla G}_\infty(\boldsymbol{x}-\boldsymbol{z}) : \boldsymbol{\mathcal{A}} : \boldsymbol{\nabla u}_\infty + O(|\boldsymbol{x}|^{-n}), \quad (|\mathbf{x}| \to \infty).$$

3 Topological sensitivity analysis

Consider the cost functionals of the form

$$J(\boldsymbol{\mathcal{C}}_a) = \mathbb{J}_a(\boldsymbol{u}_a, \nabla\boldsymbol{u}_a) \qquad \text{with} \quad \mathbb{J}_a(\boldsymbol{u}, \nabla\boldsymbol{u}) = \int_\omega \psi_a(\boldsymbol{x}, \boldsymbol{u}, \nabla\boldsymbol{u}) \, \mathrm{d}V(\boldsymbol{x}), \;\; \omega \subset \Omega, \tag{6}$$

where the density ψ_a is defined by

$$\psi_a = (1-\chi(B_a))\psi + \chi(B_a)\psi^\star = \psi + \chi(B_a)\Delta\psi, \tag{7}$$

with ψ and $\psi^\star$ (and hence also $\Delta\psi := \psi^\star - \psi$) assumed regular. The arguments $\boldsymbol{x} \in \Omega$, $\boldsymbol{u} \in \mathbb{R}^n$, $\boldsymbol{d} \in \mathbb{R}^{n\times n}$ denote the generic arguments of a density $\psi(\boldsymbol{x}, \boldsymbol{u}, \boldsymbol{d})$, $\partial_x\psi, \partial_u\psi, \partial_d\psi$ denote the partial derivatives with respect of the corresponding arguments, and higher-order partial derivatives are denoted similarly, e.g. $\partial^2_{ud}\psi$. The topological derivative $DJ(\boldsymbol{z})$ of an inclusion of elliptic shape and elastic moduli $\boldsymbol{\mathcal{C}}$ and $\boldsymbol{\mathcal{C}}^\star$ on $\boldsymbol{z}$, will be defined through

$$J(\boldsymbol{\mathcal{C}}_a) = J(\boldsymbol{\mathcal{C}}) + a^n DJ(\boldsymbol{z}) + o(a^n).$$

A particularly interesting case in non-destructive control is when $B_a \subset \Omega\backslash\omega$, and ω is a set of control volumes. In that case the topological derivative reads [2]

$$DJ(\boldsymbol{z}) = -\nabla\boldsymbol{p}(\boldsymbol{z}) : \boldsymbol{\mathcal{A}} : \nabla\boldsymbol{u}(\boldsymbol{z}),$$

and the adjoint state $\boldsymbol{p}$ satisfies the variational formulation

$$\int_\Omega \boldsymbol{\varepsilon}[\boldsymbol{p}] : \boldsymbol{\mathcal{C}} : \boldsymbol{\varepsilon}[\boldsymbol{q}] dV = \int_\Omega \chi_\omega \left\{ \partial_d\psi : \nabla\boldsymbol{q} + \partial_u\psi \cdot \boldsymbol{q} \right\} dV, \forall \boldsymbol{q} \in W(0).$$

References

[1] Habib Ammari and Hyeonbae Kang. *Polarization and Moment Tensors: with applications to inverse problems and effective medium theory*, volume 162. Springer, 2007.

[2] Marc Bonnet and Gabriel Delgado. The topological derivative in anisotropic elasticity. *Quarterly Journal of Mechanics and Applied Mathematics*, 66(4):557–586, 2013.

[3] SA Nazarov, J Sokolowski, and M Specovius-Neugebauer. Polarization matrices in anisotropic heterogeneous elasticity. *Asymptotic Analysis*, 68(4):189–221, 2010.

A 3D segmentation in X ray tomography

Badreddine Rjaibi* Lamia Jaafar Belaid† Walid Mourou ‡

Abstract: We propose in this work two methods for a 3D segmentation problem in X-ray tomography. The algorithms proposed are based on the topological gradient approach and edge detection. More precisely, the first algorithm is based on a coupled method between the 2D watershed algorithm and a marching cubes algorithm. The second algorithm concerns a 3D extension of the 2D watershed algorithm using markers technic. Experimental results obtained on noisy data illustrate the efficiency of ours approaches and show a good visualization of a given volume.
Keywords: Marching cubes, tomographic reconstruction, Topological gradient, segmentation, watershed.

1 A 3D segmentation in X ray tomography

The goal of ours approaches is to give a volume visualization of the anomaly present inside the human body.

1.1 A 3D segmentation Using a 2D Watershed algorithm coupled with Marching cubes algorithm

The first approach is based on the 2D Watershed algorithm by marker coupled with marching cubes algorithm.
This segmentation algorithm process in to three steps:

1. Acquisition of the slices reconstructs by the topological gradient approach [1].
2. Segmentation by marker of every slice which contains the object target by the method proposed by [2].
3. Application of the algorithm of the marching cube to the cube formed by segmented slices [3].

1.2 A 3D segmentation using a 3D extension of the 2D watershed algorithm by marker of one slice only

The second approach is a 3D extension of the 2D Watershed algorithm by marker of one slice only.
This segmentation algorithm process in to five steps:

1. Acquisition of the reconstructed slices and their edges: The reconstruction of slices and the detection of edges are made by the approach presented in section 2.
2. Construction of 3D edge by a stack of 2D edges.
3. Marking of objects to be segmented: one click on a portion of object to be segmented in a single slice only.

*LAMSIN-ENIT, Campus Universitaire, BP37, 1002 le Belvédère, Tunis, Tunisie, badreddine.rjaibi@lamsin.rnu.tn,
†University of Dammam College of Sciences PO Box 838, 31113 Dammam, KSA, Ljaafar@ud.edu.sa,
‡LAMSIN-ENIT, Campus Universitaire, BP37, 1002 le Belvédère, Tunis, Tunisie, walid.mourou@lamsin.rnu.tn

4. Calculation of the 3D watershed with calculation of the volume.
5. 3D display.

2 Numerical results

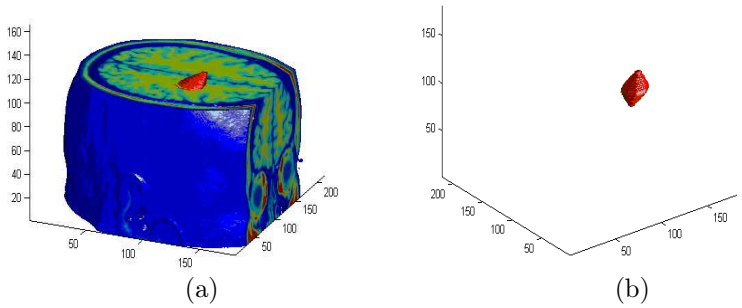

Figure 1: (a): 3D representation of the lesion of the global image , (b): 3D representation of the lesion which the volume is 19147 voxels.

We present in the Figure 2 a zoom on the result obtained by the two proposed approaches for a 3D segmentation in tomography.

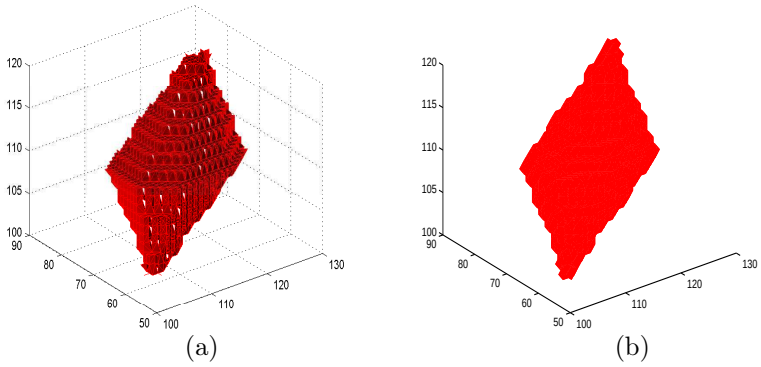

Figure 2: (a): Zoom on the lesion segmented by the technique of Marching Cubes, (b): zoom on the lesion segmented by the 3D watershed algorithm with Marking.

References

[1] D. AUROUX, L. JAAFAR BELAID, B. RJAIBI, *application of the topological gradient method to tomography* In ARIMA Proc. TamTam'09. 2010.

[2] L. JAAFAR BELAID, W. MOUROU, *image segmentation: A new watershed transformation algorithm* Image Analysis and Stereology. Volume 28-pp. 93-102. 2009.

[3] WILLIAM E. LORENSEN, HARVEY E. CLINE, *Marching Cubes: A High Resolution 3D Surface Construction Algorithm* SIG. Volume 32. 1987.

Error Estimation in Shape Optimization

Bernhard Kiniger*

Abstract: In this talk we consider a model shape optimization problem. The state variable solves an elliptic equation on a star-shaped domain where the radius is given via a control function. We reformulate the problem on a fixed reference domain, show existence of an optimal control including higher regularity. The problem is discretized using finite elements. We show a-priori error estimates for the error between the optimal control and its fully discretized counterpart and apply the dual-weighted residual method for a-posteriori error estimation. We finish the presentation with some numerical results.
Keywords: shape optimization, error estimation

1 Introduction

We consider the following shape optimization problem governed by a linear elliptic equation:

$$\min_{q\in H^2_{\mathrm{per}}((0,2\pi)),u\in H^1_0(\Omega_q)} J(\Omega_q,u)=\frac{1}{2}\left\|u-u_d^q\right\|^2_{L^2(\Omega_q)}+\frac{\alpha}{2}\left\|q\right\|^2_{H^2((0,2\pi))}, \tag{1}$$

subject to

$$\begin{cases} -\Delta u+u=f^q & \text{in } \Omega_q,\\ \qquad u=0 & \text{on } \Gamma_q, \end{cases} \tag{2}$$

where the domain Ω_q is star-shaped with respect to the origin and radius given by the control q, see Figure 1. The data functions u_d^q and f^q are restrictions of sufficiently smooth functions defined on a sufficiently large holding-all domain, and $\alpha>0$.

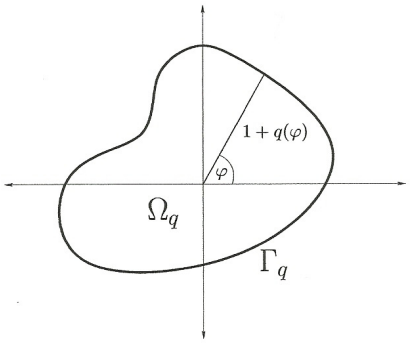

Figure 1: The domain Ω_q

In order to solve (1) we use the method of mapping [6]. We use a transformation F to reformulate (2) on a fixed reference domain Ω_0. Using results presented in [4], it is possible to proof the existence of an optimal control $\overline{q}$ with corresponding optimal state $\overline{u}$ and optimal transformation $\overline{F}$. Furthermore it is possible to show higher regularity of the optimal control, $\overline{q}\in H^4((0,2\pi))$.

*Chair of Optimal Control, Technische Universität München, Center for Mathematical Sciences, Boltzmannstraße 3, 85748 Garching b. München, Germany; kiniger@ma.tum.de

2 Error Estimation

In order to derive error estimates, we discretize problem (1). The control is being discretized using piecewise cubic polynomials, the state and the transformation are discretized using (bi)linear finite elements. In addition, we also have to approximate Ω_0 with a polygonal domain $\Omega_{0,h}$. It is possible to show that there exists a sequence $\left(\overline{q}_{\sigma,h,k}\right)_{\sigma,h,k>0}$ of optimal controls to the fully discretized problems converging to the optimal control $\overline{q}$ of the continuous problem. Here, σ, h and k are the discretization parameters for the control, the state and the transformation, respectively.

2.1 A-priori Error Estimates

By generalizing the methods used in [5] and using a weak assumption on the coercivity of the second derivative of the reduced cost functional we can proof our main result, namely

$$\left\|\overline{q} - \overline{q}_{\sigma,h,k}\right\|_{H^2((0,2\pi))} \leq c\left(\sigma^2 + h^2 + k^2\right). \tag{3}$$

2.2 A-posteriori Error Estimates

The so-called dual weighted residual method [1] is widely used for a-posteriori error estimates in the context of finite elements. We will show how to adapt this method for a-posteriori error estimation with respect to the discretization of the control, i.e. the shape of the domain.

2.3 Numerical Results

The problem has been implemented using the toolkits Gascoigne [2] and RoDoBo [3]. We will present some numerical results verifying our claims.

3 Acknowledgments

This work was done under the supervision of Boris Vexler whose help and support is warmly thanked.

References

[1] R. Becker and R. Rannacher. An optimal control approach to a posteriori error estimation in finite element methods. *Acta Numerica*, pages 1–102, 2001.

[2] Roland Becker, Malte Braack, Thomas Dunne, Dominik Meidner, Thomas Richter, Michael Schmich, Winnifried Wollner, and Boris Vexler. Gascoigne: The Finite Element Toolkit. http://www.gascoigne.uni-hd.de/.

[3] Roland Becker, Dominik Meidner, and Boris Vexler. RoDoBo: A C++ library for optimization with stationary and nonstationary PDEs. http://www.rodobo.org.

[4] B. Kiniger. A transformation approach in shape optimization: Existence and regularity results. *Numer. Funct. Anal. Optim.*, submitted.

[5] B. Kiniger and B. Vexler. A priori error estimates for finite element discretizations of a shape optimization problem. *ESAIM: Mathematical Modelling and Numerical Analysis*, 47:1733–1763, 11 2013.

[6] F. Murat and J. Simon. Studies on optimal shape design problems. *Lecture Notes in Computer Science*, 41, 1976.

Dérivation par rapport à la forme du système de Navier-Stokes non stationnaire avec des conditions aux bords de type Navier

Bsaies Chaima* Raja Dziri†

Mots clés : Dérivation par rapport à la forme- Equations de Navier-Stokes non stationnaires-conditions aux bords de type Navier.

Résumé

Nous nous intéressons dans ce travail à l'étude de la dérivabilité par rapport à la forme de la vitesse de l'écoulement d'un fluide Newtonien, visqueux et incompressible afin d'établir une condition nécessaire d'optimalité de premier ordre associée au problème de minimisation par rapport à la forme de la traînée visqueuse dûe à la pésence d'un obstacle tridimensionnel S :

$$(\mathcal{P}) \quad \min_{\Omega\in\mathcal{A}_d} J(\Omega) = \min_{\Omega\in\mathcal{A}_d} \mu \int_0^T \int_\Omega \epsilon(u_\Omega)..\epsilon(u_\Omega)$$

où $J(\Omega)$ est l'énergie visqueuse dissipée, D est un domaine suffisament grand mais borné de $\mathbb{R}^3$, $\mathcal{A}_d$ est l'ensemble des domaines admissibles et u_Ω est la vitesse du fluide.

Le choix des conditions aux bords de type Navier est motivé par le fait que la présence de rugosité sur S peut affecter considérablement le comportement du fluide au voisinage de l'obstacle (cf. [3] et [4]). Ce qui rend la question pertinente d'un point de vue optimisation de forme. Dans la pratique, on a souvent recourt à ce qu'on appelle les "lois de paroi" (ou "wall laws") où la frontière rugueuse est remplacée par une frontière artificielle régulière et une condition aux limites homogéneisée qu'est la condition de Navier. Plus précisement, la condition de non glissement : $u = 0$ sur le bord est remplacée par les conditions aux limites de Navier qui exprime le fait que la composante tangentielle de la vitesse de l'écoulement est proportionnelle aux contraintes tangentielles :

$$\begin{cases} \mu(\varepsilon(u).n)_{tg} + \beta u_{tg} = 0 \\ u.n = 0 \qquad \text{(condition de non-pénétration)} \end{cases}$$

où $\varepsilon(u)$: tenseur de déformation, μ : coefficient de viscosité et β : coefficient de frottement

Dans notre étude de la dérivabilité par rapport à la forme, on a adopté la méthode des vitesses introduite par J.Sokolowski et J-P.Zolésio, voir par exemple [1] et [2].
La démarche consiste dans un premier temps à prouver l'existence et l'unicité d'une solution pour $\Omega \in \mathcal{A}_d$ sous certaines hypothèses portant sur la régularité des données sur le bord pour l'existence. Pour l'uncité et comme dans le cas classique de conditions aux bords de Dirichlet, il a fallu imposer plus de régularité sur les données et rajouter une contrainte supplémentaire satisfaite pour les grandes viscosités, cf. [5] et [6]. Pour le calcul la dérivée par rapport à la forme du système de Navier-Stockes, on a utilisé la transformation de Piola [7] et le théorème des fonctions implicites faible introduit par J.-P. Zolésio, [8].

*FST-Département de Maths, chaimabsaies@yahoo.fr
†FST-Département de Maths, raja.dziri@fst.rnu.tn

Références

[1] **J.Sokolowski, J.-P. Zolésio**, *Introduction to Shape Optimization : Shape Sensitivity Analysis*, Springer- Verlag, Berlin, 1992.

[2] **M. C. Delfour and J. P. Zolésio**, *Shapes and geometries : metrics, analysis differential calculus and optimization*, Siam, 2011.

[3] **W. Jager and A. Mikelic**, *On the roughness-unduced effective boundary conditions for an incompressible viscous flow*, J. Differential Equations 170, 1, 96-122, 2001.

[4] **A. Russo, A. Tartaglione**, *On the Navier problem for stationary Navier-Stokes equations*, J. Differential Equations 251, 2387-2408, 2011.

[5] **R. Temam**, *Theory and numerical analysis of the analysis of the Navier-Stockes equations*, North-holland, 1977.

[6] **J.L.Lions**, *Quelques méthodes de résolution des probèmes aux limites non linéaires*, Dunod Guathier-Villars, 1969.

[7] **S. Boisgerault**, *Optimisation de forme : système non linéaires et mécanique des fluides, Thèse de doctorat*, Ecole des Mines de Paris-Informatique Temps réel, Robotique, Automatique, 2000.

[8] **J.-P. Zolésio** , *Identification de domaines par déformation*, Thèse de doctorat d'état, Université de Nice, France, 1979.

Index